NONLINEAR OPTICAL PROPERTIES AND STRUCTURE OF POLED TELLURITE GLASSES AND RELATED MATERIALS

AIKO NARAZAKI

2000

DEPARTMENT OF MATERIAL CHEMISTRY
GRADUATE SCHOOL OF ENGINEERING
KYOTO UNIVERSITY

Contents

General introduction

Oxide glasses are attractive as well as useful materials in the fields of optics and optoelectronics because of high transparency and processability. For instance, optical fiber glasses contribute to the prosperity of not only information science but also various aspects of human activity in the present information-oriented society. In addition to the outstanding linear optical properties, the nonlinear optical properties of glass have become of technological interest, with the development of the laser. The large electric field of laser beams makes higher-order nonlinear terms in the material polarization large enough for the effective nonlinear optical phenomena including second- and third-harmonic generation, multiphoton absorption, intensity-dependent refractive index, and so forth. The glasses with these nonlinear optical properties can be utilized in many applications such as a frequency converter, electro-optics and optical-switching device, and therefore, possess ability to play a central roll in the field of optoelectronics.

Poled oxide glasses are promising materials because of the second-order nonlinear optical properties induced by poling, and have been studied extensively since the discovery of second-harmonic generation (SHG) in Ge-doped silica glass fiber [1] and thermally/electrically poled silica glass [2]. The second-harmonic generation is one of the second-order nonlinear phenomena; an incident light is efficiently converted to a second-harmonic wave with twice the initial frequency. In addition to the practical interest, a great deal of attention has been paid to the fundamental or scientific problem why the poled oxide glasses exhibit second-harmonic generation. This question comes from the fact that the second-order nonlinearity strictly needs a lack of inversion symmetry in material structure so that it should

completely vanish in glasses which possess isotropic and centro-symmetric structure. In other words, glasses originally do not show second-harmonic generation which arises from the inside of the glass. As a result, the induction of second-order nonlinearity into glass materials has been an attractive subject from the fundamental standpoint.

With an increase of interest in poled glasses in the last decade, poling techniques have been developed rapidly. They are divided into some groups dependent on the types of exciting source: optical poling [1, 3], thermal poling [2, 4], poling with electron-beam radiation [5, 6] and UV-excited poling [7–9]. All of these involve distinct advantages and induction mechanisms of nonlinear optical properties. In the present thesis, thermal poling which takes advantage of the flexibility of glass structure and reflects the temperature dependence of the flexibility is chosen. Namely, the second order nonlinearity of the thermally/electrically poled oxide glasses is investigated. Hereafter, the technical term of poling stands for thermal poling, unless otherwise stated, in this work.

As for the poled oxide glasses, the second-harmonic generation has been investigated most extensively and widely in silica-based glasses [2, 10–18]. The characteristic behavior in these materials is that the region with second-order nonlinearity, that is, the SHG-active structure, was mainly created in the vicinity of the glass surface contacted with an anode during poling. This reveals the existence of a common factor for the induction of the second-order nonlinearity. On the other hand, poled tellurite glasses as well as the silica-based glasses offer the second-harmonic generation, as first reported by Tanaka *et al.* in 1993 [19]. Tellurite glasses possess many attractive linear optical properties such as high refractive index and good IR transmittance in addition to low melting point and relatively high chemical durability. Besides, large third-order nonlinear susceptibility has been reported in various tellurite glass systems [20], which is larger by two orders of magnitude compared with those for most of the silica-based glasses. In addition to the above excellent properties, the tellurite glasses exhibit fragility to some extent at around their relatively low glass transition temperatures. From this point, it is expected that their temperature dependence of second-order nonlinearity gives us some valuable aspects on the structural change and the variation of ionic motion related to glass network at around their glass transition temperatures. Therefore, in the present thesis, the nonlinear optical properties with second-order and structure of poled tellurite glasses are throughly investigated.

As shown above, the poled oxide glasses exhibit the interesting nonlinear optical properties with second-order from both fundamental and practical viewpoints. Moreover, poling is an attractive technique for a modification of glass structure such as controlled crystallization, owing to the structural flexibility of amorphous state. However, there exist many unresolved problems on the poled oxide glass materials. For instance, a complete clarification of the induction mechanism of the second-order nonlinearity has not been attained. This hinders further developments of optoelectronic devices in this field. Also, the influence of a large electric field by poling on not only the nonlinear optical properties but also the structure of oxide glasses is not thoroughly clarified. The studies on the relaxation behavior of the induced second-order nonlinearity are scarce despite of its importance for better understanding of the induction process as well as practical applications. The ability of poling to improve crystallinity in glass-ceramics is also little known. In particular, since the problem how the ferroelectric-like behavior of glass-ceramics is accomplished is quite interesting, a promising method is desired to overcome this problem. The present thesis was undertaken to resolve such problems. The respective chapters are outlined as follows.

In Chapter 1, a theoretical approach to second-harmonic generation of poled oxide glasses, so-called the Maker fringe theory, is presented. Second-harmonic generation in poled tellurite glasses is examined and analyzed by this theory in order to evaluate their second-order nonlinearity. Especially, the dependence of second-harmonic intensity on poling temperature is examined. All the tellurite glass systems employed in this thesis exhibit a common characteristic that there is an optimum poling tempera-

ture at which the second-harmonic intensity experiences a maximum. This optimum poling temperature is further discussed in connection with the glass transition temperature. Moreover, the compositional dependence of second-harmonic intensity is investigated in mixed alkali tellurite glasses.

In Chapter 2, the variation of second-harmonic intensity with angle of incidence, namely, the Maker fringe pattern is investigated in detail for poled tellurite glasses. As a result, the induction mechanism of second-order nonlinearity described as $\chi^{(2)} = 3\chi^{(3)} \cdot E_{dc}$ is suggested. Here, E_{dc} denotes a static electric field created in the glass by poling. Based on this mechanism, long-term and large second-order nonlinearity are realized in ZnO-TeO_2 and WO_3-TeO_2 glass systems, respectively.

In Chapter 3, the relaxation behavior of second-harmonic intensity is demonstrated for the WO_3-TeO_2 glass system with the large second-order nonlinearity as presented in Chapter 2. The relaxation time which is also an important factor for clarification of the induction mechanism of second-order nonlinearity as well as practical application is calculated with a stretched exponential decay function. The effect of poling temperature on the relaxation time is studied. Second-harmonic generation is also examined at elevated temperatures so that a determination of the activation energy for the relaxation process is carried out by the Arrhenius plot.

In Chapter 4, surface structure of poled tellurite glasses is investigated by means of X-ray photoelectron spectroscopic and infrared reflectance techniques. The information on a surface state also allows us to characterize the second-order nonlinearity because the SHG-active layer is located at the glass surface as revealed in the previous chapters.

In Chapter 5, second-harmonic generation in tellurite glass-ceramics containing $BaTiO_3$ crystallites is discussed. The Maker fringe theory is modified for the purpose of application to the glass-ceramics. Also, the poling effect on both the ferroelectricity of $BaTiO_3$ and second-harmonic generation is experimentally examined.

In Summary, the central results and discussions through the whole of this thesis are summarized.

References

[1] U. Österberg and W. Margulis, Opt. Lett. **11**, 516 (1986).

[2] R. A. Myers, N. Mukherjee, and S. R. J. Brueck, Opt. Lett. **16**, 1732 (1991).

[3] D. M. Krol and J. R. Simpson, Opt. Lett. **16**, 1650 (1991).

[4] H. Nasu, H. Okamoto, A. Mito, J. Matsuoka, and K. Kamiya, Jpn. J. Appl. Phys. **32**, 180 (1993).

[5] P. G. Kazansky, A. Kamal, and P. S. J. Russell, Opt. Lett. **18**, 693 (1993).

[6] P. G. Kazansky, A. Kamal, and P. S. J. Russell, Opt. Lett. **18**, 1141 (1993).

[7] T. Fujiwara, D. Wong, Y. Zhao, S. Fleming, S. Poole, and M. Sceats, Electron. Lett. **31**, 573 (1995).

[8] T. Fujiwara, M. Takahashi, and A. J. Ikushima, Appl. Phys. Lett. **71**, 1032 (1997).

[9] M. Takahashi, T. Fujiwara, T. Kawachi, and A. J. Ikushima, Appl. Phys. Lett. **71**, 993 (1997).

[10] X.-C. Long, R. A. Myers, and S. R. J. Brueck, Opt. Lett. **19**, 1819 (1994).

[11] R. A. Myers, X. Long, and S. R. J. Brueck, Proc. SPIE **2289**, 98 (1994).

[12] P. G. Kazansky, L. Dong, and P. S. J. Russell, Electron. Lett. **30**, 1345 (1994).

[13] K. Tanaka, K. Kashima, K. Hirao, N. Soga, S. Yamagata, A. Mito, and H. Nasu, Jpn. J. Appl. Phys. **34**, 175 (1995).

[14] J. M. Dell, M. J. Joyce, and G. O. Stone, Proc. SPIE **2289**, 185 (1994).

[15] H. Imai, S. Horinouchi, Y. Uchida, H. Yamasaki, K. Fukao, G. Zhang, T. Kinoshita, K. Mito, H. Hirashima, and K. Sasaki, J. Non-Cryst. Solids **196**, 63 (1996).

[16] O. Sugihara, T. Hirama, H. Fujimura, and N. Okamoto, Opt. Rev. **3**, 150 (1996).

[17] H. Takebe, P. G. Kazansky, and P. S. J. Russell, Opt. Lett. **21**, 468 (1996).

[18] M. Qiu, F. Pi, G. Orriols, and M. Bibche, J. Opt. Soc. Am. B **15**, 1362 (1998).

[19] K. Tanaka, K. Kashima, K. Hirao, N. Soga, A. Mito, and H. Nasu, Jpn. J. Appl. Phys. **32**, L843 (1993).

[20] S. H. Kim, T. Yoko, and S. Sakka, J. Am. Ceram. Soc. **76**, 2486 (1993).

Chapter 1

Poling-induced second-order nonlinearity in tellurite glass systems

1.1 Theory of second-harmonic generation for poled oxide glasses

1.1.1 Maker fringe theory

In the present thesis, second-harmonic generation (SHG) is measured for the estimation of nonlinear optical properties with second-order in poled tellurite glasses and glass-ceramics. Second-harmonic generation is a second-order nonlinear phenomenon which comes from the second-order nonlinear polarization term $P_{2\omega} = \chi^{(2)} \cdot \vec{E}_{\omega} \quad \vec{E}_{\omega}$ in Eq. (1.1):

$$\begin{aligned} P &= P_{\omega} + P_{2\omega} + P_{3\omega} + \cdots \\ &= \chi^{(1)} \cdot \vec{E}_{\omega} + \chi^{(2)} \cdot \vec{E}_{\omega} \quad \vec{E}_{\omega} + \chi^{(3)} \cdot \vec{E}_{\omega} \quad \vec{E}_{\omega} \quad \vec{E}_{\omega} + \cdots , \end{aligned} \tag{1.1}$$

where P is the polarization and $\vec{E}_{\omega}$ is the electric field of an incident light. Namely, the incident light is efficiently converted into a second-harmonic wave with twice the initial frequency. This phenomenon has attracted a great deal of attention because of not only its potential application to optical devices but also non-distractive method for investigating a buried interface. The Maker fringe method [1] has been employed most extensively for the SHG measurements. As for the poled oxide glasses, this method is notably useful because it informs us not only the magnitude of non-zero

tensor components of the second-order nonlinear susceptibility but also other important aspects such as symmetry and thickness of a SHG-active structure.

SHG measurements utilizing the Maker fringe method are carried out under a configuration described below (Fig. 1.2). An intense laser beam is incident on a plate-like glass sample which is rotated around an axis perpendicular to the incident plane. As a result, the second-harmonic intensity generated from the poled glass is obtained as a function of incident angle. The angular dependence of second-harmonic intensity, so-called Maker fringe pattern, is analyzed with the following Maker fringe equations:

$$I_{2\omega} = C\, d_{eff}{}^2\, t_\omega{}^4\, T_{2\omega}\, R(\theta)\, I_\omega{}^2 [1/(n_\omega{}^2 - n_{2\omega}{}^2)^2] \sin^2\Psi \ . \tag{1.2}$$

$$t_\omega = \frac{2\cos\theta}{n_\omega \cos\theta + \cos\theta_\omega} \ . \tag{1.3}$$

$$T_{2\omega} = \frac{2 n_{2\omega} \cos\theta_{2\omega} (n_\omega \cos\theta + \cos\theta_\omega)(n_{2\omega} \cos\theta_\omega + n_\omega \cos\theta_{2\omega})}{(n_{2\omega} \cos\theta + \cos\theta_{2\omega})^3} \ . \tag{1.4}$$

where I is the power of light, C is the constant, $R(\theta)$ represents the multiple reflection coefficient, n is the refractive index and d_{eff} is the effective second-order nonlinear coefficient which is described in detail in the next section. Here, subscripts ω and 2ω denote the fundamental and second-harmonic waves, respectively. Ψ is a function of SHG-active layer thickness, L, as follows:

$$\Psi = (2\pi L/\lambda)(n_\omega \cos\theta_\omega - n_{2\omega} \cos\theta_{2\omega}) \ . \tag{1.5}$$

The last term of Eq. (1.2), $\sin^2\Psi$, causes the oscillation of second-harmonic intensity in the Maker fringe pattern: the generated second-harmonic intensity varies with angle of incidence. By analyzing this oscillation pattern using Eqs. (1.2)-(1.5), we can determine the thickness of the SHG-active region. Here, it should be mentioned that the application of Maker fringe method is restricted to some extent due to the assumption of high transparency in the spectral range of interest. This problem is tackled in Chapter 5 by modifying the last term of Eq. (1.2). As for the poled tellurite

glasses employed in this work, however, it is out of a question.

1.1.2 Effective second-order nonlinear coefficient of poled glasses

The second-order nonlinear polarization $P_{2\omega}$ which causes second-harmonic generation depends on the second-order nonlinear susceptibility tensor with $3^3 = 27$ components of $\chi^{(2)}_{ijk}$ ($i, j, k = x, y, z$) as well as an amplitude of the incident electric field | $\vec{E}_\omega$ |:

$$P_{2\omega\, i} = \chi^{(2)}_{ijk} \cdot \vec{E_\omega}_j \quad \vec{E_\omega}_k \ . \tag{1.6}$$

The number of tensor components can be reduced to 18 because the ijk and ikj components are identical. Thus, the second-order nonlinear tensor is represented by $\chi^{(2)}_{mn}$ with subscripts m and n as described in Table 1.1.

Table 1.1: Second-order nonlinear tensor components $\chi^{(2)}_{mn}$.

	1	2	3	4	5	6
m	x	y	z			
n	xx	yy	zz	$yz\,(zy)$	$zx\,(xz)$	$xy\,(yx)$

$\chi^{(2)}$ is related to the second-order nonlinear coefficient d as follows:

$$\chi^{(2)} = 2\, d \ . \tag{1.7}$$

both of them are used for evaluating the second-order nonlinearity of poled tellurite glasses and glass-ceramics. d can be written by Eq. (1.8) for poled oxide glasses under the assumptions that that the Kleinman symmetry [2] is satisfied and that the electro dipoles are isotropic [3] and oriented perpendicular to the sample surface with $C_{\infty v}$ symmetry:

$$d = \begin{pmatrix} \cdot & \cdot & \cdot & \cdot & d_{15} & \cdot \\ \cdot & \cdot & \cdot & d_{24} & \cdot & \cdot \\ d_{31} & d_{32} & d_{33} & \cdot & \cdot & \cdot \end{pmatrix} \ . \tag{1.8}$$

with the following relation:

$$d_{15} = d_{24} = 2d_{31} = 2d_{32} = \frac{2}{3}d_{33} \ . \tag{1.9}$$

Therefore, the poled oxide glass has only one independent tensor component. If the second-harmonic measurement is carried out under *pp*-polarization, the effective second-order nonlinear coefficient, d_{eff}, is written as follows:

$$\begin{aligned} d_{eff} &= 2d_{31}\sin\theta_\omega\cos\theta_\omega\cos\theta_{2\omega} + (d_{31}\cos^2\theta_\omega + d_{33}\sin^2\theta_\omega)\sin\theta_{2\omega} \\ &= \frac{2}{3}d_{33}\sin\theta_\omega\cos\theta_\omega\cos\theta_{2\omega} + d_{33}(\frac{1}{3}\cos^2\theta_\omega + \sin^2\theta_\omega)\sin\theta_{2\omega} \end{aligned} \tag{1.10}$$

It is predicted that the poled glass offers two kinds of the refractive indices, one is for a light propagated along anisotropic axis and another is for a light propagated along two residual equivalent axes. Nonetheless, it is difficult to separate such two components by using the ellipsometry method and a difference is expected less than a few percent in the poled tellurite glasses. Hence, the difference between refractive indices for ordinary and extraordinary rays is ignored at the present time.

1.2 Effect of poling temperature on second-harmonic generation in tellurite glass systems

1.2.1 Introduction

Nonlinear optical properties with second-order of poled glass materials have the focus of growing scientific and practical interest. From the fundamental standpoints, the main interest lies in the fact that the second-order nonlinearity which rigorously needs a lack of inversion symmetry in the light wavelength scale is induced in some kinds of glasses by poling, despite of optical isotropy of glass. The ability to tailor the nonlinear optical properties with second-order has been utilized in many practical applications such as a frequency doubler of light and linear electro-optical devices.

Not only the silica glass [4–8] but also tellurite glass are one of the representative amorphous materials which exhibit second-harmonic generation when the poling is carried out [9–11]. The main goal of the present thesis is the clarification of the above problem, namely, the induction mechanism of second-order nonlinearity in tellurite glasses, as well as its optimization for the practical needs.

There are several factors which possibly affect the magnitude of second-order nonlinearity induced in poled glasses: glass composition and poling conditions, such as temperature, voltage, and atmosphere, and so forth. Thus, it is desired that the effect of not only poling conditions but also glass composition on the second-order nonlinearity is studied perfectly for the fundamental and practical interest. In this section, the poling temperature effect on the second-harmonic generation is investigated systematically in various tellurite glass systems containing the network modifying cations with mono- and divalent states. Consequently, the characteristic dependence of second-harmonic intensity on the poling temperature was revealed, as shown in Fig. 1.6. A startling fact is that a similar phenomenon was observed in poled silica glass [12]. From this, it is instructive to clarify the effect of poling temperature. In particular, this phenomenon is interesting in connection with thermally induced change of glass structure because the poling temperature is very close to glass transition temperature. Also, the linear relation between glass transition temperature and the poling temperature corresponding to maximum second harmonic intensity, which is hereafter referred to as an optimum poling temperature, is demonstrated and discussed.

1.2.2 Experimental procedure

1.2.2.1 Sample preparation

Glass samples were prepared from Na_2CO_3, ZnO and TeO_2. The purity of raw materials was 99.5, 99 and 99 %, respectively. The raw materials

were mixed thoroughly to make $30NaO_{\frac{1}{2}}\cdot 70TeO_2$ and $10NaO_{\frac{1}{2}}\cdot 20ZnO\cdot 70TeO_2$ compositions, and melted in a platinum crucible at 850 °C for 20 min in air. The melt was poured onto a carbon plate to obtain glass. The glass transition temperature was measured using differential thermal analysis (Rigaku, TG-DTA8112BH). After the glass was annealed at around the glass transition temperature for 20 min, it was cut into a plate. Both sides of surfaces of the plate-like glass were polished to measure the second-harmonic generation. The thickness of the resultant glass sample was 1.00 mm.

Poling of the glass sample was performed as follows. A schematic illustration of the poling apparatus is shown in Fig. 1.1. The glass sample was sandwiched in between two commercial borosilicate glass plates with a thickness of 0.15 mm and contacted physically with electrodes made of stainless steel. The commercial borosilicate glass plates were used to avoid precipitation of metallic tellurium which occurred on the cathode-side glass surface when the glass sample was contacted directly to the electrodes made of stainless steel [11]. The use of commercial borosilicate glass plates was also effective to avoid discharge between the electrodes. The glass sample sandwiched with the electrodes was put into an electric furnace and heated to an aimed temperature. After the glass sample was held at the temperature for 30 min, the voltage of 3 kV was applied for 20 min. Then, the glass sample was taken out from the furnace and quenched to room temperature with the constant voltage. The voltage was removed after the temperature of the glass sample was decreased to the room temperature. It should be noted that the actual voltage applied to the glass sample was less than 3 kV because of the use of borosilicate glass plates as mentioned above.

1.2.2.2 Characterization

The second-harmonic intensity of poled glass samples was measured using Maker fringe method. A setup for SHG measurement is illustrated schematically in Fig. 1.2. The intensity of second-harmonic wave from

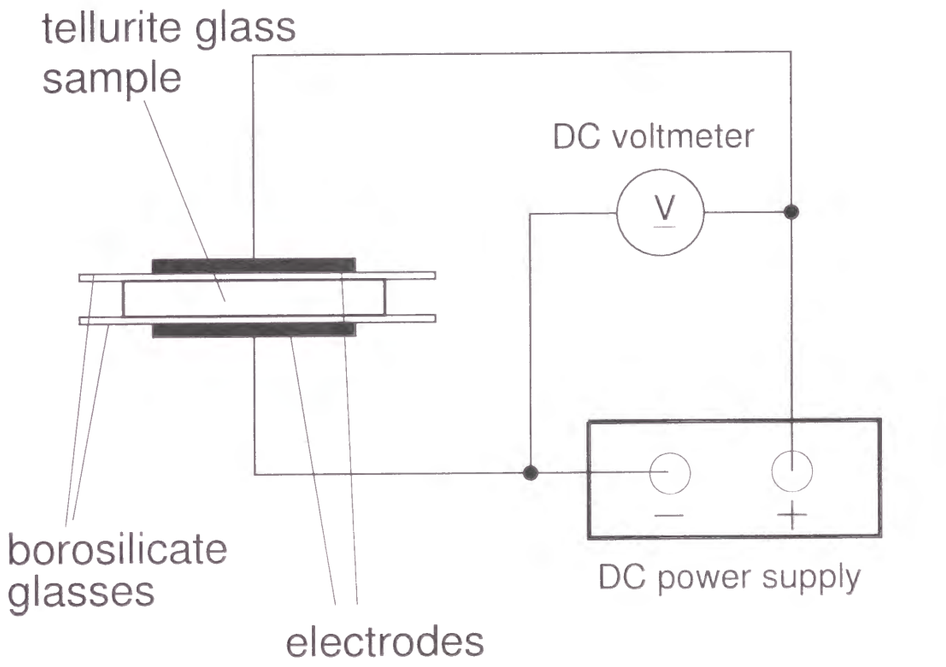

Fig. 1.1: Apparatus for poling the tellurite glass sample.

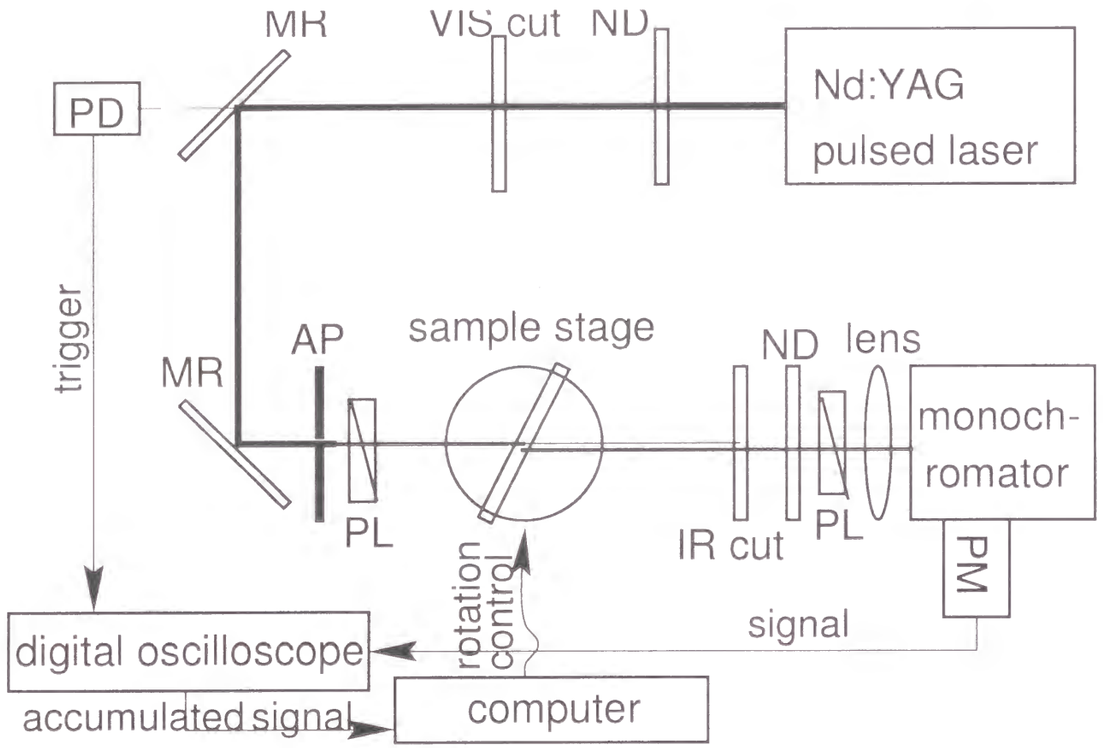

Fig. 1.2: Schematic illustration of equipment for second-harmonic generation measurements. The second-harmonic wave is detected with a photomultiplier tube after the elimination of fundamental wave by using an IR cut filter and a monochromator. The meanings of abbreviations are as follows. ND: ND filter; VIS cut: VIS cut filter; MR: mirror; AP: aperture; PL: polarizer; IR cut: IR cut filter; and PM: photomultiplier.

poled glass sample was measured using a pulsed Nd:YAG laser (Spectra Physics. GCR-11) which operated in a Q-switched mode with a 10 Hz repetition rate. After the pulse at 1064 nm with 9 ns duration was p-polarized. it was incident on the sample which was rotated around an axis perpendicular to the incident plane so that angle of incidence varied from $-65°$ to $65°$. The output light from the poled glass sample was passed through both an IR cut filter and a monochromator (Spex. 270M) to eliminate the fundamental wave at 1064 nm completely. The p-polarized second-harmonic wave was passed through a monochromator (Spex. 270M) and detected with a photomultiplier (Hamamatsu Photonics. R955). The signal from the photomultiplier was accumulated using a digital oscilloscope (Hewlett Packard 54522A). For the determination of input light power. Y-cut quartz with thickness of 1.046 mm and $d_{11} = 0.34$ pm/V was used as a reference material under the condition of p-excitation and p-detection.

X-ray diffraction measurements were carried out for both as-annealed and poled glasses with CuKα radiation (Rigaku. RAD-C). For each surface of bulk sample. the diffraction angle was scanned from $2\theta = 10$ to $70°$ at an interval of $0.05°$. The scan speed was $2°$/min.

Refractive indices at 532 and 1064 nm were measured using an ellipsometer (Yokojiri. DVA-36VW) for poled glass samples to estimate second-order nonlinear coefficient.

Table 1.2: Glass composition, glass transition temperature and optimum poling temperature of Na_2O-ZnO-TeO_2 glasses.

Glass composition (mol%)	Glass transition temperature (°C)	Optimum poling temperature (°C)
$30NaO_{\frac{1}{2}}\cdot 70TeO_2$	250	225
$10NaO_{\frac{1}{2}}\cdot 20ZnO\cdot 70TeO_2$	300	260
$30ZnO\cdot 70TeO_2$	326	280

1.2.3 Results

Table 1.2 shows glass transition temperatures of Na_2O-ZnO-TeO_2 glasses. The glass transition temperature increases with a replacement of Na by Zn. The variation of second-harmonic intensity with angle of incidence for $30NaO_{\frac{1}{2}}\cdot 70TeO_2$ glass poled at 220 °C with 3 kV is shown in Fig. 1.3. The Maker fringe pattern is observed, although minimum values of intensity are not zero in contrast with the theory of Maker fringe. For $30NaO_{\frac{1}{2}}\cdot 70TeO_2$ glass poled at 225 °C, the dependence of second-harmonic intensity on incident angle is plotted in Fig. 1.4. When the anode-side surface of this glass was etched mechanically with about 30 μm, the second-harmonic generation disappered, which indicates that the origin of SHG exists in thin layer near the anode-side surface. In this figure, the solid curve is a theoretical one drawn by using the refractive indices shown in Table 1.3 and by assuming that the poled region is 28 μm. This value, 28 μm, is coincident with the fact that the mechanical etching of 30 μm of anode-side glass surface makes the second-harmonic wave disappear. The agreement between the experimental data and theoretical curve is rather good. From this analysis, $d_{33} = 0.082$ pm/V is obtained. Figure 1.5 shows the dependence of second-harmonic intensity on angle of incidence for $30ZnO\cdot 70TeO_2$ glass poled at 280 °C. The solid circles denote experimental result, and the solid curve represents theoretical one drawn with $L = 27\,\mu$m and $d_{33} = 0.45$ pm/V, where L is the length of poled region. The values of d_{33} thus obtained are summarized in Table 1.3.

Table 1.3: Refractive indices at 532 and 1064 nm (n_{532} and n_{1064}) and d_{33} values of poled Na_2O-ZnO-TeO_2 glasses. Each glass was poled at the optimum poling temperature listed in Table 1.2.

Glass composition	n_{532}	n_{1064}	d_{33} (pm/V)
$30NaO_{\frac{1}{2}}\cdot 70TeO_2$	2.00	1.95	0.082
$10NaO_{\frac{1}{2}}\cdot 20ZnO\cdot 70TeO_2$	2.02	1.97	0.23
$30ZnO\cdot 70TeO_2$	2.05	2.00	0.45

The variation of second-harmonic intensity with poling temperature for $30NaO_{\frac{1}{2}}\cdot 70TeO_2$ glass is shown in Fig. 1.6. The second-harmonic intensity exhibits a maximum at 225 °C which is 25 °C below the glass transition temperature. In other words, the optimum poling temperature is 225 °C. Figure 1.7 shows the variation of second-harmonic intensity with poling temperature for $10NaO_{\frac{1}{2}}\cdot 20ZnO\cdot 70TeO_2$ glass. This glass manifests a maximum of second-harmonic intensity as well and the optimum poling temperature is 260 °C. The optimum poling temperature of the Na_2O-ZnO-TeO_2 glasses are summarized in Table 1.2.

In poled $30NaO_{\frac{1}{2}}\cdot 70TeO_2$ glasses, devitrification was observed at the anode-side glass surface. Figure 1.8 shows X-ray diffraction patterns of as-annealed glass sample and the anode-side surface of poled glass samples with $30NaO_{\frac{1}{2}}\cdot 70TeO_2$ composition. Two peaks at around $2\theta = 18.4°$ and 27.7° can be assigned to Te_4O_9 and TeO_2 crystals, respectively. This fact clearly indicates that some electrochemical reactions occurred at interface between anode and glass surface and these reactions become vigorous when the poling temperature is increased.

1.2.4 Discussion

As for the poled silica glasses, the initial stage of poling is considered to be due to a migration of cations such as Na^+, as suggested by Myers *et al.* [13]. The migration of cations leaves thin space charge layer near the anode, and the external voltage drops drastically in this region. In other words, a large electric field is applied to the thin layer in the glass near the anode. This large electric field is frozen in the anode-side surface region of the glass, leading to the second-harmonic generation. This phenomenon

can also take place in the tellurite glasses containing mobile cations such as Na^+ and Zn^{2+}. The electric dipoles created as a result of pairing of these mobile cations with non-bridging oxide ions can contribute to the second-harmonic generation. Additionally, it is speculated that, in the vicinity of

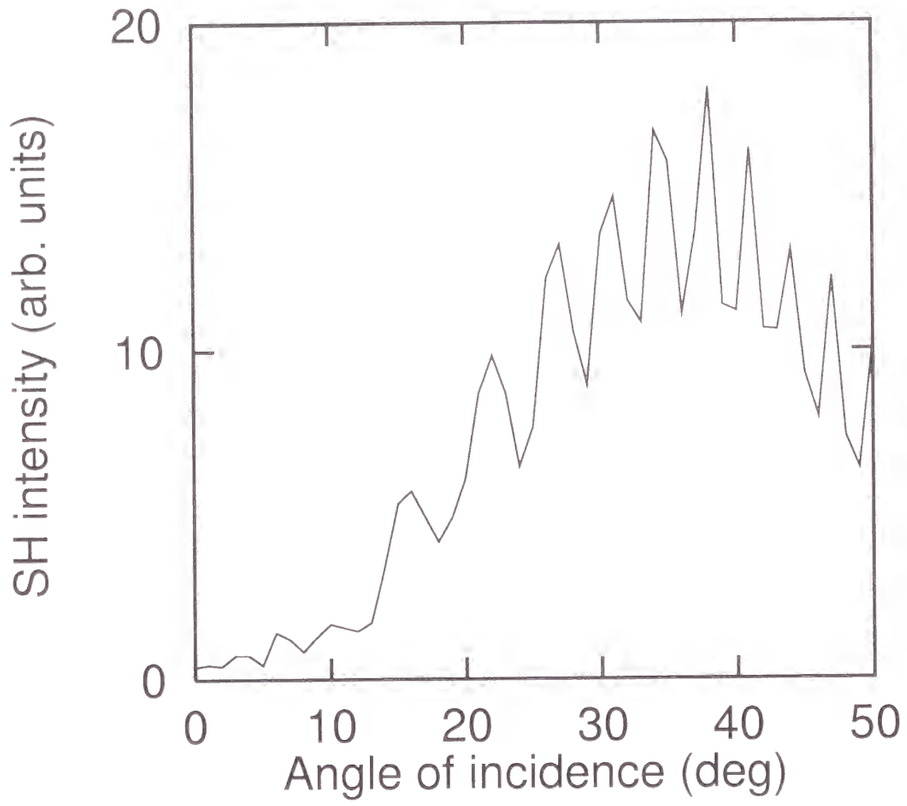

Fig. 1.3: Maker fringe pattern of $30NaO_{\frac{1}{2}}{\cdot}70TeO_2$ glass poled at 220 °C with 3 kV.

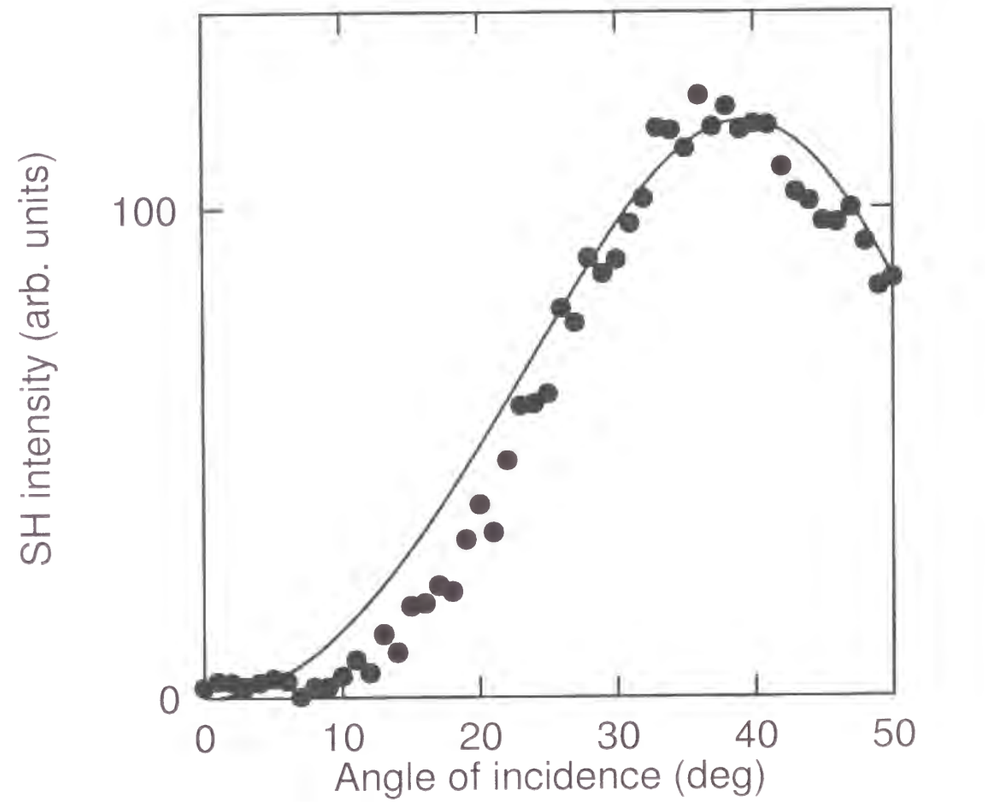

Fig. 1.4: Maker fringe pattern of $30NaO_{\frac{1}{2}}{\cdot}70TeO_2$ glass poled at 225 °C with 3 kV. The circles denote the fringe pattern obtained experimentally. The solid curve represents the theoretical fringe pattern drawn with $d_{33} = 0.082$ pm/V, $L = 28\mu$m, $n_{532} = 2.00$ and $n_{1064} = 1.95$.

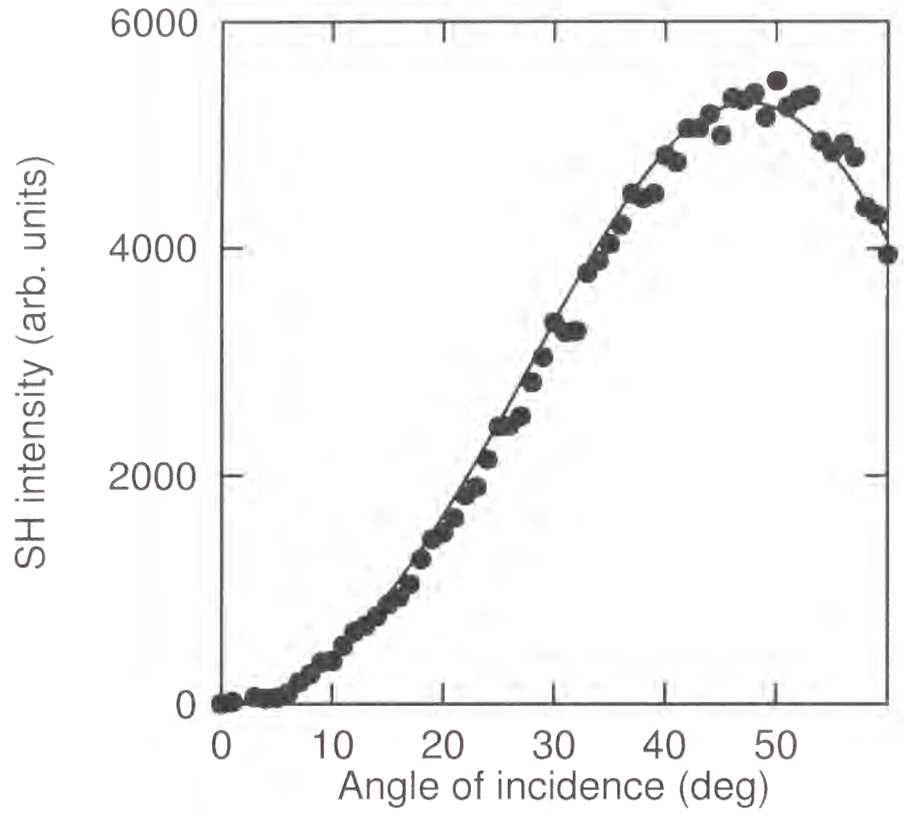

Fig. 1.5: Maker fringe pattern of $30ZnO{\cdot}70TeO_2$ glass poled at 280 °C with 3 kV. The circles and solid curve denote the experimental and theoretical Maker fringe patterns. respectively. The theoretical one was drawn with $d_{33} = 0.45$ pm/V, $L = 27\mu$m, $n_{532} = 2.05$ and $n_{1064} = 2.00$.

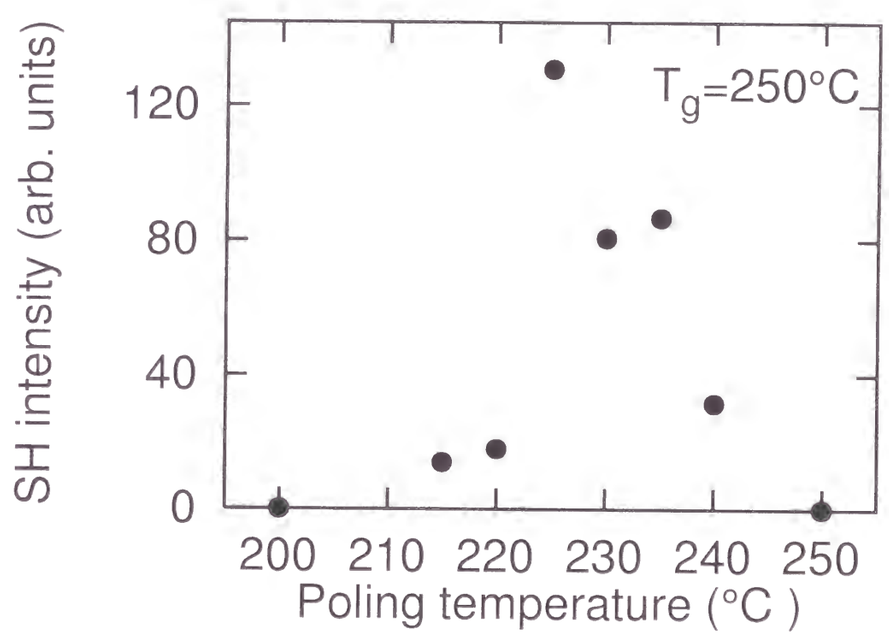

Fig. 1.6: Poling temperature dependence of second-harmonic intensity for $30NaO_{\frac{1}{2}}{\cdot}70TeO_2$ glass poled with 3 kV for 20 min.

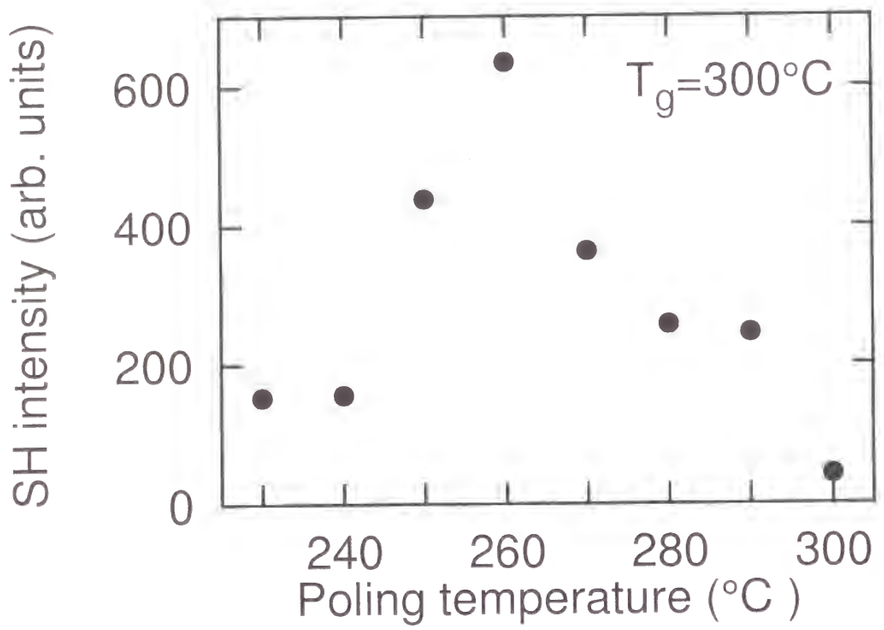

Fig. 1.7: Poling temperature dependence of second-harmonic intensity for $10NaO_{\frac{1}{2}}{\cdot}20ZnO{\cdot}70TeO_2$ glass poled with 3 kV for 20 min.

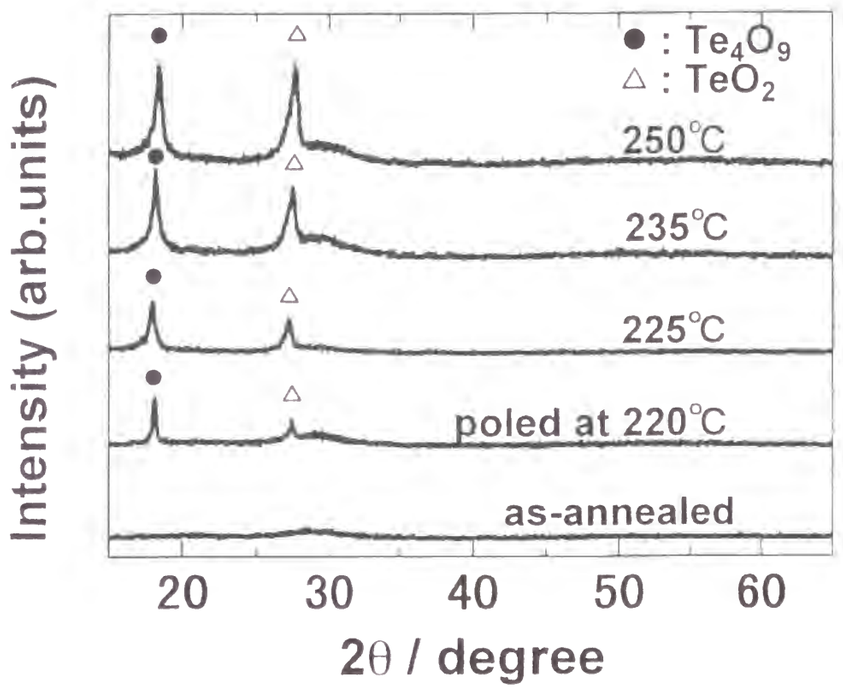

Fig. 1.8: X-ray diffraction patterns of as-annealed and poled $30NaO_{\frac{1}{2}}{\cdot}70TeO_2$ glasses. The surfaces of bulk glasses were examined in these measurements. It should be noted that for poled glasses devitrification was observed only in the anode-side surface. The circle and triangle denote the diffraction lines of Te_4O_9 and TeO_2 crystals, respectively.

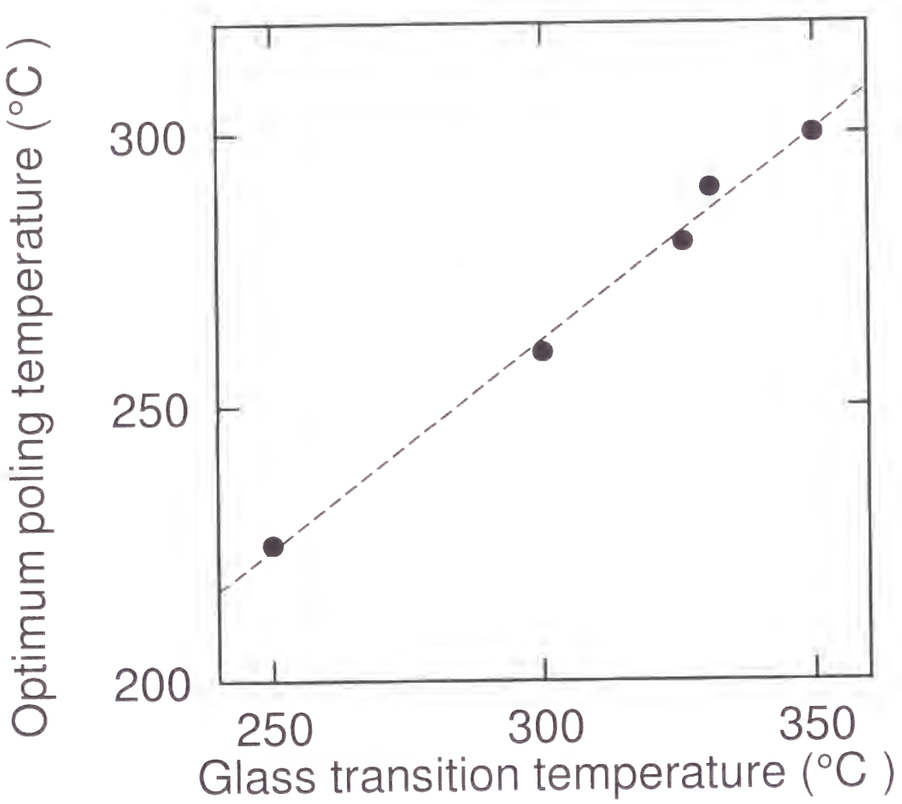

Fig. 1.9: Relation between optimum poling temperature and glass transition temperature observed in Na_2O-ZnO-TeO_2 and MgO-ZnO-TeO_2 glass systems. The broken line was drawn by a least square method.

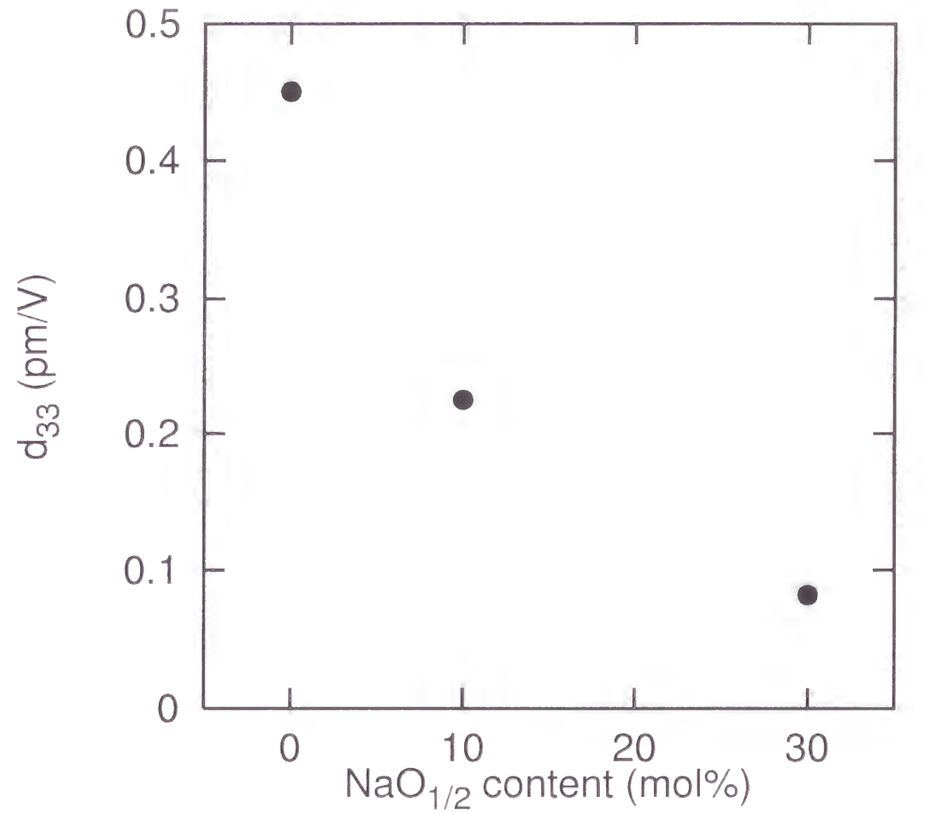

Fig. 1.10: Compositional dependence of second-order nonlinear optical coefficient for $x$$NaO_{1/2}$·(30-$x$)ZnO·70$TeO_2$ glasses (x =0, 10, 30) poled at the optimum poling temperature with 3 kV.

the glass transition temperature, the induced large electric field leads to an orientation of asymmetrical tellurite structural units such as TeO_4 trigonal bipyramid and TeO_3 trigonal pyramid which possess electric dipoles. Further experiments, however, are needed to ascertain this possibility.

Similarly to MgO-ZnO-TeO_2 glass system [14,15], the Na_2O-ZnO-TeO_2 glasses show a peculiar dependence of second-harmonic intensity on poling temperature; both systems possess optimum poling temperatures. Namely, the second-harmonic intensity increases as the poling temperature increases up to the optimum poling temperature and become almost zero when the poling temperature is close to the glass transition temperature. The increase in second-harmonic intensity with an increase in poling temperature below the optimum poling temperature can be naturally attributed to the increase in the mobility of cations, which form larger electric dipoles.

Figure 1.9 shows the relationship between optimum poling temperature and glass transition temperature for both the MgO-ZnO-TeO_2 and Na_2O-ZnO-TeO_2 glasses. The optimum poling temperature is proportional to the glass transition temperature. This linear relation between them implies that the formation of electric dipoles is influenced by the structural relaxation around the glass transition temperature. Based on these results, two types of possible mechanisms exist. One of them is the effect of thermal fluctuation on the orientation of electric dipoles works more efficiently at higher temperature. Another possible explanation is some electrochemical reactions between glass surfaces and electrodes at elevated temperatures, which decrease the origin of SHG. As shown in Fig. 1.8, the precipitation of Te_4O_9 and TeO_2 crystalline phases was observed at the anode-side surface, suggesting the some oxidation reactions take place irreversibly. Besides, it was also found that the crystallization becomes vigorous with raising poling temperature. Such oxidation reactions possibly reduce the space charge built near the anode-side surface. Therefore, the decrease in second-harmonic intensity near the glass transition temperature, that is, the existence of optimum poling temperature is attributable to the some oxidation reactions.

For Na_2O-ZnO-TeO_2 glass system, the maximum second-order nonlinear optical coefficients are listed in Fig. 1.10. The second-order nonlinear coefficient increases as a function of the concentrational ratio of ZnO to Na_2O. This was explained by considering the electrochemical reactions such as crystallization, which becomes more remarkable with increasing the Na_2O content.

1.2.5 Conclusions

The second-harmonic intensity was measured using the Maker fringe method for Na_2O-ZnO-TeO_2 glass system. The similar dependence of second-harmonic intensity on the poling temperature was observed in the Na_2O-ZnO-TeO_2 glasses as well as MgO-ZnO-TeO_2 glasses; the second-harmonic intensity increased, made a maximum and then decreased with raising poling temperature. This decrease is attributable to some electrochemical reactions at the anode-side surface, which break up the frozen electric field and diminish the second-harmonic generation near the glass transition temperature. It was also revealed that the optimum poling temperature, where the maximum second-harmonic intensity was attained, is proportional to the glass transition temperature.

1.3 Effect of glass composition on second-harmonic generation in Li_2O-Na_2O-TeO_2 glasses

1.3.1 Introduction

As described in Chapter 1.2, the second-order nonlinearity significantly depends on poling temperature for poled tellurite glasses containing ZnO, MgO, and Na_2O; all the glasses exhibited the optimum poling temperatures which are defined as a temperature giving rise to a maximum second-harmonic intensity. Myers *et al.* [16] examined poling temperature depen-

dence of second-harmonic intensity for silica glass and found a similar phenomenon that the second-harmonic intensity increases, shows a maximum, and then decreases with an increase in the poling temperature. Besides, it was revealed for tellurite glasses that the optimum poling temperature is proportional to the glass transition temperature. This is interesting because it suggests that the process of the breakdown of macroscopic inversion symmetry in tellurite glasses is connected with structural relaxation in the glass transition range. Further investigation on the linear relation between the optimum poling temperature and glass transition temperature is made by an application of the Maker fringe theory in Chapter 2.1.

On the other hand, glass compositions as well as poling conditions possibly affect the nonlinear susceptibility with second-order of glass materials. For instance, in the Na_2O-ZnO-TeO_2 glass system, the substitution of ZnO for $NaO_{1/2}$ increased the second-order nonlinear coefficient at their optimum poling temperatures. This was explained by considering the electrochemical reactions such as crystallization, which becomes more remarkable with increasing the Na_2O content. In other words, the lower thermal stability of glass brings about more vigorous crystallization, resulting in a decrease of second-order nonlinearity.

In this work, the compositional dependence of second-harmonic generation is examined for Li_2O-Na_2O-TeO_2 glass system. Komatsu *et al.* reported that $10Li_2O{\cdot}10Na_2O{\cdot}80TeO_2$ glass showed higher thermal stability than $20R_2O{\cdot}80TeO_2$ glasses (R = Li, Na) because of the so-called mixed alkali effect [17]. This fact enables us to study the effect of thermal stability of glass on the second-harmonic generation. In addition, it is shown that the above-described proportional relationship between optimum poling temperature and glass transition temperature also holds for lithium sodium tellurite glass.

1.3.2 Experimental procedure

Glass was prepared from reagent-grade Li_2CO_3, Na_2CO_3 and TeO_2 powders as starting materials. The raw materials were mixed thoroughly to make $10Li_2O{\cdot}10Na_2O{\cdot}80TeO_2$ composition, and melted in air at 850 °C for 30 min using a platinum crucible. The melt was poured onto a stainless steel plate to obtain glass. The resultant glass was annealed at around glass transition temperature determined by means of differential scanning calorimetry (Rigaku, DSC-8230B), and cut into a rectangular parallelepiped of about 7 mm x 7 mm x 1 mm using a saw pasted with diamond powders. After the glass surfaces were polished, the plate-like glass was sandwiched in between two commercial borosilicate glass plates and was directly brought into contact with electrodes made of stainless steel. Then, the glass sample was poled at several temperatures for 20 min with 3 kV. If the tellurite glass sample was directly sandwiched in between the electrodes made of stainless steel, some black precipitates were observed in the glass after the poling. Presumably, an electric discharge took place in thin air layer between cathode and tellurite glass surface to cause some oxidation-reduction reactions as well as an increase in temperature of the tellurite glass surface, resulting in the precipitation from the glass; the air layer is present when the tellurite glass sample is directly brought into contact with the electrodes, because of the roughness of tellurite glass surface. It should be noted that the actual voltage applied to the tellurite glass sample is smaller than 3 kV because the borosilicate glass plates are inserted.

The second-harmonic intensity of the glass samples was measured just after the poling by utilizing Maker fringe method [18]. The incident light was a *p*-polarized fundamental wave of a pulsed Nd:YAG laser (Spectra Physics, GCR-11); the wavelength was 1064 nm. The *p*-polarized second-harmonic wave with 532 nm was passed through a monochromator (Spex. 270M), and detected by means of a photomultiplier (Hamamatsu Photonics, R955). The output signals were detected and counted by using a digital oscilloscope (Hewlett Packard, 54522A).

1.3.3 Results and discussion

Figure 1.11 shows the DSC patterns for both the $10Li_2O{\cdot}10Na_2O{\cdot}80TeO_2$ and $18Na_2O{\cdot}82TeO_2$ ($30NaO_{\frac{1}{2}}{\cdot}70TeO_2$) glasses. Whereas an endothermic peak due to glass transition appears in both curves, an exothermic peak due to a crystallization is observed only for the $18Na_2O{\cdot}82TeO_2$ glass. The exothermic peak at about 450 °C in the DSC curve of $18Na_2O{\cdot}82TeO_2$ glass is ascribable to crystallization. Namely, a crystallization does not take place in the $10Li_2O{\cdot}10Na_2O{\cdot}80TeO_2$ glass when the heating temperature is below 450 °C. In other words, thermal stability of $10Li_2O{\cdot}10Na_2O{\cdot}80TeO_2$ glass is higher than that of $18Na_2O{\cdot}82TeO_2$ glass. This result is coincident with thermal analysis data reported by Komatsu *et al* [17]. The glass transition temperature of $18Na_2O{\cdot}82TeO_2$ glass, i.e., 255 °C, is somewhat higher than the value reported previously, that is, 250 °C, due to the difference in method to evaluate the glass transition temperature. The previous value was obtained by means of differential thermal analysis (DTA).

The variation of second-harmonic intensity with angle of incidence is shown in Fig. 1.12 for $10Li_2O{\cdot}10Na_2O{\cdot}80TeO_2$ glass poled at 220 °C. The Maker fringe pattern is ambiguous, indicating that the length of poled region is shorter than the coherence length. This fact suggests that the efficiently poled region is restricted near the anode-side glass surface [13]. The initial stage of the poling is a migration of mobile cations such as Li^+ and Na^+ ions. Since the migration of these ions leaves negative charges due to non-bridging oxide ions in the glass surface region, a space charge layer is formed in the vicinity of the anode-side glass surface. This layer is composed of cations such as Li^+ and Na^+ and oxide ions which are separated from each other in direction of the external electric field. In addition, such a situation leads to a large electric field near the anode-side surface [19]. It is possible that this very large electric field causes orientation of TeO_4 and TeO_3 tellurite structural units with non-bridging oxygen which possess permanent electric dipoles. The breakdown of macroscopic inversion symmetry is brought about by the creation of space charge layer and/or the orientation of tellurite structural units. The former is a major contribution.

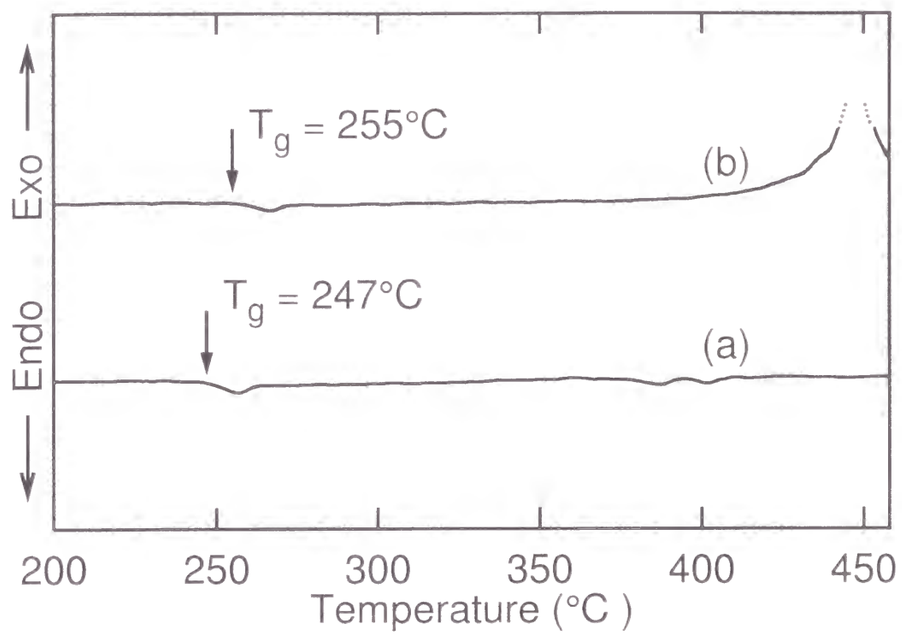

Fig. 1.11: Differential scanning calorimetry curves of (a) $10Li_2O{\cdot}10Na_2O{\cdot}80TeO_2$ glass and (b) $18Na_2O{\cdot}82TeO_2$ glass.

The poling temperature dependence of second-harmonic intensity for $10Li_2O{\cdot}10Na_2O{\cdot}80TeO_2$ glass is shown in Fig. 1.13 (a). The second-harmonic intensity increases, takes a maximum, and then decreases with an increase in the poling temperature. The poling temperature corresponding to the maximum second-harmonic intensity, i.e., the optimum poling temperature, is 220 °C. The optimum poling temperatures are plotted as a function of glass transition temperature for several kinds of tellurite glasses involving the $10Li_2O{\cdot}10Na_2O{\cdot}80TeO_2$ glass in Fig. 1.14. A linear relationship is observed between optimum poling temperature and glass transition temperature irrespective of the glass composition. One possible mechanism for

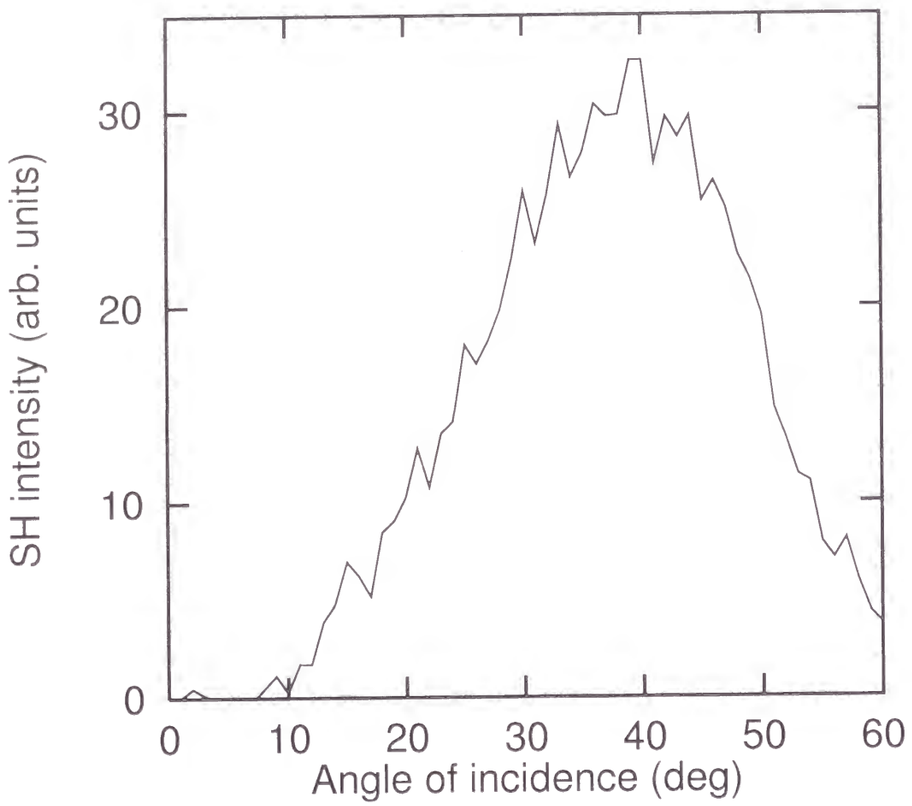

Fig. 1.12: Variation of second-harmonic intensity with angle of incidence for $10Li_2O{\cdot}10Na_2O{\cdot}80TeO_2$ glass poled at 220 °C for 20 min.

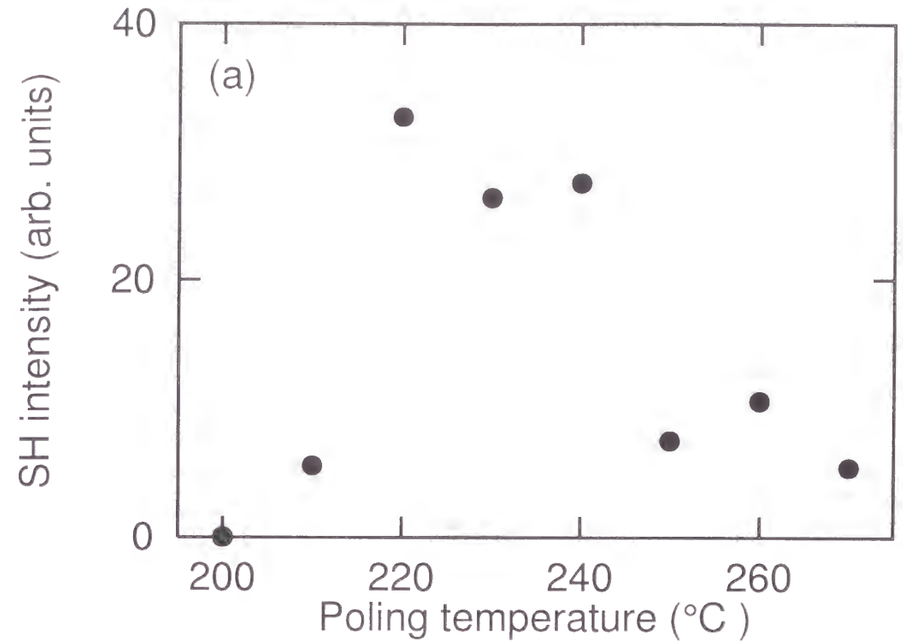

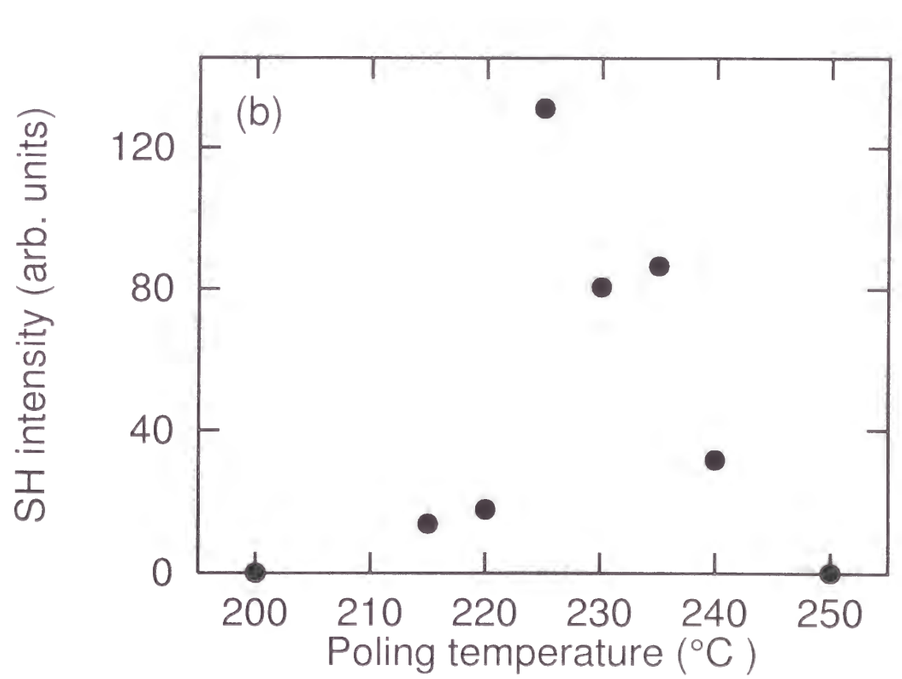

Fig. 1.13: Poling temperature dependence of second-harmonic intensity for (a) $10Li_2O{\cdot}10Na_2O{\cdot}80TeO_2$ glass and (b) $18Na_2O{\cdot}82TeO_2$ glass poled with 3 kV.

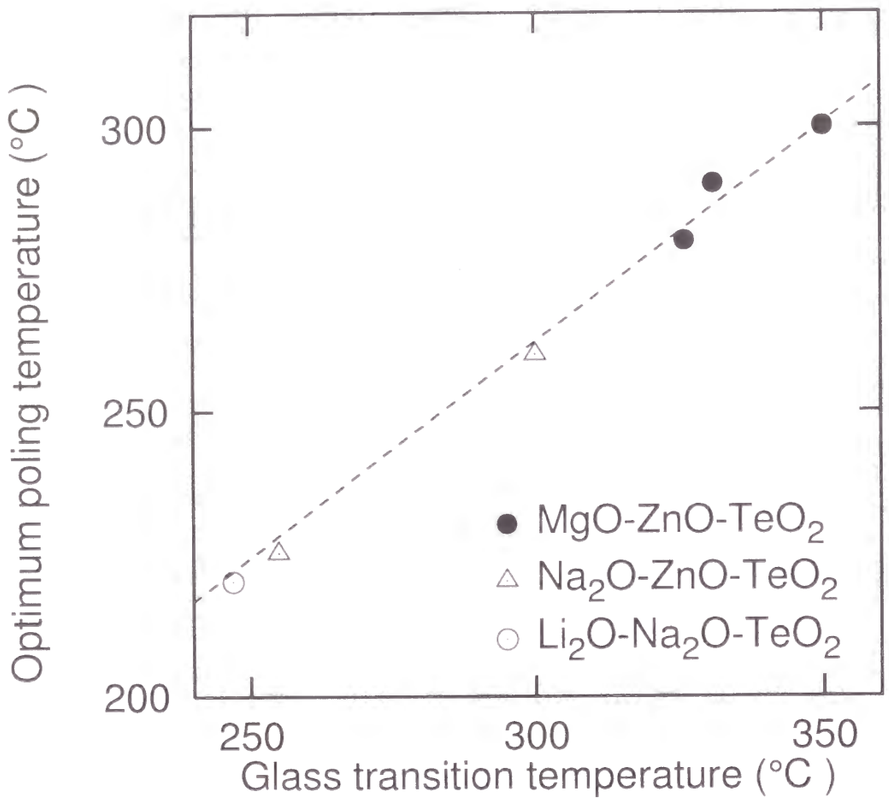

Fig. 1.14: Relation between glass transition temperature and optimum poling temperature for tellurite glasses including 10Li2O·10Na2O·80TeO2 glass. The datum for the 10Li2O·10Na2O·80TeO2 glass is indicated by an open circle.

the decrease in the second-harmonic intensity with an increase in the poling temperature near the glass transition temperature is migration of oxide ions. Carlson et al. [20] found that when a soda lime silicate glass is poled at its annealing temperature with 100 V/3 mm in vacuum (10^{-6} mmHg), oxide ions move to the anode, so that oxygen molecules are evolved. A similar phenomenon may occur in the present tellurite glasses to reduce the electric field in the space charge layer when the poling temperature is close to the glass transition temperature. Consequently, the optimum temperature which is relevant to the glass transition temperature exists. Nevertheless, further experiments are required to demonstrate this assumption. In Fig. 1.13 the poling temperature dependence of second-harmonic intensity for $18Na_2O{\cdot}82TeO_2$ glass reported previously is also shown for comparison. Whereas the second-harmonic intensity is zero for the $18Na_2O{\cdot}82TeO_2$ glass poled just around the glass transition temperature, the second-harmonic generation is still observed in the $10Li_2O{\cdot}10Na_2O{\cdot}80TeO_2$ glasses poled at temperatures higher than the glass transition temperature. This phenomenon can be connected with the thermal stability of these glasses. As found in Fig. 1.11, the $10Li_2O{\cdot}10Na_2O{\cdot}80TeO_2$ glass is more stable against heat than the $18Na_2O{\cdot}82TeO_2$ glass. It is speculated that the migration of oxide ions at high temperatures, which reduces the second-harmonic intensity, is suppressed in the $10Li_2O{\cdot}10Na_2O{\cdot}80TeO_2$ glass because of its high thermal stability.

1.3.4 Conclusions

The poling temperature dependence of second-harmonic intensity for $10Li_2O{\cdot}10Na_2O{\cdot}80TeO_2$ glass exhibits an optimum poling temperature which gives a maximum second-harmonic intensity. The linear relationship between optimum poling temperature and glass transition temperature observed for tellurite glasses containing Na_2O, MgO and ZnO holds for the present tellurite glasses containing both Li_2O and Na_2O as well. Thus, we

conclude that the structural relaxation in the glass transition range affects the process to break the inversion symmetry in these tellurite glasses. The thermal stability of the glasses also has an influence on the poling temperature dependence of second-harmonic intensity. The $10Li_2O{\cdot}10Na_2O{\cdot}80TeO_2$ glass shows higher thermal stability than $18Na_2O{\cdot}82TeO_2$ glass as revealed from the DSC measurements. Subsequently, the temperature range within which the poling is effective is wider for the $10Li_2O{\cdot}10Na_2O{\cdot}80TeO_2$ glass than for the $18Na_2O{\cdot}82TeO_2$ glass.

References

[1] J. Jerphagnon and S. K. Kurtz, J. Appl. Phys. **41**, 1667 (1970).

[2] D. A. Kleinman, Phys. Rev. **126**, 1977 (1962).

[3] K. D. Singer, M. G. Kuzyk, and J. E. Sohn, J. Opt. Soc. Am. **4**, 968 (1987).

[4] H. Nasu, H. Okamoto, A. Mito, J. Matsuoka, and K. Kamiya, Jpn. J. Appl. Phys. **32**, L406 (1993).

[5] A. Okada, K. Ishii, K. Mito, and K. Sasaki, Appl. Phys. Lett. **60**, 2853 (1992).

[6] P. G. Kazansky, L. Dong, and P. S. J. Russell, Electron. Lett. **30**, 1345 (1994).

[7] O. Sugihara, T. Hirama, H. Fujimura, and N. Okamoto, Opt. Rev. **3**, 150 (1996).

[8] H. Takebe, P. G. Kazansky, and P. S. J. Russell, Opt. Lett. **21**, 468 (1996).

[9] K. Tanaka, K. Kashima, K. Hirao, N. Soga, A. Mito, and H. Nasu, Jpn. J. Appl. Phys. **32**, L843 (1993).

[10] K. Tanaka, K. Kashima, K. Kajihara, K. Hirao, N. Soga, A. Mito, and H. Nasu, Proc. SPIE **2289**, 167 (1994).

[11] K. Tanaka, K. Kashima, K. Hirao, N. Soga, A. Mito, and H. Nasu, J. Non-Cryst. Solids **185**, 123 (1995).

[12] R. A. Myers, X. Long, and S. R. J. Brueck, SPIE **2289**, 98 (1994).

[13] R. A. Myers, N. Mukherjee, and S. R. J. Brueck, Opt. Lett. **16**, 1732 (1991).

[14] K. Tanaka, A. Narazaki, K. Hirao, and N. Soga, J. Appl. Phys. **79**, 3798 (1996).

[15] K. Tanaka, A. Narazaki, K. Hirao, and N. Soga, J. Non-Cryst. Solids **203**, 49 (1996).

[16] R. A. Myers, X. Long, and S. R. J. Brueck, Proc. SPIE **2289**, 98 (1994).

[17] T. Komatsu, R. Ike, R. Sato, and K. Matusita, Phys. Chem. Glasses **36**, 216 (1995).

[18] P. D. Maker, R. W. Terhune, M. Nisenoff, and C. M. Savage, Phys. Rev. Lett. **8**, 21 (1962).

[19] T. M. Proctor and P. M. Sutton, J. Am. Ceram. Soc. **43**, 173 (1960).

[20] D. E. Carlson, K. W. Hang, and G. F. Stockdale, J. Am. Ceram. Soc. **55**, 337 (1972).

Chapter 2

Realization of long relaxation time and large second-order nonlinearity in poled tellurite glasses

2.1 Induction of second-order nonlinearity with long decay time in ZnO-TeO_2 glass

2.1.1 Introduction

Some interesting characteristics of second-harmonic generation in poled tellurite glasses were revealed in Chapter 1. With an increase in poling temperature, the second-harmonic intensity increases, takes a maximum value, and decreases. It was also found that the poling temperature corresponding to the highest second harmonic intensity, namely, optimum poling temperature, is proportional to the glass transition temperature. The close relation between the optimum poling temperature and the glass transition temperature indicates an intrinsic mechanism for inducing the second-order nonlinearity in tellurite glass systems. Besides, it can be suggested that the tellurite glass network structure containing non-bridging oxygens with negative charge takes part in a process which decreases the second-harmonic intensity in the vicinity of the glass transition temperature. This is a striking result from the conventional standpoints that the glass network is rigid enough to prevent the ionic conduction of non-

bridging oxygen as well as its viscous flow below the glass transition temperature. In the present chapter, further efforts are made to exploit the peculiar dependence of second-harmonic intensity on the poling temperature; the two-step poling procedure which informs the reversibility of the decrease in second-harmonic intensity just below the glass-transition temperature. Moreover, the long lifetime of second-order nonlinearity is realized in ZnO-TeO_2 glass system in addition to an attempt for achieving large second-order nonlinear susceptibility in WO_3-TeO_2 glasses.

Optical second-order nonlinearity observed in poled glass materials is a subject of great interest from both fundamental and practical standpoints. The fundamental interest finds its origin in the fact that a disappearance of inversion symmetry is induced in a disordered system such as glass and is frozen even after a high voltage is removed. From a practical viewpoint, the poled glasses will be useful as a frequency doubler of light and a linear electro-optical device. Since the discovery of second-harmonic generation in poled silica glass by Myers *et al.* [1], the silica-based glasses have been investigated most extensively [2 -8]. Tellurite glass is also known to exhibit second-harmonic generation when the thermal poling is carried out [9 15]. A peculiar point of tellurite glass is its low glass transition temperature, which is very close to the poling temperature. This fact enables us to analyze in detail a change of glass structure in the vicinity of the glass transition temperature under an applied high voltage. In this section, the second-harmonic generation in $30ZnO{\cdot}70TeO_2$ glass with a two-step poling procedure is investigated for the purpose of the clarification of the cause for the decrease in second-harmonic intensity just below the glass transition temperature. The two-step poling procedure gives us a new sight for the induction mechanism of second-harmonic generation. The relaxation behavior of second-harmonic intensity is also examined at room temperature in $30ZnO{\cdot}70TeO_2$ and $30NaO_{\frac{1}{2}}{\cdot}70TeO_2$ glasses, and discussed the difference in relaxation behavior between these two systems in the light of the mobility of Na^+ and Zn^{2+} ions. As a result, in ZnO-TeO_2 glass system, the second-order nonlinearity with long decay time is attained.

2.1.2 Experimental procedure

2.1.2.1 Sample preparation

Glass samples were prepared from ZnO, Na_2CO_3 and TeO_2. The purity of these raw materials was 99, 99.5 and 99 %, respectively. The powders of the raw materials were mixed thoroughly to make $30ZnO{\cdot}70TeO_2$ and $30NaO_{\frac{1}{2}}{\cdot}70TeO_2$ compositions and melted in a platinum crucible at 850 to 900 °C for 20 min in air. The melt was rapidly cooled by pouring onto an alumina plate to obtain glass. The glass transition temperature was measured using differential thermal analysis (Rigaku, TG-DTA8112BH). After the glass was annealed at around the glass transition temperature for 20 min, it was cut into a plate. Both surfaces of the plate-like glass were polished for measurements of second-harmonic generation. The resultant glass specimen had a thickness of 1.00 mm.

Poling of the glass sample was performed as follows. The glass sample was sandwiched in between two commercial borosilicate glass plates with a thickness of 0.15 mm and contacted physically with electrodes made of stainless steel. The glass sample sandwiched in the electrodes was put into an electric furnace and held at an aimed temperature for 30 min. After the voltage of 3 kV was applied for 20 min at the temperature, the glass sample was taken out from the furnace and kept at room temperature for 60 min with the constant voltage applied. In addition to the above-described poling, the two-step poling treatment was carried out for the $30ZnO{\cdot}70TeO_2$ glass. Under the constant voltage of 3 kV, the glass sample was heated at 300 °C for 20 min in the first step and succeedingly heated at 280 °C for 20 min in the second step. Then, it was quenched to the room temperature with the constant voltage. It should be noted that the actual voltage applied to the glass sample was less than 3 kV because of the use of borosilicate glass plates. The actual voltage applied to the sample was estimated to be 1.7 kV, when the dielectric constants of $30ZnO{\cdot}70TeO_2$ and

borosilicate glasses were assumed to be 21 [16] and 7.9 [17], respectively.

2.1.2.2 Optical measurements

Second-harmonic generation of the poled glass samples was measured using Maker fringe method. A pulsed Nd:YAG laser (Spectra Physics, GCR-11), which operated in a Q-switched mode with a 10 Hz repetition rate, was used as a light source. After the pulse at 1064 nm with 9 ns duration was p-polarized, it was incident on the sample at $-65°$ to $65°$. The beam diameter was about 1 mm. The output light from the poled glass sample was passed through both IR cut filters and a monochromator (Spex, 270M) to eliminate the fundamental wave at 1064 nm completely. The second-harmonic wave at 532 nm thus obtained was detected with a photomultiplier (Hamamatsu Photonics, R955). The signal from the photomultiplier was integrated by using a digital oscilloscope (Hewlett Packard 54522A). The second-harmonic intensity from a Y-cut quartz with a thickness of 1.046mm and $d_{11} = 0.34$ pm/V was also measured for the purpose of determining input light power and calculating second-order nonlinear optical coefficient of the samples.

Refractive indices at 532 and 1064 nm were measured using an ellipsometer (Yokojiri, DVA-36VW) for the $30ZnO{\cdot}70TeO_2$ glass poled at 280 °C to estimate second-order nonlinear coefficient.

2.1.3 Results

Figure 2.1 shows the dependence of second-harmonic intensity on poling temperature for $30ZnO{\cdot}70TeO_2$ glass with an accuracy of $\pm 10\%$. The closed circles denote the second-harmonic intensity for the glasses poled at the specified temperatures for 20 min, whereas the closed triangle represents the intensity for the glass treated with two-step poling procedure. As found from the results of one-step poling (closed circles), a maximum clearly appears at 280 °C, which corresponds to an optimum poling temperature. The second-harmonic intensity for the glass poled in two steps is

almost the same as the intensity obtained for the glass poled at 300 °C, and much lower than for the glass poled at the optimum poling temperature equal to 280 °C. Namely, the change to cause the decrease in second-harmonic intensity just below the glass transition temperature is an irreversible process.

The variation of second-harmonic intensity with angle of incidence for $30ZnO{\cdot}70TeO_2$ glasses poled in two steps and in single step at 280 °C is shown by the solid curves in Figs. 2.2(a) and 2.3, respectively. The broken curve in Fig. 2.2(b) graphically represents the theoretical Maker fringe pattern drawn using Eqs. (1.2)-(1.10) on the assumption that $L = 1$ mm, which corresponds to the glass sample thickness, $n_\omega = 2.00$ and $n_{2\omega} = 2.05$. Although the theoretical pattern is in accordance with the experimental one regarding the spacing between minima, the theoretical intensity at the minima is different from the experimental one; the former is zero while the latter shows non-zero values. The Maker fringe pattern such as the experimental fringe in Fig. 2.2(a) is obtained if the second-harmonic waves with different amplitude are generated from surface layers of the glass which are separated by about 1 mm and interfere with each other. By contrast, the experimental fringe in Fig. 2.3 which exhibits a minimum only at the incident angle of 0 ° indicates that the second-harmonic waves are produced only in a thin layer with a thickness around the coherence length $\simeq 5\,\mu$m. Moreover, this thin layer was found to be near the glass surface which had been contacted with the anode during poling because the second-harmonic generation was not observed when the anode-side surface with about 30 μm was etched mechanically. The application of Eqs. (1.2)-(1.10) with $L = 27\mu$m and $d_{33} = 0.45$ pm/V, which is indicated by the broken curve in Fig. 2.3, results in a good agreement with the experimental pattern.

Figure 2.4 shows the variation of second-harmonic intensity with time after the high voltage is removed. The open and closed circles represent the intensity for $30ZnO{\cdot}70TeO_2$ glass poled at 280 °C and $30NaO_{\frac{1}{2}}{\cdot}70TeO_2$ glass poled at 220 °C, respectively. For $30NaO_{\frac{1}{2}}{\cdot}70TeO_2$ glass, the optimum

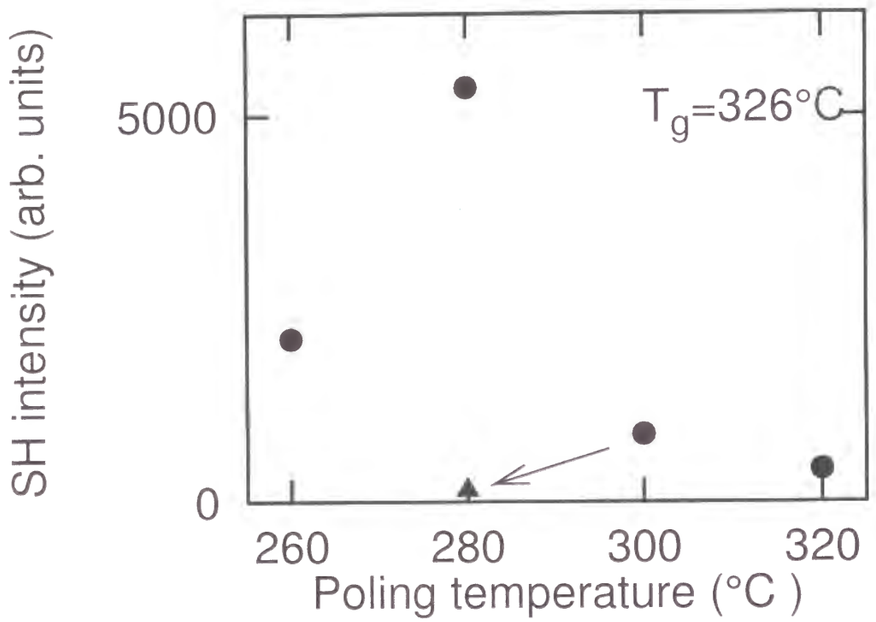

Fig. 2.1: Poling temperature dependence of second-harmonic intensity for $30ZnO{\cdot}70TeO_2$ glass. The closed circles correspond to the intensity for glasses poled at each of the temperatures for 20 min. The closed triangle represents the intensity for the glass after two-step poling; the sample was finally poled at 280 °C for 20 min after the initial poling at 300 °C for 20 min.

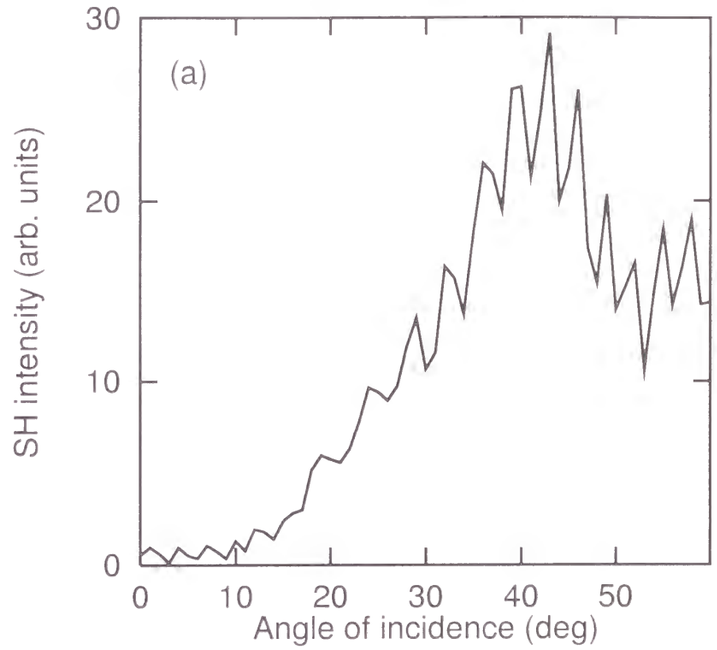

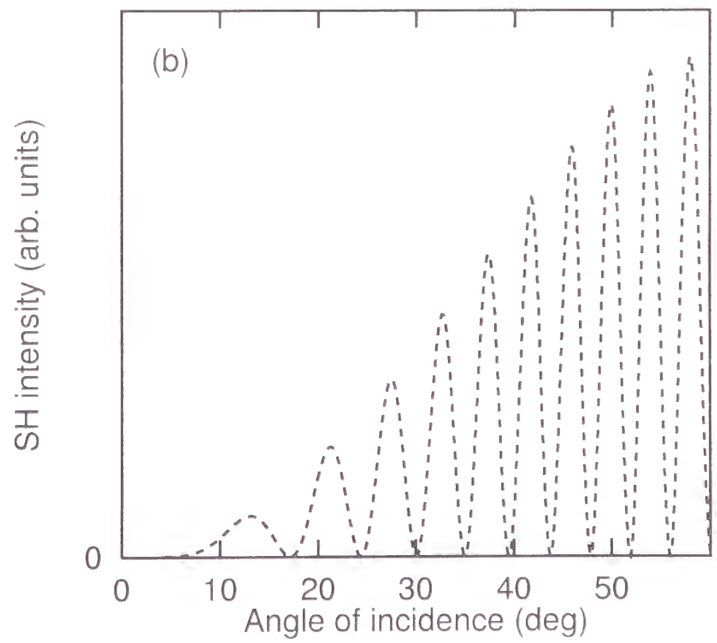

Fig. 2.2: (a) Experimental Maker fringe pattern of $30ZnO{\cdot}70TeO_2$ glass poled in two steps. (b) Theoretical Maker fringe pattern drawn by using Eqs. (1.2)-(1.10) with $L = 1$ mm, $n_{2\omega} = 2.05$ and $n_{\omega} = 2.00$.

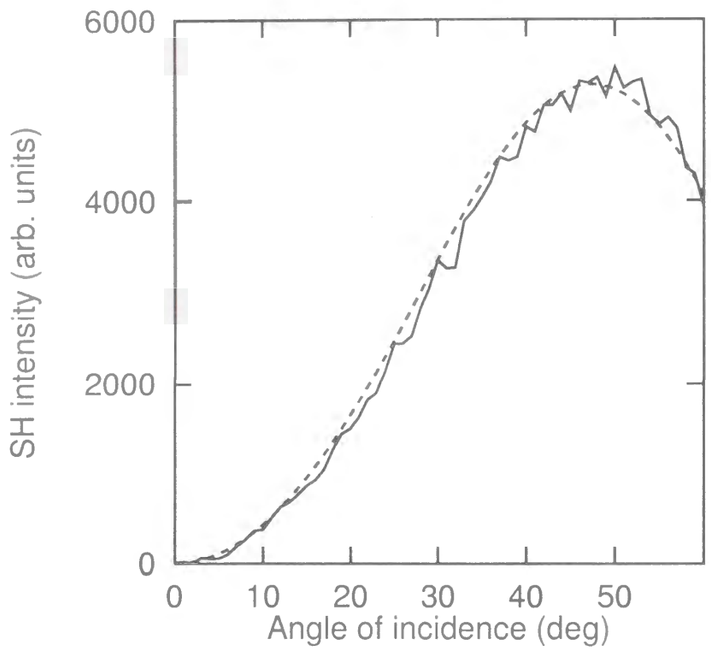

Fig. 2.3: Maker fringe patterns for $30ZnO{\cdot}70TeO_2$ glass poled at 280 °C with 3 kV. The solid and broken curves denote the experimental and theoretical patterns, respectively. The theoretical curve was drawn with $d_{33} = 0.45$ pm/V, $L = 27\,\mu$m, $n_{2\omega} = 2.05$ and $n_\omega = 2.00$

poling temperature is 225 °C, which is about 30 °C below the glass transition temperature. The second-harmonic intensity of the $30ZnO{\cdot}70TeO_2$ glass does not decay in a few weeks. On the contrary, the intensity keeps more than 90 % of its initial value even after one year. In contrast, a decay of second harmonic intensity was observed in the $30NaO_{\frac{1}{2}}{\cdot}70TeO_2$ glass. The relaxation time τ was determined by fitting the following function $f(t)$ to the experimental data indicated by the closed circles:

$$f(t) = \exp\{-(\frac{t}{\tau})^\beta\}. \tag{2.1}$$

which is generally used for the purpose of analyzing non-exponential relaxation behavior. The broken curve was drawn on the assumption of $\tau = 10$ h and $\beta = 0.6$. The agreement between experimental data and theoretical curve was rather good. It is concluded that the relaxation time for the decay of second-harmonic intensity is about 10 h in the case of $30NaO_{\frac{1}{2}}{\cdot}70TeO_2$ glass. The fact that the value of β is less than 1 means that the relaxation time has a rather broad distribution. The same analysis was performed by Qiu *et al.* [18] for soda-lime silicate glass recently.

2.1.4 Discussion

In general, the application of high voltage at high temperatures to glass containing mobile cations causes a migration of cations toward a cathode, resulting in a formation of depletion region and a pile-up of the cations beneath the anode- and cathode-side glass surfaces, respectively. The depletion region is likely to develop to greater extent if the mobility of cations is much larger than that of non-bridging oxide ions. Carlson reported that Na^+ ion-depleted layer was formed over about 1 μm below the anode-side glass surface when $20Na_2O{\cdot}80SiO_2$ (wt%) glass was heated with 100 V for 2.5 h at 475 °C [19]. Moreover, the pile of mobile cations was observed in the thin layer near the anode [20]. Such a pile of cations can be explained as follows. In the depletion region a large net negative charge is left. The cations are attracted to the depletion region by the large Coulomb force.

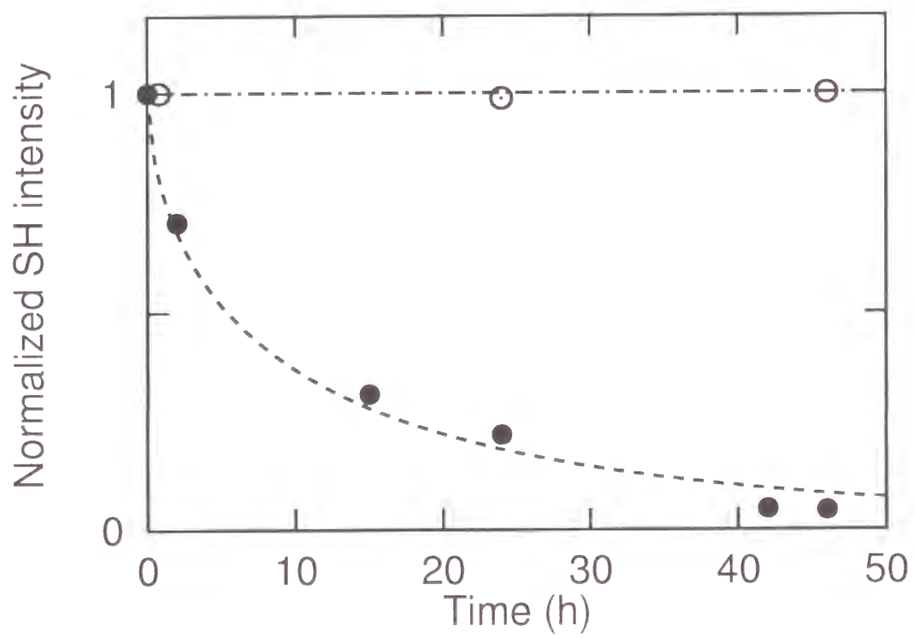

Fig. 2.4: Relaxation behavior of the second-harmonic intensity for $30ZnO{\cdot}70TeO_2$ (open circles) and $30NaO_{\frac{1}{2}}{\cdot}70TeO_2$ (closed circles) glasses. The broken curve was drawn by using Eq. (2.1) with $\tau = 10\,\mathrm{h}$ and $\beta = 0.6$. For $30ZnO{\cdot}70TeO_2$ glass, the intensity does not decay in a few weeks and shows more than 90 % of its initial intensity even after one year. It should be noted that the initial intensity of $30ZnO{\cdot}70TeO_2$ glass is about fifty times larger than for $30NaO_{\frac{1}{2}}{\cdot}70TeO_2$ glass.

Then, this Coulomb force becomes to balance with the opposite external electric force, giving a pile of cations near the anode.

Similarly, when the poling is performed for the glass composition of $30ZnO{\cdot}70TeO_2$ and $30NaO_{\frac{1}{2}}{\cdot}70TeO_2$, a thin layer with Zn^{2+} and Na^{+} ions depleted is thought to be developed near the anode-side surface to which the major part of the external electric field is applied. The depletion layer has a space charge composed of non-bridging oxygens. A pair of separated charges with opposite signs, namely non-bridging oxygen in the depletion layer and cation accumulated near the anode, creates an electric field in the opposite direction of the external electric field. Thus, the thermal poling of tellurite glasses produces a strong electric field in the thin layer beneath the anode and breaks the macroscopic inversion symmetry of the glass structure. This frozen electric field E_{dc} in the glass induces the observable second-order nonlinear susceptibility $\chi^{(2)}$ via both an orientation of non-bridging oxide ions in the depleted region and the third-order nonlinear effect, i.e., $\chi^{(3)} \cdot E_{dc}$. The magnitude of $\chi^{(2)} = 3\chi^{(3)} \cdot E_{dc}$ was estimated for $30ZnO{\cdot}70TeO_2$ glass as follows. When the poling is carried out at 280 °C, the actual voltage of 1.7 kV is approximately applied to the thickness of $L = 27\,\mu\mathrm{m}$ near the anode, leading to that E_{dc} is about 6×10^7 V/m. Therefore, using $\chi^{(3)} = 1.10 \times 10^{-20}$ $\mathrm{m^2/V^2}$ reported by Berthereau *et al.* [21], $\chi^{(2)}$ can be calculated as 2.1 pm/V. The magnitude of estimated $\chi^{(2)}$ is about twice as large as the value obtained experimentally, i.e., $\chi^{(2)} = 0.90$ pm/V. This is explained by considering the possibility that E_{dc} is overestimated. Therefore, it is feasible that the process of $\chi^{(3)} \cdot E_{dc}$ plays a dominant role in the induction of second-order nonlinearity for the poled $30ZnO{\cdot}70TeO_2$ glass.

The poling temperature dependence of second-harmonic intensity indicated by closed circles in Fig. 2.1 has been commonly observed in MgO-ZnO-TeO_2 , Na_2O-ZnO-TeO_2 and Li_2O-Na_2O-TeO_2 glass systems, as depicted in Chapter 1. Up to the optimum poling temperature, i.e., 280 °C, the second-harmonic intensity increases with an increase in poling temperature. Based upon the above-described mechanism of induction of second-

harmonic generation, such an increase in the intensity is attributed to an augmentation in easiness to form the internal dc electric field. At higher temperatures, the depletion of cations is promoted near the anode-side surface more easily [22]. Consequently, the larger internal electric field and the larger second-harmonic generation are induced. In fact, Proctor and Sutton revealed experimentally that the development of voltage which dropped near the anode electrode occurred more drastically at higher temperature for lead borosilicate glass [23]. The Maker fringe pattern shown in Fig. 2.3 is also explainable when considered the previous mechanism that an origin of the second-harmonic generation exists only in a thin layer beneath the anode-side glass surface. This situation is schematically presented in Fig. 2.5(a), where a distribution of d_{33} as well as electric field is illustrated.

On the other hand, the fact that second-harmonic intensity decreases just below the glass transition temperature cannot be explained under the above-described model which assumes the mobile cations and rigid non-bridging oxide ions, and needs consideration that the change in behavior of both cations and non-bridging oxide ions. The linear relation between optimum poling temperature and glass transition temperature shown in Fig. 1.14 supports an idea that the decrease in second-harmonic intensity results from the behavior of glass network structure, which includes an increase in mobility of non-bridging oxygens. On a plausible assumption that the glass network plays an important role in the decrease in second-harmonic intensity, two types of mechanisms for the diminish of the second-harmonic intensity are possible, as follows. One of them includes the conduction of non-bridging oxide ions toward an anode-side and subsequent evaporation into the air in the form of O_2, which decreases the internal electric field in the depletion layer [19]. The oxidation reaction to change the valence of Te^{4+}, which reduces the negative charge in the depletion region, is also possible. In another mechanism, when the poling temperature approaches to the glass transition temperature, the non-bridging oxygens begin to vibrate more vigorously, leading to a larger

thermal fluctuation of electric dipoles and hence a reduction in orientation. The fact that which is more reasonable is clear from the experiments of two-step poling process.

In the latter case, the internal electric field does not change so that the orientation of dipoles and second-harmonic intensity should recover if the poling is performed again at the optimum poling temperature after the initial poling at higher temperature. In contrast, since the former mechanism includes an irreversible electrochemical reaction such as the evaporation, the second poling process at the optimum poling temperature does not bring about an increase in second-harmonic intensity. The result shown in Fig. 2.1 clearly indicates that the decrease in second-harmonic intensity occurs irreversibly just below the glass transition temperature. Thus, the former mechanism is more plausible, although further experiments are required to determine what kinds of electrochemical reactions are predominant.

As described at the top of this section, the dipole moment along the external electric field is induced in the thin depletion layer near the anode side surface. Nevertheless, the profile of Maker fringe pattern such as Fig. 2.2(a) suggests the presence of more than two layers, which are separated with each other by the sample thickness and generate second-harmonic waves with different amplitude. This profile of Maker fringe pattern is generally observed in the tellurite glass with low second-harmonic intensity such as the glass poled at a temperature close to the glass transition temperature. In support of this observation, we conclude that the decrease in space charge in the depletion layer beneath the anode-side glass surface leads to a less voltage drop near the anode-side, resulting in such a situation that the external electric field is likely applied to the whole bulk glass and second-order nonlinearity is induced in the other regions, as shown in Fig. 2.2(b).

The second-harmonic intensity of $30ZnO{\cdot}70TeO_2$ glass did not decay in a few weeks but lasts more than one year, whereas a rapid relaxation of intensity was observed at room temperature for $30Na_2O{\cdot}70TeO_2$ glass.

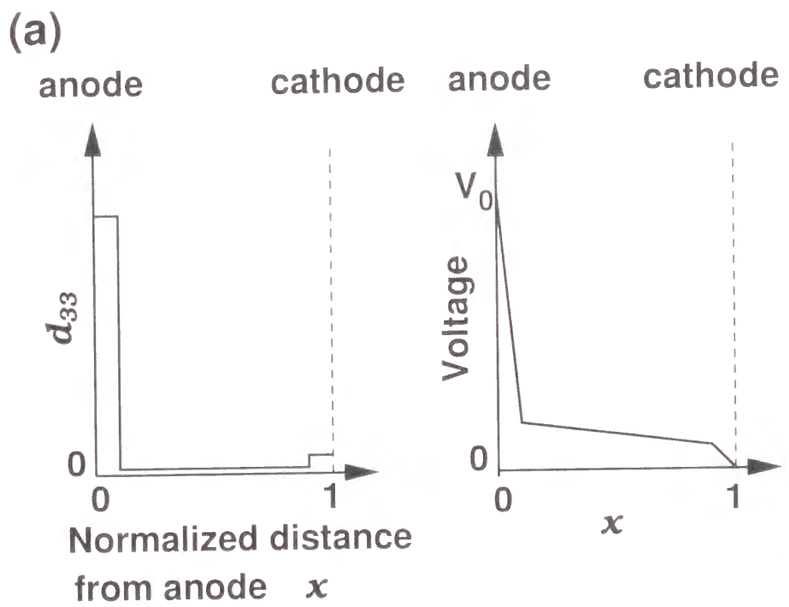

Fig. 2.5: Schematic diagrams for variation of second-order nonlinear optical coefficient d_{33} and applied voltage with normalized distance from anode-side glass surface x for the $30ZnO{\cdot}70TeO_2$ glass poled by single-step (a) and two-step (b) processes.

as demonstrated in Fig. 2.4. It is reasonable to argue that in oxide glasses alkali ions diffuse more easily than divalent cations, because the alkali ion is approximately bonded to only one non-bridging oxygen and needs less energy to break the bond to diffuse. In the $Na_2O{\cdot}9SiO_2$ glass, for example, self-diffusion coefficient of sodium ions D^*_{Na} is ca. $10^{-12}\,cm^2/s$ at 210 °C, whereas that of calcium ions D^*_{Ca} is ca. 10^{-16} cm^2/s at 450 °C [24]. Therefore, the rapid relaxation of second-harmonic intensity in the $30NaO_{\frac{1}{2}}{\cdot}70TeO_2$ glass is ascribable to the diffusion of sodium ions caused by the concentration gradient which was made during the poling. Considering this fact, a glass containing a large amount of alkali ions is not suitable for an application to devices, and it is necessary to choose glass composition containing relatively mobile divalent cations with small size such as Zn^{2+} ions for the purpose of realizing a long-lasting polarization.

2.1.5 Conclusions

It is known for various tellurite glasses that with an increase in poling temperature, the second-harmonic intensity increases, manifests a maximum at the optimum poling temperature and then decreases. In the present work, the second-harmonic intensity was measured for $30ZnO{\cdot}70TeO_2$ glass after two-step poling procedure; the glass was first poled at 300 °C and succeedingly poled at 280 °C corresponding to its optimum poling temperature. Because the second-harmonic intensity did not recover the maximum value obtained by single-step poling at 280 °C, it is concluded that the decrease in second-harmonic intensity occurred irreversibly just below the glass transition temperature. This result is interpreted by suggesting the mechanisms to induce and to reduce the second-harmonic generation as follows. Up to the optimum poling temperature, the formation of a thin depleted layer of mobile cations beneath the anode and the subsequent orientation of non-bridging oxygens in the depletion layer produce the strong electric field in the opposite direction of the external field, leading to the

second-harmonic generation. On the other hand, in the vicinity of the glass transition temperature, some oxidation reactions such as $O^{2-} \rightarrow \frac{1}{2}O_2 + 2e^-$ and $Te^{4+} \rightarrow Te^{6+} + 2e^-$, which reduce the internal electric field, presumably take place. Besides, it was successfully shown that the second-harmonic intensity of $30ZnO{\cdot}70TeO_2$ glass kept its initial value at room temperature while the intensity decayed with an average relaxation time of 10 h for $30NaO_{\frac{1}{2}}{\cdot}70TeO_2$ glass. The latter phenomenon is attributed to the larger diffusion coefficient of sodium ions compared with divalent zinc ions.

2.2 Large second-order nonlinearity of poled WO_3-TeO_2 glasses

2.2.1 Introduction

The scientific interest concerning the second-harmonic generation in poled oxide glass lies in the fact that a disappearance of macroscopic inversion symmetry is realized in a disordered solid such as a glass which has been considered to be a prototype of optically isotropic materials. From such a viewpoint, the present thesis on the second-harmonic generation in poled tellurite glasses is carried out in order to obtain information about atomistic origin for the second-order nonlinearity and mechanism to induce the second-harmonic generation. For instance, the process to create the polarization or internal dc electric field, which is frozen in the glass at room temperature and gives rise to the second-order nonlinearity, is significantly affected by the structural relaxation at glass transition for several tellurite glasses; optimum poling temperature, which corresponds to a maximum second-harmonic intensity in the poling temperature dependence of second-harmonic intensity, correlates with the glass transition temperature, as discussed in the previous chapters.

The poled oxide glasses also have attracted attention because of their

potential application to devices in the field of optoelectronics. They can be used as a frequency doubler and an optical modulator. For fabrication of those optoelectronics devices, glass materials which possess large second-order nonlinear susceptibility are required. Recently, Fujiwara *et al.* obtained $\chi^{(2)} = 6.8\,\mathrm{pm/V}$ for Ge-doped silica glass by utilizing UV poling [25]. This value is comparable to those of some crystalline materials such as $LiNbO_3$. This large value was accomplished by the precipitation of crystallites with a large third-order nonlinearity after applying large electric field ($\sim$15 kV/mm) to the glass without a discharge in air layer between glass surface and electrode.

The tellurite glasses are also important materials from a point of view of application in the field of optoelectronics. They have large optical third-order nonlinear susceptibility. Also, they are practically used as host materials for optical fiber amplifiers. In the present investigation, an attempt to attain the large second-order nonlinear susceptibility was made. As a result, it was successfully shown that the large second-order nonlinear susceptibility, i.e., 2.1 pm/V was attained in the WO_3-TeO_2 glass system. This value is fairly large compared with those of poled silica-based glasses except the above example reported by Fujiwara *et al.* [25].

2.2.2 Experimental procedure

Glass was prepared from reagent-grade WO_3 (99.9%) and TeO_2 (99.9%) powders as starting materials. The raw materials were mixed thoroughly to make $20WO_3{\cdot}80TeO_2$ composition, and melted in air at 850 °C for 30 min using a platinum crucible. After melting, the melt was poured onto a carbon plate and cooled to room temperature in air. The glass thus obtained was annealed around its glass transition temperature determined by differential scanning calorimetry (Rigaku, DSC-8230B). The annealed glass was cut into a rectangular parallelepiped using a saw pasted with diamond powder, and the surfaces of the resultant glass sample were polished for

measurements of optical properties. The thickness of the glass samples was 0.60 and 0.86 mm. The plate-like glass sample was sandwiched in between two commercial borosilicate glass plates with a thickness of 0.15 mm and physically contacted with electrodes made of stainless steel. Then, the glass sample was poled at various temperatures for 20 min with a dc voltage of 3 kV applied. The use of commercial borosilicate glass plates comes from the fact that an electric discharge in thin air layers between electrodes and tellurite glass surface possibly leads to crystallization on the tellurite glass surface, if the tellurite glass sample was directly sandwiched in between the electrodes made of stainless steel. The actual dc voltage applied to the tellurite glass sample is smaller than 3 kV because of the insertion of borosilicate glass.

Maker fringe method was applied to measurements of second-harmonic intensity for the poled glass samples. The measurements were carried out just after the poling. The *p*-polarized fundamental wave of a pulsed Nd:YAG laser (Spectra Physics, GCR-11), the wavelength of which was 1064 nm, was used as an incident light. The *p*-polarized component of the second-harmonic wave with 532 nm was passed through a monochromator (Spex, 270M), and detected by using a photomultiplier (Hamamatsu Photonics, R955). The intensity of the second-harmonic wave was determined by means of a digital oscilloscope (Hewlett Packard, 54522A).

2.2.3 Results

The effect of poling temperature on the second-harmonic intensity is depicted for $20WO_3{\cdot}80TeO_2$ glass samples of 0.60 and 0.86 mm thick in Figs. 2.6 and 2.7, respectively. The second-harmonic intensity increases, takes a maximum, and then decreases with an increase in the poling temperature for both glass samples. As argued previously, the decrease in the second-harmonic intensity with an increase in the poling temperature is connected with structural relaxation at around the glass transition temperature such as the ionic motion of non-bridging oxygens and/or some electrochemical reactions. Figures 2.6 and 2.7 also indicate that the maximum second-harmonic intensity is larger for the samples of 0.60 mm thick than of 0.86 mm thick. Furthermore, the poling temperature of maximum second-harmonic intensity, i.e., optimum poling temperature, is lower for the samples of 0.60 mm thick than of 0.86 mm thick. The electric field applied to the glass sample of 0.60 mm is larger than that for the glass sample of 0.86 mm because the voltage applied to the samples is equal to each other, so that the optimum poling temperature shifts to a lower temperature side in the former sample. In addition, the larger electric field leads to the larger second-harmonic intensity.

Figure 2.8 shows the Maker fringe pattern for $20WO_3{\cdot}80TeO_2$ glass with a thickness of 0.60 mm poled at 250 °C. The solid circles represent the dependence of second-harmonic intensity on angle of incidence obtained experimentally. The fringe pattern is ambiguous, suggesting that the length of poled region is shorter compared with the coherence length. The measurements of second-harmonic generation were also carried out for glass samples after the anode-side surface was mechanically etched.

Figure 2.9 shows the dependence of second-harmonic intensity on the etched thickness. The second-harmonic intensity is zero after etching with 20 μm. These facts suggest that the efficiently poled region is restricted near the anode-side glass surface.

2.2.4 Discussion

The solid line in Fig. 2.8 denotes the theoretical curve drawn using Eqs. (1.2)-(1.10). From the fitting, $L = 15\mu$m and $\chi^{(2)} = 2.1$ pm/V were obtained when $n_\omega = 2.105$ and $n_{2\omega} = 2.168$ were used. The length of poled region, i.e., $L = 15\mu$m, is coincident with the etched thickness dependence of second-harmonic intensity shown in Fig. 2.9. The value of second-order nonlinear susceptibility, 2.1 pm/V, is fairly large compared with the poled

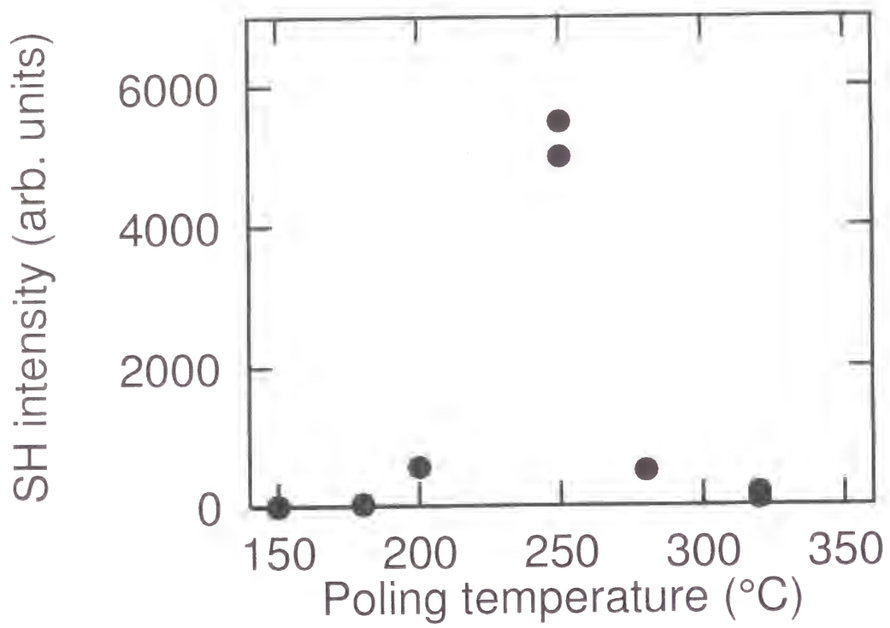

Fig. 2.6: Dependence of second-harmonic intensity on poling temperature for $20WO_3{\cdot}80TeO_2$ glass sample of 0.60 mm thick.

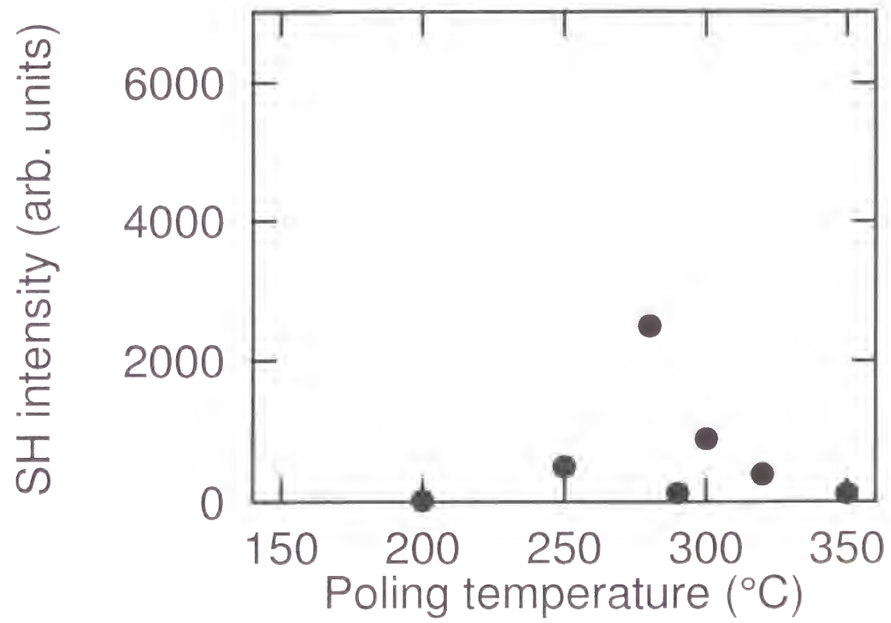

Fig. 2.7: Dependence of second-harmonic intensity on poling temperature for $20WO_3{\cdot}80TeO_2$ glass sample of 0.86 mm thick.

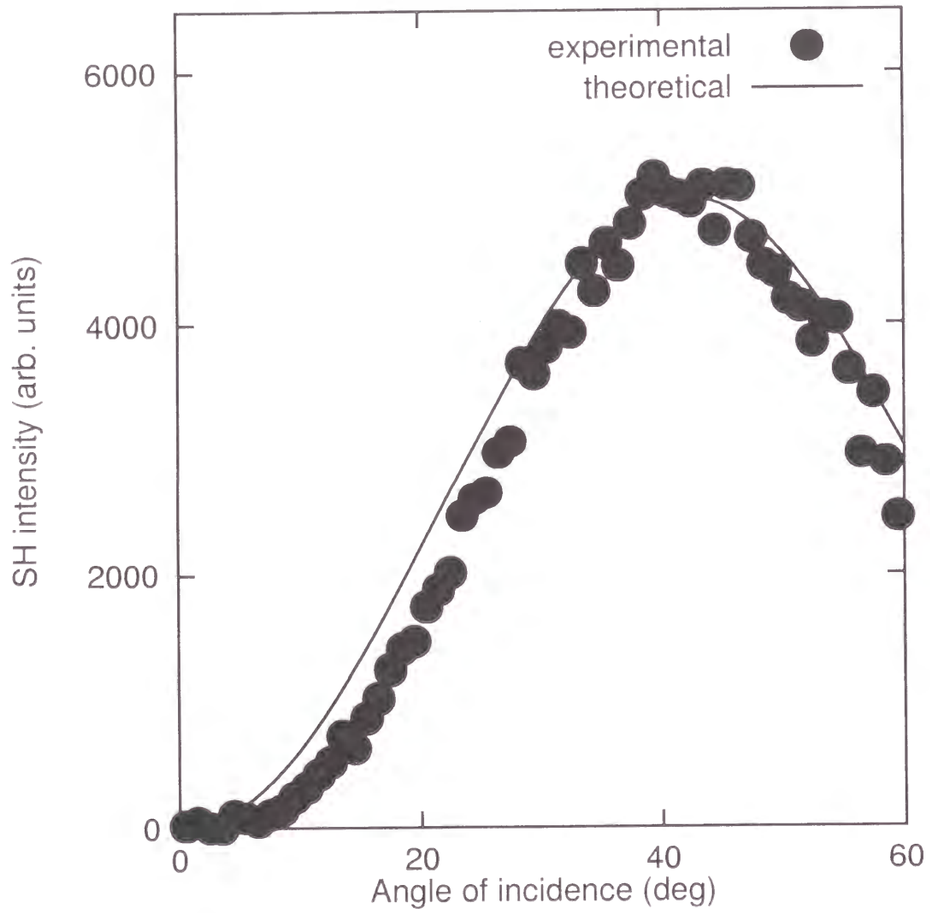

Fig. 2.8: Variation of second-harmonic intensity with angle of incidence (Maker fringe pattern) for $20WO_3{\cdot}80TeO_2$ glass sample of 0.60 mm thick poled at 250 °C for 20 min. The applied voltage is 3 kV.

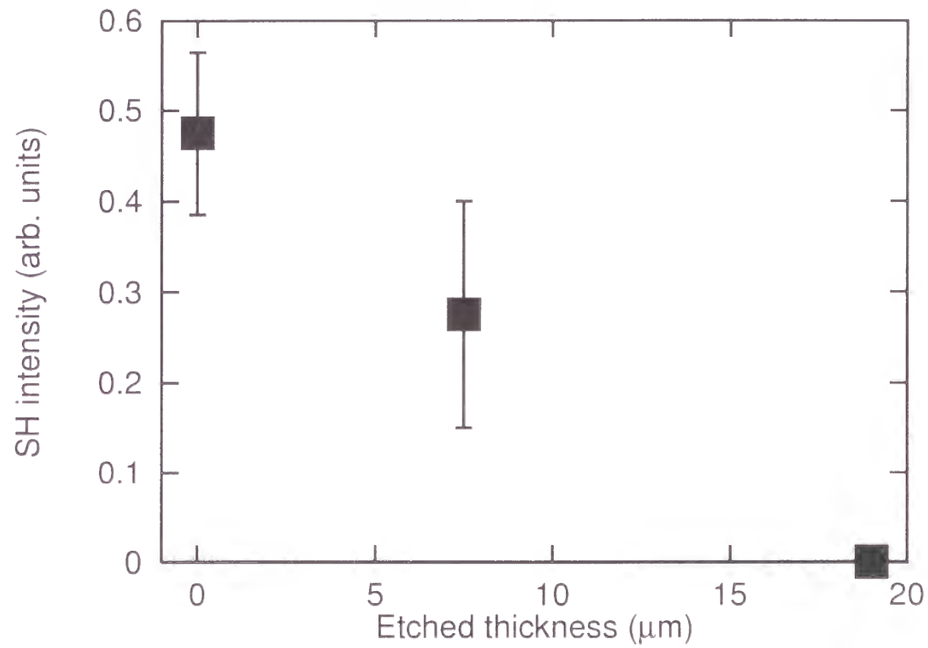

Fig. 2.9: Dependence of second-harmonic intensity on etched thickness for $20WO_3{\cdot}80TeO_2$ glass sample of 0.60 mm thick poled at 250 °C for 20 min. The anode-side glass surface was mechanically etched.

silica and tellurite glasses reported thus far: it is about 40% of $\chi^{(2)}_{22}$ of $LiNbO_3$ crystal. It is suggested that this large value is attributable to large $\chi^{(3)}$ of $20WO_3{\cdot}80TeO_2$ glass. Although the $\chi^{(3)}$ value of WO_3-TeO_2 glasses has not been measured to our knowledge, it is expected that they possess large $\chi^{(3)}$ since the linear refractive index of WO_3-TeO_2 glasses is larger than those of other tellurite glasses. According to Ghosh [26], the linear refractive indices of $20WO_3{\cdot}80TeO_2$, $10Nb_2O_5{\cdot}90TeO_2$, $30NaO_{\frac{1}{2}}{\cdot}70TeO_2$ $25ZnO{\cdot}75TeO_2$, and $20BaO{\cdot}80TeO_2$ glasses are about 2.13, 2.13, 1.95, 2.05, and 2.05, respectively at a wavelength of 1.05 μm. The Miller's rule predicts that $\chi^{(3)}$ is proportional to the fourth power of the linear susceptibility, $\chi^{(1)}$. Hence, it is anticipated that the $\chi^{(3)}$ of $20WO_3{\cdot}80TeO_2$ glass is almost equal to that of $10Nb_2O_5{\cdot}90TeO_2$, and is larger than those of $30NaO_{\frac{1}{2}}{\cdot}70TeO_2$, $25ZnO{\cdot}75TeO_2$, and $20BaO{\cdot}80TeO_2$ glasses. In fact, the value of $\chi^{(3)}$ for $10Nb_2O_5{\cdot}90TeO_2$ glass is larger by about 30% than that for $25ZnO \cdot 75TeO_2$ glass [21]. The large $\chi^{(3)}$ possibly leads to large $\chi^{(2)}$ via $\chi^{(2)} = 3\,\chi^{(3)} \cdot E_{dc}$ process.

2.2.5 Conclusions

The poled $20WO_3{\cdot}80TeO_2$ glass possesses fairly large $\chi^{(2)}$, which is presumably brought about by large $\chi^{(3)}$ via $\chi^{(2)} = 3\,\chi^{(3)} \cdot E_{dc}$ process. Considering the large $\chi^{(3)}$ of tellurite glasses, it is possible to obtain much larger $\chi^{(2)}$ in the tellurite glasses by inducing larger E_{dc}. Application of high voltage to tellurite glass thin film may be effective for that purpose.

References

[1] R. A. Myers, N. Mukherjee, and S. R. J. Brueck, Opt. Lett. **16**, 1732 (1991).

[2] H. Nasu, H. Okamoto, A. Mito, J. Matsuoka, and K. Kamiya, Jpn. J. Appl. Phys. **32**, L406 (1993).

[3] J. M. Dell, M. J. Joyce, and G. O. Stone, Proc. SPIE **2289**, 185 (1994).

[4] P. G. Kazansky, L. Dong, and P. S. J. Russell, Electron. Lett. **30**, 1345 (1994).

[5] K. Tanaka, K. Kashima, K. Hirao, N. Soga, S. Yamagata, A. Mito, and H. Nasu, Jpn. J. Appl. Phys. **34**, 175 (1995).

[6] T. Fujiwara, D. Wong, Y. Zhao, S. Fleming, S. Poole, and M. Sceats, Electron. Lett. **31**, 573 (1995).

[7] H. Takebe, P. G. Kazansky, and P. S. J. Russell, Opt. Lett. **21**, 468 (1996).

[8] H. Imai, S. Horinouchi, Y. Uchida, H. Yamasaki, K. Fukao, G. Zhang, T. Kinoshita, K. Mito, H. Hirashima, and K. Sasaki, J. Non-Cryst. Solids **196**, 63 (1996).

[9] K. Tanaka, K. Kashima, K. Hirao, N. Soga, A. Mito, and H. Nasu, Jpn. J. Appl. Phys. **32**, L843 (1993).

[10] K. Tanaka, K. Kashima, K. Kajihara, K. Hirao, N. Soga, A. Mito, and H. Nasu, Proc. SPIE **2289**, 167 (1994).

[11] K. Tanaka, K. Kashima, K. Hirao, N. Soga, A. Mito, and H. Nasu, J. Non-Cryst. Solids **185**, 123 (1995).

[12] K. Tanaka, A. Narazaki, K. Hirao, and N. Soga, J. Appl. Phys. **79**, 3798 (1996).

[13] K. Tanaka, A. Narazaki, K. Hirao, and N. Soga, J. Non-Cryst. Solids **203**, 49 (1996).

[14] A. Narazaki, K. Tanaka, K. Hirao, and N. Soga, J. Appl. Phys. **83**, 3986 (1998).

[15] A. Narazaki, K. Tanaka, K. Hirao, and N. Soga, J. Appl. Phys. **85**, 2046 (1999).

[16] M. J. Redman and J. H. Chen, J. Am. Ceram. Soc. **50**, 523 (1967).

[17] A. A. Appen and G. Fuxi, Fiz. Tverd. Tela (Leningrad) **1**, 1529 (1959).

[18] M. Qiu, F. Pi, G. Orriols, and M. Bibiche, J. Opt. Soc. Am. B **15**, 1362 (1998).

[19] D. E. Carlson, J. Am. Ceram. Soc. **57**, 291 (1974).

[20] D. E. Carlson, K. W. Hang, and G. F. Stockdale, J. Am. Ceram. Soc. **57**, 295 (1974).

[21] A. Berthereau, Y. L. Luyer, R. Olazcuaga, G. L. Flem, M. Couzi, L. Canioni, P. Segonds, L. Sarger, and A. Ducasse, Mater. Res. Bull. **29**, 933 (1994).

[22] T. M. Proctor and P. M. Sutton, J. Chem. Phys. **30**, 212 (1959).

[23] T. M. Proctor and P. M. Sutton, J. Am. Ceram. Soc. **43**, 173 (1960).

[24] R. Terai and R. Hayami, J. Non-Cryst. Solids **18**, 217 (1975).

[25] T. Fujiwara, M. Takahashi, and A. J. Ikushima, Appl. Phys. Lett. **71**, 1032 (1997).

[26] G.Ghosh, J. Am. Ceram. Soc. **78**, 2828 (1995).

Chapter 3

Relaxation of second-order nonlinearity in poled tellurite glasses

3.1 Relaxation behavior of second-harmonic generation in poled tellurite glasses

3.1.1 Introduction

Poled oxide glasses with second-order nonlinearity have attracted considerable attention from the practical viewpoint because of their potential applications to electro-optics [1] and nonlinear optics [2, 3]. As well as the technical interest, the problem how the second-order nonlinearity can be induced in glass materials which originally exhibit no second-order nonlinear phenomena is quite interesting from the basic viewpoint. Hence, the effect of glass composition [4–6] and poling conditions [7–9] on second-order nonlinearity has been investigated extensively. The information on relaxation behavior of second-harmonic intensity is also important to deduce the mechanism and to realize long lifetime of second-order nonlinearity [7]. As for soda-lime silicate glass, Qiu *et al.* reported that the second-harmonic intensity decayed more rapidly when the poling was made at lower temperatures [10]. As well, non-exponential relaxation behavior was observed in the soda-lime silicate glass by Garcia *et al.* [9]. However, little is known about the relaxation mechanism of second-harmonic generation because of a lack of quantitative and systematic studies on it. For that reason, the

purpose of this research is to examine the relaxation behavior of second-order nonlinearity and discuss its mechanism.

It is known that poled tellurite glasses as well as silicate glasses show second-harmonic generation (SHG) [11]. In particular, tellurite glasses possess large third-order nonlinear susceptibility $\chi^{(3)}$ than silica and silicate glasses [12, 13], which is responsible for large second-order nonlinear susceptibility $\chi^{(2)}$ via $\chi^{(2)} = 3\chi^{(3)} \cdot E_{dc}$ process. Actually, as investigated in Chapter 2, it was revealed that WO_3-TeO_2 glasses exhibit large second-order nonlinear susceptibility, $\chi^{(2)}_{33} = 2.1\,\mathrm{pm/V}$. Nonetheless, the relaxation of second-order nonlinearity in tellurite glasses has been little reported.

In this chapter, second-harmonic intensity was measured as a function of time at room temperature and elevated temperatures for poled $20WO_3{\cdot}80TeO_2$ glasses. For the purpose of investigating the effect of poling temperature on relaxation behavior of second-order nonlinearity, poling was performed at various temperatures. The variation of second-harmonic intensity with time was analyzed using a stretched exponential decay function to determine relaxation time τ and stretched exponential parameter β which represents a deviation from an exponential decay function. τ and β thus obtained are discussed in terms of possible relaxation processes. Furthermore, temperature dependence of τ, that is, the Arrhenius plot was also carried out in the temperature range of room temperature to 150 °C in order to estimate the activation energy for the relaxation of second-order nonlinearity. From a comparison of the calculated activation energy with those for ionic conduction of alkali ions and viscous flow in tellurite glasses, it is concluded that the relaxation behavior of second-order nonlinearity relates closely to ionic conduction and diffusion in the WO_3-TeO_2 glass system.

3.1.2 Experimental procedure

3.1.2.1 Sample preparation

Glass was prepared from reagent-grade WO_3 (99.9%) and TeO_2 (99.9%) powders. These powders were mixed thoroughly to make a nominal composition of $20WO_3{\cdot}80TeO_2$ (mol%) and melted in a platinum crucible at 850 °C for 30 min in air. The melt was rapidly cooled to room temperature by pouring onto a carbon plate to obtain glass. After the glass was annealed at around the glass transition temperature determined by differential scanning calorimetry (Rigaku, DSC-8230B), it was cut into a plate. Both surfaces of the plate-like glass were polished with aqueous suspension of CeO_2 for measurements of second-harmonic generation. The glass sample of 1.00 mm thick was sandwiched in between two commercial borosilicate glass plates with a thickness of 0.15 mm and contacted physically with electrodes made of stainless steel. Then, the glass sample was set in an electric furnace, and then poled at various temperatures ranged from 230-340 °C for 20 min with a dc voltage of 3 kV applied. The borosilicate glass plates were used to prevent precipitation of metallic tellurium and discharge between the electrodes. After the poling was performed at the aimed temperature, the glass sample was taken out from the furnace and kept at room temperature for 60 min with the constant voltage applied.

3.1.2.2 SHG measurements

Second-harmonic generation of the poled glass samples was measured by Maker fringe method in a temperature range of room temperature to 150 °C. A setup for SHG measurement at elevated temperatures is illustrated schematically in Fig. 3.1. The *p*-polarized pulsed light at 1064 nm of a Q-switched Nd:YAG laser (Spectra Physics, GCR-11) was used as an incident light. The duration of the pulse was 9 ns and the repetition rate was 10 Hz. The glass sample was mounted in an electric furnace and rotated so that the input light was incident on the sample surface at −65° to

65°. Thus, the second-harmonic intensity detected as follows was plotted against angle of incidence. In this work, the second-harmonic intensity only at the angle of incidence where the intensity makes a maximum is taken into account. The output light from the poled glass sample was passed through both IR cut filters and a monochromator (Spex, 270M) to eliminate the fundamental wave at 1064 nm completely. The second-harmonic wave at 532 nm thus obtained was p-polarized, and then detected with a photomultiplier (Hamamatsu Photonics, R955). The signal from the photomultiplier was integrated by using a digital oscilloscope (Hewlett Packard 54522A). The second-harmonic intensity from a Y-cut quartz with a thickness of 1.046mm and $d_{11} = 0.34\,\mathrm{pm/V}$ was also measured as a reference for the purpose of determining input light power.

3.1.3 Results

Figure 3.2 shows the variation of second-harmonic intensity with poling temperature for $20WO_3{\cdot}80TeO_2$ glasses. The SHG measurements were carried out at room temperature as soon as the application of a dc voltage was removed. The glass transition temperature was determined to be 350 °C. Similarly to various tellurite glass systems shown in the previous chapter, the second-harmonic intensity increases, manifests a maximum, and then decreases just below its glass transition temperature, with increasing poling temperature.

Figure 3.3 shows the relaxation of second-harmonic intensity measured at room temperature for poled $20WO_3{\cdot}80TeO_2$ glasses. The closed circles, open circles and closed triangles correspond to the normalized second-harmonic intensity for the glasses poled at 240, 260 and 280 °C, respectively. The solid curves were drawn by fitting stretched exponential decay function $f(t)$ of Eq. (2.1) to the experimental data, leading to the determination of the relaxation time τ and stretched exponential parameter β. This function is generally used for the purpose of analyzing non-exponential

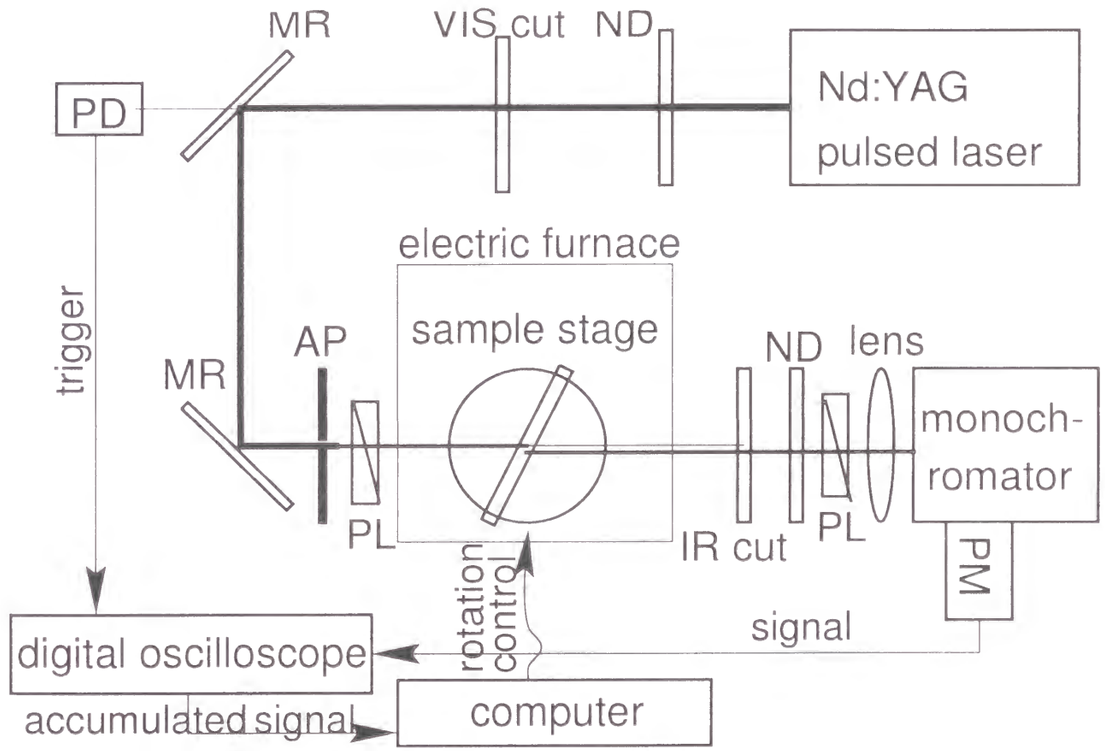

Fig. 3.1: Schematic illustration of equipment for second-harmonic generation measurements. For the SHG measurement at elevated temperatures, the tellurite glass sample was placed in an electric furnace and rotated.

relaxation behavior. Such non-exponential behavior comes from heterogeneous or homogeneous process; the former is a superposition of exponential processes with distributed relaxation time, whereas the latter consists of intrinsically non-exponential processes [14]. τ and β thus obtained are listed in Table 3.1. τ increases monotonically with an increase in poling temperature. $\beta = 1$ for the glasses poled at 240-270 °C. while β for the glass poled at 280 °C is 0.6.

In order to investigate the temperature dependence of τ and estimate the activation energy E_a for relaxation of second-order nonlinearity, the second-harmonic generation was also measured at elevated temperatures. The poling temperature was kept at 260 °C since the experimental second-harmonic intensity exhibited an exponential relaxation behavior for the glass poled at 260 °C. The results were analyzed with the Arrhenius equation:

$$\ln \tau = \frac{E_a}{RT} - \ln A, \tag{3.1}$$

where R is the gas constant, A is the frequency factor for the relaxation process. The decay of second-harmonic intensity at elevated temperatures is shown in Fig. 3.4. The closed circles and triangles denote the normalized second-harmonic intensity measured at 100 and 150 °C. respectively. The solid curves represent the decay functions of Eq. (2.1) with parameters listed in Table 3.2. The relaxation time decreases from 45 h measured at room temperature to 0.75 h at 100 °C and 0.15 h at 150 °C. In Fig. 3.5, τ given in Table 3.2 is plotted against reciprocal of T. The solid straight line was drawn by the method of least squares. The coincidence between experimental data and Eq. (2.1) implies a thermally activated relaxation process, namely, Arrhenius behavior in the poled $20WO_3{\cdot}80TeO_2$ glass. The activation energy calculated from the slope of the Arrhenius plot is 47 kJ·mol^{-1}.

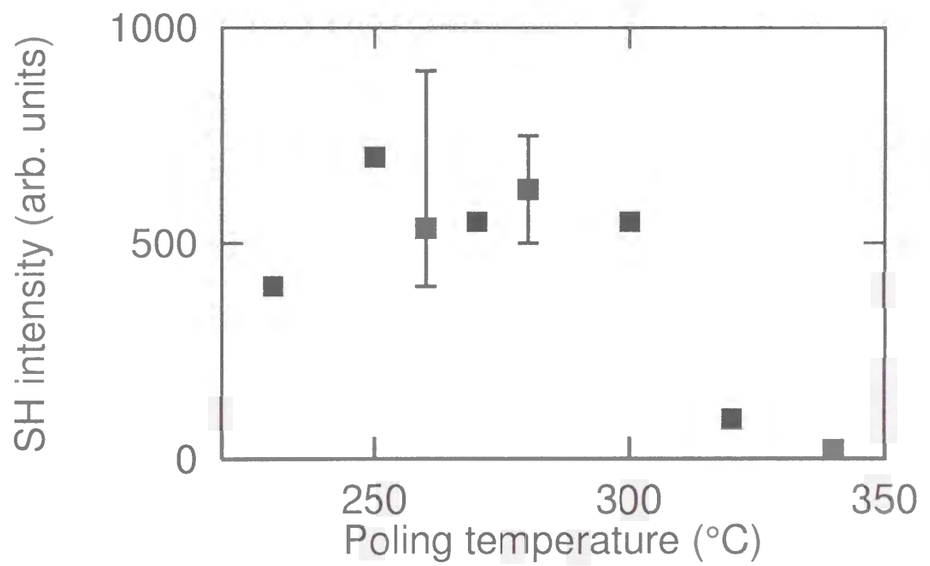

Fig. 3.2: Poling temperature dependence of second-harmonic intensity for $20WO_3{\cdot}80TeO_2$ glasses.

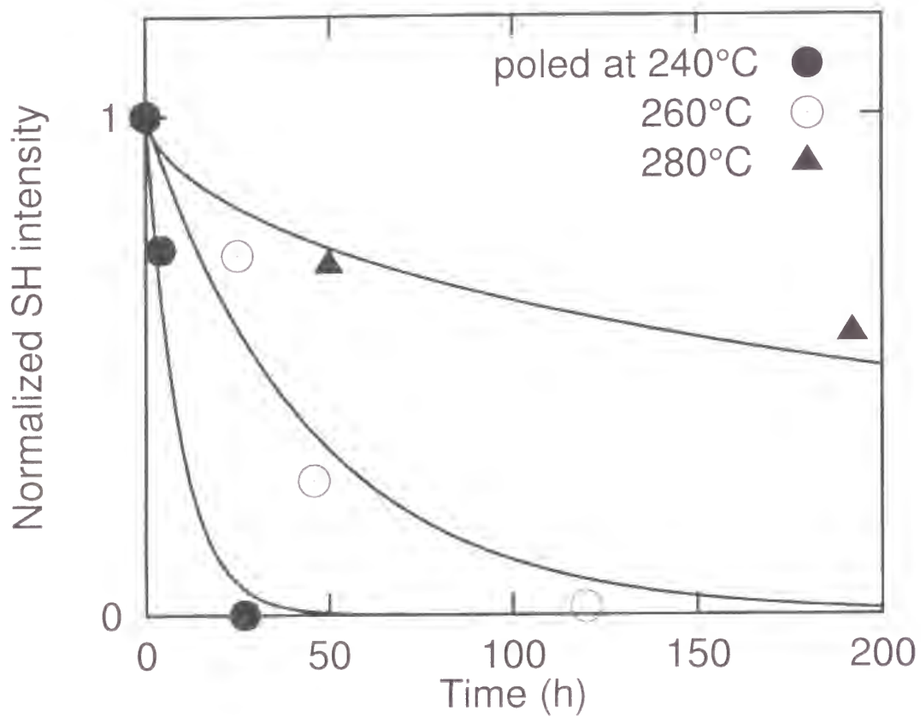

Fig. 3.3: Relaxation behavior of second-harmonic generation measured at room temperature for $20WO_3{\cdot}80TeO_2$ glasses poled at 240 (closed circles), 260 (open circles) and 280 °C (closed triangles), respectively. The second-harmonic intensity is normalized by the initial intensity. The time corresponds to a period after the high voltage was removed. The broken curves were drawn using Eq. (2.1) with the fitting parameters τ and β listed in Table 3.1.

Table 3.1: Relaxation time, τ, and β obtained by fitting the stretched exponential function to the experimental data of decay of second-harmonic intensity measured at room temperature.

Poling temperature (°C)	τ (h)	β
240	9.0	1
250	3.2×10	1
260	4.5×10	1
270	3.0×10^2	1
280	3.6×10^2	0.6

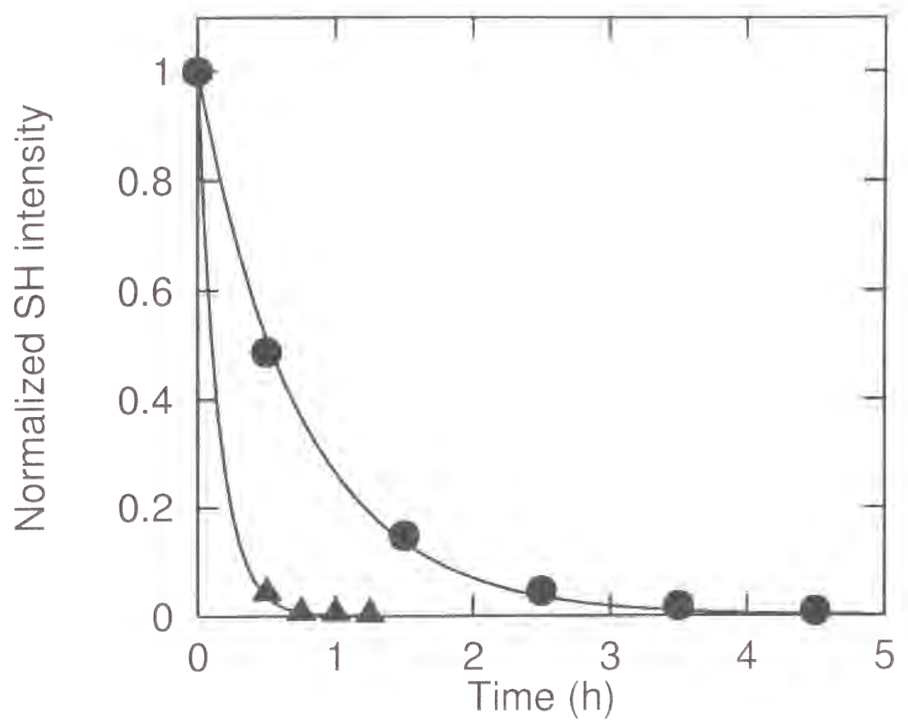

Fig. 3.4: Relaxation behavior of second-harmonic generation measured at elevated temperatures for $20WO_3{\cdot}80TeO_2$ glasses poled at 260 °C. The closed circles and triangles denote the normalized second-harmonic intensity measured at 100 and 150 °C, respectively. The experimental data were fitted using Eq. (2.1) with τ and β listed in Table 3.2.

Table 3.2: Fitting parameters for decay of second-harmonic intensity at elevated temperatures. The glass sample was poled at 260 °C.

Measurement temperature (°C)	τ (h)	β
24	4.5×10	1
100	7.5×10^{-1}	1
150	1.5×10^{-1}	1

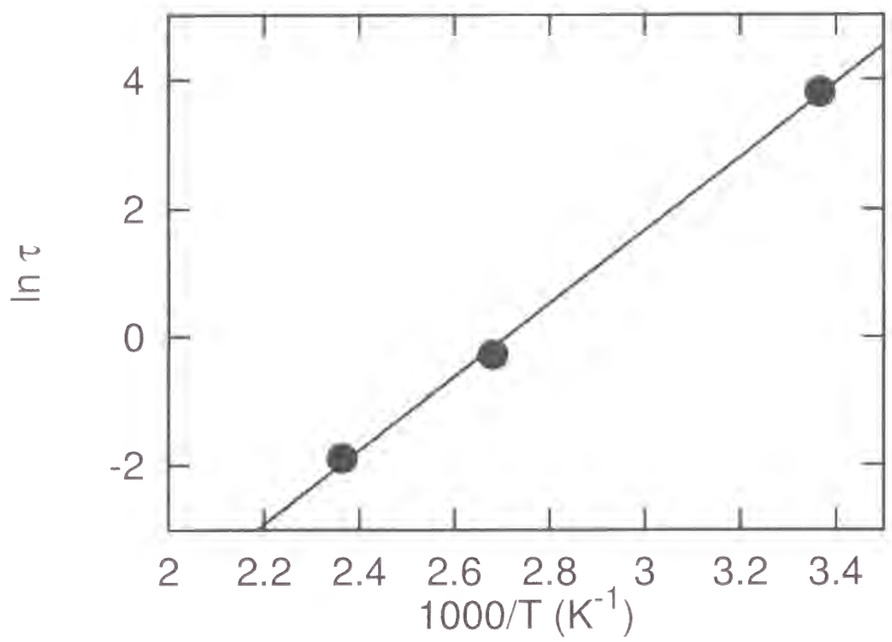

Fig. 3.5: Arrhenius plot for relaxation time τ listed in Table 3.2. The solid line was drawn by the method of least squares. From the slope of the line, th activation energy was calculated to be 47kJ·mol^{-1}.

3.1.4 Discussion

It is generally accepted for oxide glasses that a drift of mobile cations first takes place followed by a formation of a cation-depleted region beneath an anode-side glass surface when a dc voltage is applied. Then, a frozen electrostatic field E_{dc} in the cation-depleted region induces the second-order nonlinear susceptibility $\chi^{(2)}$ via a process of $\chi^{(2)} = 3\,\chi^{(3)} \cdot E_{dc}$. Such a model is based on the observation that SHG-active structure is localized only in the vicinity of the anode-side surface for most of the poled oxide glasses.

For all the $20WO_3{\cdot}80TeO_2$ glasses poled in this experiment, the second-order nonlinearity was observed only within a depth of several micrometers from the anode-side surface, which supports the $\chi^{(2)} = 3\,\chi^{(3)} \cdot E_d$ process. Although the $20WO_3{\cdot}80TeO_2$ glass does not contain mobile cations as nominal glass-constituents, Na^+ ions can be detected by X-ray photoelectron spectroscopy measurements after poling. This is because penetration of Na^+ ions from the borosilicate glass plate placed between tellurite glass sample and anode occurred under the external electric field. Thus, it is plausible that conduction of the Na^+ ions brings about the induction of E_{dc} and second-order nonlinearity. A detail of the implantation of Na^+ ions will be discussed in the following chapter. Therefore, it can be concluded that the initial increase in second-harmonic intensity with raising poling temperature is due to an increase in the amount of implanted Na^+ ions. On the other hand, the decrease in second-harmonic intensity just below its glass transition temperature of 350 °C can not be explained in terms of the increase in implanted Na^+ ions. One of possible mechanisms is a conduction of non-bridging oxygens toward an anode which diminishes E_{dc}, namely, the second-order nonlinearity, as suggested in Chapter 2.

As seen in Table 3.1, the relaxation time τ increases monotonically with raising poling temperature. This indicates an increase in the activation energy E_a and/or a decrease in the frequency factor of relaxation process for the glass poled at higher poling temperature. Supposing the above pro-

cess to induce SHG, the decay of second-harmonic intensity is caused by diffusion of Na^+ ions to the anode-side as a relaxation phenomenon which diminishes the frozen electrostatic field E_{dc}. Therefore, it can be suggested that such a relaxation process occurred with higher E_a and/or at lower frequency for the glass poled at higher temperature.

Besides, the stretched exponential parameter β deviated from 1 was obtained only for the glass poled at 280 °C, as given in Table 3.1. As mentioned above, it is feasible that heterogeneous or homogeneous process becomes dominant in the relaxation of second-harmonic generation of the glass poled at 280 °C. Supposing that the heterogeneous process is dominant, the second-order nonlinearity decays via exponential processes with different τ. Such distributed τ possibly comes from either a site-distribution of Na^+ ions or other ions with different mobility. In contrast, the homogeneous process intrinsically shows non-exponential behavior due to correlation between relaxation species. Recently, Pan *et al.* analyzed the electric modulus data with Eq. (2.1) for $x\mathrm{Na_2O}\cdot(100-x)\mathrm{TeO_2}$ glasses and revealed that β decreased from 0.75 for $x = 10\,\mathrm{mol\%}$ to 0.63 for $x = 30\,\mathrm{mol\%}$ [15]. It was also suggested that an increase in cation-cation interaction with increasing Na_2O content resulted in a decrease of β. Therefore, owing to the effect of the interaction among Na^+ ions on β, the intrinsic non-exponential relaxation is observable when concentration of relaxation species such as Na^+ ion is high enough to interact with each other. At this moment, however, it is not evident which process plays an important role in the relaxation of second-harmonic generation in the case of $\beta = 0.6$.

Additionally, the relaxation of second-order nonlinearity can be discussed in the light of temperature dependence of τ, namely, Arrhenius plot shown in Fig. 3.5. The activation energy E_a calculated from the Arrhenius plot is $47\,\mathrm{kJ\cdot mol^{-1}}$. This is smaller than the activation energy for dc conduction of Na^+ ion, $E_\sigma = 102\,\mathrm{kJ\cdot mol^{-1}}$, reported for $10\mathrm{Na_2O}\cdot90\mathrm{TeO_2}$ glass in the temperature range of 100-260 °C [15] and the activation energy for viscous flow, $E_\eta = 530\,\mathrm{kJ\cdot mol^{-1}}$, reported for $20\mathrm{Na_2O}\cdot80\mathrm{TeO_2}$ glass just

above its glass transition temperature [16]. From the fact that E_a is closer to E_σ than E_η, it can be concluded that the relaxation of second-order nonlinearity is related to ionic conduction or diffusion of Na^+ ion.

3.1.5 Conclusions

The relaxation of second-harmonic generation was evaluated in the range of room temperature to 150 °C for poled $20\mathrm{WO_3}\cdot80\mathrm{TeO_2}$ glasses. Using the stretched exponential decay function, the relaxation time τ and the stretched exponential parameter β were obtained for the glasses poled at various temperatures. τ increases monotonically with raising the poling temperature, and $\beta = 1$ for glasses other than the glass poled at 280 °C for which $\beta = 0.6$. Furthermore, the temperature dependence of τ followed the Arrhenius behavior with the activation energy for relaxation of second-harmonic generation being $47\,\mathrm{kJ\cdot mol^{-1}}$. A comparison of this with those for dc ionic conduction and viscous flow of tellurite glasses suggests the relaxation mechanism in which ionic conduction or diffusion plays a dominant role.

References

[1] X. C. Long, R. A. Myers, and S. R. J. Brueck. Opt. Lett. **19**, 1819 (1994).

[2] A. Okada, K. Ishii, K. Mito, and K. Sasaki, Appl. Phys. Lett. **60**, 2853 (1992).

[3] P. G. Kazansky, L. Dong, and P. S. J. Russell, Electron. Lett. **30**, 1345 (1994).

[4] H. Nasu, H. Okamoto, A. Mito, J. Matsuoka, and K. Kamiya, Jpn. J. Appl. Phys. **32**, 180 (1993).

[5] H. Imai, S. Horinouchi, N. Asakuma, K. Fukao, D. Matsuki, H. Hirashima, and K. Sasaki, J. Appl. Phys. **15**, 5415 (1998).

[6] A. Narazaki, K. Tanaka, K. Hirao, and N. Soga. J. Am. Ceram. Soc. **81**, 2735 (1998).

[7] A. Narazaki, K. Tanaka, K. Hirao, and N. Soga. J. Appl. Phys. **85**, 2046 (1999).

[8] H. Takebe, P. G. Kazansky, and P. S. J. Russell. Opt. Lett. **21**, 468 (1996).

[9] F. C. Garcia, I. C. S. Carvalho, E. Hering, and W. Margulis. Appl. Phys. Lett. **72**, 3252 (1998).

[10] M. Qiu, F. Pi, G. Orriols, and M. Bibche. J. Opt. Soc. Am. B **15**, 1362 (1998).

[11] K. Tanaka, K. Kashima, K. Hirao, N. Soga, A. Mito, and H. Nasu, Jpn. J. Appl. Phys. **32**, L843 (1993).

[12] S. H. Kim, T. Yoko, and S. Sakka, J. Am. Ceram. Soc. **76**, 2486 (1993).

[13] A. Berthereau, Y. L. Luyer, R. Olazcuaga, G. L. Flem, M. Couzi, L. Canioni, P. Segonds, L. Sarger, and A. Ducasse, Mater. Res. Bull. **29**, 933 (1994).

[14] A. Heuer, S. C. Kuebler, U. Tracht, H. W. Spiess, and K. Okun, *Structure and Dynamics of Glasses and Glass Formers*, Vol. 455 of *Symposium Proceedings* (Materials Research Society, Pittsburgh, Pennsylvania, 1997), pp. 105 116.

[15] A. Pan and A. Ghosh, Phys. Rev. B **59**, 899 (1999).

[16] T. Komatsu, R. Ike, R. Sato, and K. Matusita, Phys. Chem. Glasses **36**, 216 (1995).

Chapter 4

Surface structure of poled tellurite glasses

4.1 XPS and IR studies on the surface structure of poled ZnO-TeO_2 glasses

4.1.1 Introduction

The SHG-active region is formed preferentially beneath the anode-side glass surface which was contacted with an anode during poling. as suggested so far. This is a common feature of many poled oxide glasses with second-order nonlinearity. Therefore, it is important to investigate surface structure of poled glass materials for characterization of the SHG-active structure. In this chapter, the poling effect on surface structure is studied throughly by means of IR reflectance and X-ray photoelectron spectroscopy (XPS) techniques for ZnO-TeO_2 and WO_3-TeO_2 glass systems. The obtained results are discussed in terms of a difference between them, leading to better understanding of the role of divalent cations in the second-order nonlinearity.

First, the surface of poled $30ZnO{\cdot}70TeO_2$ glass was examined because no decay of second-harmonic intensity was observed for about one year after poling. The estimated relaxation time is much longer than other tellurite glasses without divalent cations, such as Na_2O-TeO_2 and WO_3-TeO_2 compositions. In order to make clear which factors play an dominant role

in the induction of the long-lasting second-order nonlinearity, this composition was chosen. The IR reflectance technique was used to explore glass network structure at the near-surface region of the poled $30ZnO{\cdot}TeO_2$ glass. TeO_4 trigonal bipyramids are the basic structural unit of tellurite glasses and they are connected with each other in 3-dimensional space, leading to glass network structure. On the other hand, an addition of network modifying oxides such as ZnO gives rise to TeO_3 trigonal pyramids which are considered to restrict the glass formation. Thus, IR reflectance peaks attributable to two types of TeO_n polyhedra [1]. Hence, the IR reflectance was measured for the purpose of studying the change in glass network structure caused by poling. Also, XPS measurement was carried out for the purpose of probing the concentration of each glass-constituent atom for the as-annealed and poled glasses. The results thus obtained are discussed in relation to the induction mechanism of second-order nonlinearity in the $30ZnO{\cdot}70TeO_2$ glass.

4.1.2 Experimental procedure

4.1.2.1 Sample preparation

Glass samples were prepared from ZnO and TeO_2 as starting materials using the conventional melt-quenching method. The purity was 99 and 99.9 %, respectively. The powders of raw materials were mixed thoroughly to make a nominal composition of $30ZnO{\cdot}70TeO_2$ and melted in a platinum crucible at 900 °C for 20 min in air. The melt was rapidly cooled by pouring onto a carbon plate to obtain glass. The glass was annealed around its glass transition temperature. The as-annealed glass was cut into a plate, and then both surfaces of the plate-like glass were polished with aqueous suspension of CeO_2 for optical measurements. The resultant glass specimen had a thickness of 1.00 mm.

Poling of the glass sample was performed as follows. The glass sample was sandwiched in between two commercial borosilicate glass plates with

a thickness of 0.15 mm and contacted physically with electrodes made of stainless steel. The commercial borosilicate glass plates were used to avoid precipitation of metallic tellurium which occurred on the cathode-side glass surface when the glass sample was directly brought into contact with the electrodes made of stainless steel. The use of commercial borosilicate glass plates was also effective to avoid discharge between the electrodes. The glass sample sandwiched with the electrodes was put into an electric furnace and heated at an aimed temperature for 30 min. In this work, poling temperature was set in the range of 260-300 °C. After the voltage of 3 kV was applied for 40 min at the temperature, the glass sample was taken out from the furnace and kept at room temperature for 60 min with the voltage applied. It should be noted that the actual voltage applied to the sample was estimated to be 1.7 kV, when the dielectric constants of $30ZnO{\cdot}70TeO_2$ and borosilicate glasses were assumed to be 21 and 7.9, respectively.

4.1.2.2 Analysis of glass near-surface region

Both the as-annealed and poled glass specimens thus obtained were subjected to IR and XPS measurements. The IR reflectance spectra were measured with an FT-IR spectrometer (Japan Spectroscopic, FT/IR-550) in the wave number range of 4000 to 400 cm^{-1} in air. Samples were placed at an angle of incidence of 10°. The reference was an aluminum mirror. The obtained data were corrected by subtracting the reflectance due to atmospheric CO_2. The glass composition was investigated with an XPS (ULVAC-phi, MT-5500) using MgKα X-ray as an excitation source in the pressure range of 10^{-8} to 10^{-9} Pa.

4.1.2.3 Optical measurements

Second-harmonic generation of the poled glass samples was measured using the Maker fringe method. A pulsed Nd:YAG laser (Spectra Physics,

GCR-11), which operated in a Q-switched mode with a 10 Hz repetition rate, was used as a light source. After the pulse at 1064 nm with 9 ns duration was *p*-polarized, it was incident on the sample at $-65°$ to $65°$. The beam diameter was about 1 mm. The output light from the poled glass sample was passed through both IR cut filters and a monochromator (Spex. 270M) to eliminate the fundamental wave at 1064 nm completely. The second-harmonic wave at 532 nm was detected with a photomultiplier (Hamamatsu Photonics, R955). The signal from the photomultiplier was integrated by using a digital oscilloscope (Hewlett Packard 54522A). The second-harmonic intensity from a Y-cut quartz with a thickness of 1.046mm and $d_{11} = 0.34$ pm/V was also measured for the purpose of determining input light power.

4.1.3 Results

Figure 4.1 shows the reflectance spectra in the range of 4000-400 cm^{-1} for the as-annealed and poled $30ZnO{\cdot}70TeO_2$ glasses. As for the anode-side surface region with second-order nonlinearity, there is no evident change in reflectance after poling in the vicinity of 3000 cm^{-1}, where the absorption band caused by the free OH groups appears as reported by Bürger *et al.* for several tellurite glasses [2].

The reflectance spectra from 1400 to 400 cm^{-1} were illustrated in Fig. 4.2. A broad reflectance peak at 700-600 cm^{-1} was observed in all the spectra. The reflectance around 600 cm^{-1} from the anode-side surface is smaller compared with both the as-annealed and cathode-side surfaces. Mochida *et al.* reported transmission IR spectra from 4000 to 350 cm^{-1} for the $30ZnO{\cdot}70TeO_2$ glass [1]; the absorption at 635 and 675 cm^{-1} can be assigned to the vibrational modes of the Te-O_{ax} bond in TeO_4 trigonal bipyramid and the Te-O bond in TeO_3 trigonal pyramid, respectively. Here, *ax* stands for the axial position of the TeO_4 trigonal bipyramid. Thus, the above-described broad peak at 700-600 cm^{-1} can be identified as a super-

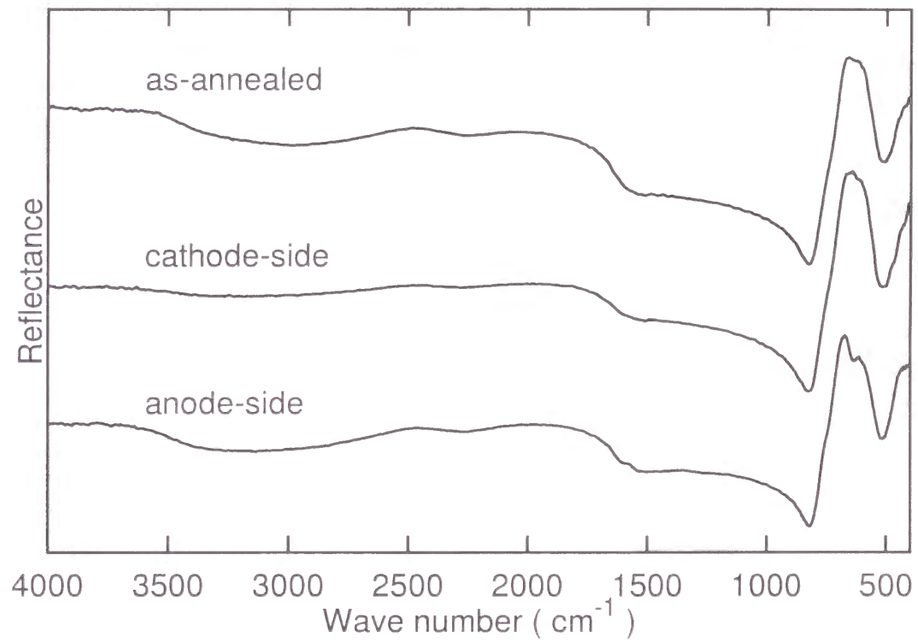

Fig. 4.1: Reflectance spectra from 4000-400 cm^{-1} for $30ZnO{\cdot}70TeO_2$ glasses. The spectra from the top to the bottom correspond to the reflectance from the as-annealed, cathode-side and anode-side surfaces, respectively. The poling was carried out with an external voltage of 3 kV at 280 °C for 40 min.

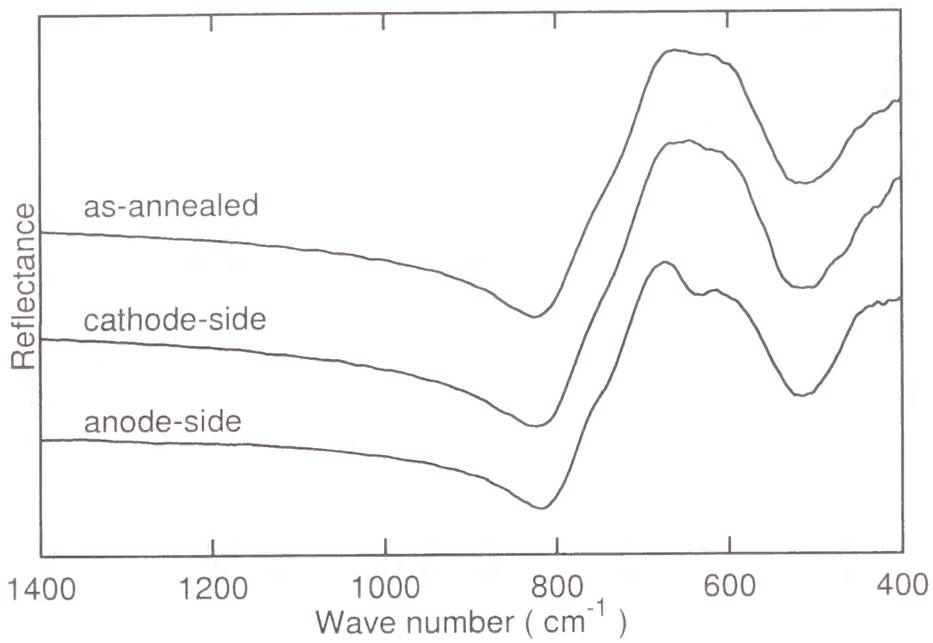

Fig. 4.2: Reflectance spectra from 1400-400 cm^{-1} for the as-annealed and poled $30ZnO{\cdot}70TeO_2$ glasses.

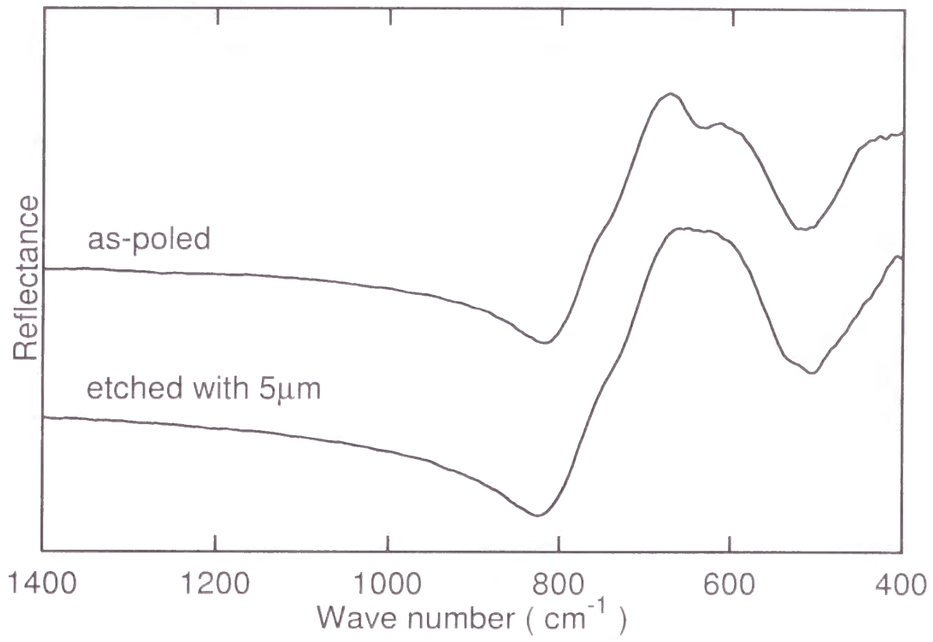

Fig. 4.3: IR reflectance from the anode-side surface of the poled $30ZnO{\cdot}70TeO_2$ glass after the original surface was removed mechanically with a thickness of 5 μm.

position of both the reflectance at 635 and 675 cm^{-1} due to Te-O_{ax} and TeO_3, respectively. Therefore, the decrease in reflectance at 635 cm^{-1} at the anode-side surface suggests a breaking of Te-O_{ax} bonds after poling.

Figure 4.3 shows the IR reflectance for the anode-side surface etched with a thickness of 5 μm. The intensity at 635 cm^{-1} was recovered after the mechanical etching. This indicates that the decrease in relative number of Te-O_{ax} bonds takes place just only beneath the anode-side surface.

Table 4.1 lists the concentration ratios of network modifying cations estimated from the XPS data for both the as-annealed and anode-side surfaces. The atomic concentration was obtained from the peak area divided by atomic sensitivity. In order to discuss the change in the number of Zn and Na ions, their concentrations were normarized by that of Te ions on the assumption that the number of Te ions is not varied throughout the bulk glass even after poling. The concentration of Zn^{2+} ions in poled glasses is lower than that of the original glass. Although the original glass does not contain sodium ions except those as impurities, an increase in Na^+ content is observed at the anode-side in comparison with the as-annealed glass. It is feasible that this increase is due to an implantation of Na^+ from the borosilicate glass which was placed between the anode and tellurite glass sample during the poling, as described above.

Table 4.1: Concetration ratio of modifying cations to Te obtained by the XPS measurements for the anode-side surfaces of poled $30ZnO{\cdot}70TeO_2$ glasses. The concentration raito for as-annealed glass surface is also presented.

Poling temperature (°C)	Concentration ratio	
	Zn/Te	Na/Te
260	0.13	0.088
280	0.10	0.10
300	0.11	0.10
as-annealed	0.14	0.040

Table 4.2: Concentration ratio obtained by the XPS measurements for the cathode-side surfaces of poled glasses with a nominal composition of $30ZnO{\cdot}70TeO_2$.

Poling temperature (°C)	Concentration ratio	
	Zn/Te	Na/Te
280	0.19	0.079
300	0.19	0.031

The variation of concetration ratio at the cathode-side surface is shown in Table 4.2. The concentration of Zn^{2+} ions increases compared to the as-annealed glass, whereas the ratio of Na^+ is lower than the anode-side.

The dependence of second-harmonic intensity on incident angle, namely, Maker fringe pattern is depicted for the poled $30ZnO{\cdot}70TeO_2$ glasses in Fig. 4.4. The solid curve and closed and open circles denote the Maker fringe patterns corresponding to the poling temperatures of 260, 280 and 300 °C, respectively. The second-harmonic intensity manifests a maximum at a certain temperature which we defined as an optimum poling temperature. This behavior is similar to those of various tellurite glasses reported previously [3–5]. In the present case, the optimum poling temperature is 280 °C.

4.1.4 Discussion

The poling induces the second-order nonlinearity in various kinds of tellurite glasses. The SHG-active region exists mainly in a thin layer beneath the anode-side surface in poled tellurite as well as other poled oxide glasses. For instance, the SHG-active layer ranged from the anode-side surface to 27 μm depth in the $30ZnO{\cdot}70TeO_2$ glass poled at 280 °C for 20 min [5]. One possible explanation for the localization of the induced second-order nonlinearity is as follows. When an external voltage is applied during poling, relatively mobile cations in glasses such as Na^+ drift toward a cathode to screen the applied voltage. Assuming the blocking anode [6, 7], this

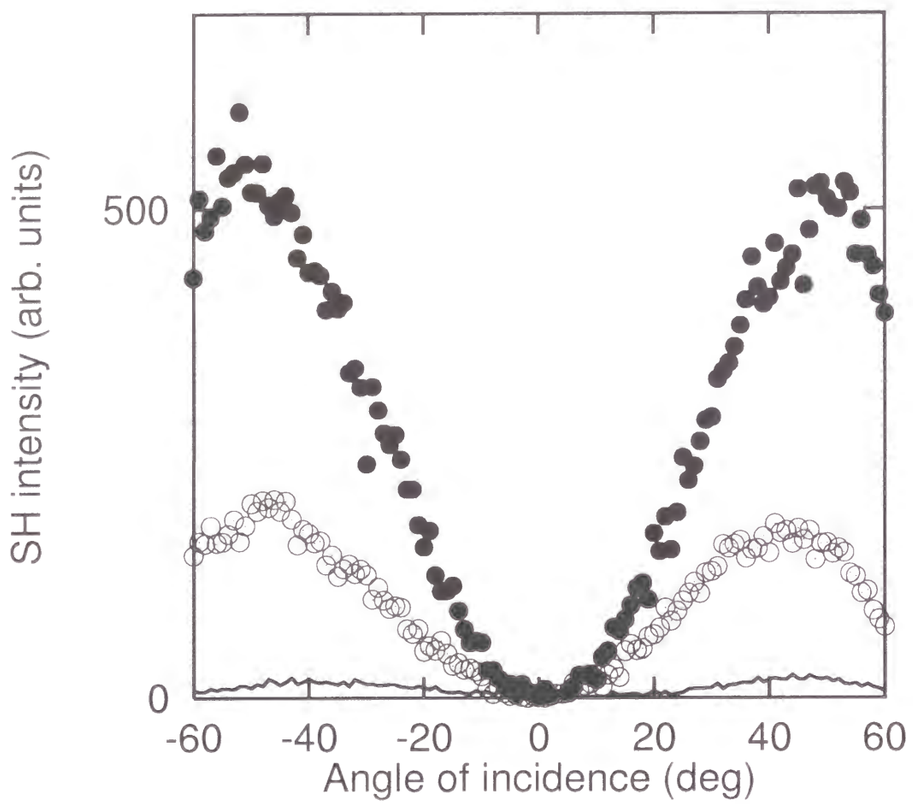

Fig. 4.4: The variation of the second-harmonic intensity with incident angle, namely, Maker fringe pattern for the $30ZnO{\cdot}70TeO_2$ glass. The solid curve, closed and open circles represent the second-harmonic intensity for the specimens poled at 260, 280 and 300 °C, respectively. An external voltage of 3 kV was applied at the aimed temperature for 40 min.

results in a creation of cation-depleted layer with net minus charge at the anode-side because the anions in oxide glasses, i.e., non-bridging oxygens are stuck more strongly to the glass network and immobile. The depleted region at the anode-side surface creates the second-order nonlinear susceptibility, $\chi^{(2)}$, via the process of $\chi^{(2)} = 3\,\chi^{(3)} \cdot E_{dc}$ where $\chi^{(3)}$ is the third-order nonlinear susceptibility the tellurite glasses originally possess. E_{dc} is the frozen electric field in the cation-depleted region.

The IR reflectance from the anode-side surface depicted in Fig. 4.1 shows a decrease in intensity at around 635 cm^{-1} assigned to the vibration mode of the Te-O_{ax} bond in TeO_4 trigonal bipyramid in ZnO-TeO_2 system [1]. According to this assignment, it can be concluded that poling treatment brought about a breaking of the tellurite glass network. Mochida *et al.* also reported dependence of IR absorption on ZnO and Na_2O content in ZnO-TeO_2 and Na_2O-TeO_2 binary glass systems: when ZnO or Na_2O content became higher, the absorption assigned to the Te-O_{ax} bond decreased accompanied by an increase in absorption at around 675 cm^{-1} assigned to the Te-O bonds in TeO_3 polyhedra. However, the poled $30ZnO{\cdot}70TeO_2$ glasses employed in the present experiments did not show the increase in intensity at 675 cm^{-1}. Hence, the decrease in Te-O_a bonds was caused not only by a change in amount of network modifying cations but also by additional poling effect. Moreover, the fact that the reflectance at 635 cm^{-1} recovered after the anode-side surface was removed with 5 μm thickness indicates that the structural change observed by IR spectroscopy is restricted in a thinner layer than the SHG-active region. Thus, presumably the decrease in Te-O_{ax} bonds is not directly related to the induction process of the second-order nonlinearity.

The glass compositions obtained for the anode-side surface in Table 4.1 exhibit common characteristics irrespective of the poling temperature. The percentage of Zn decreased by about 30 % after poling, whereas the ratio of Na in poled glass became twice as large as that of the as-annealed one. In contrast to the results of anode-side surface, the evaluated compositions for the cathode-side show that the concentration of Zn is higher than that

of the as-annealed surface (Table 4.2). Therefore, it can be speculated that when the external electric field is applied, Zn^{2+} cations drift toward the cathode to screen the external electric field followed by their depletion and accumulation at the anode- and cathode-side surfaces, respectively. As for Na^+ ions implanted from the borosilicate glass placed between the anode and the tellurite glass sample, they conduct through the tellurite glass, making a slight accumulation in the vicinity of the anode-side surface. Consequently, it is plausible that the observed Zn^{2+} ion-depleted and/or Na^+ ion-accumulated layer at the anode-side can contribute to the second-order nonlinearity through the above-mentioned process.

In addition, It can be discussed from a difference in the relaxation behavior of the second-harmonic intensity which ion, Zn^{2+} or Na^+, contributes more predominantly to the induction of second-order nonlinearity. As shown in Fig. 2.4 for $30ZnO{\cdot}70TeO_2$ and $30NaO_{1/2}{\cdot}70TeO_2$ glasses, the decay time of the second-harmonic intensity remarkably depends on the glass composition; the decay time for the former is about 10 years, whereas the intensity for the latter decreased rapidly in several hours. Since Na^+ ion is the only mobile cation that can form the space charge layer during poling in the $30NaO_{1/2}{\cdot}70TeO_2$ glass, the relaxation of the second-harmonic intensity is caused by a redistribution of Na^+ ions to an equilibrium state which decreases E_{dc}. Thus, the longer decay time for the poled $30ZnO{\cdot}70TeO_2$ glass suggests that divalent zinc cations with lower mobility than Na^+ ions, play an important role in the formation and relaxation of the second-order nonlinearity.

As shown in Fig. 4.4, the second-harmonic intensity exhibits a maximum at the optimum poling temperature of 280 °C. According to the XPS data of the anode-side, the ratio of Zn is the least at the optimum poling temperature, leading to a freeze of the largest static electric field and then the largest second-order nonlinear susceptibility among the present glasses.

4.1.5 Conclusions

Effect of poling on surface structure was investigated by means of both IR reflectance and X-ray photoelectron spectroscopies for the $30ZnO{\cdot}70TeO_2$ glasses with second-order nonlinearity. Since the second-order nonlinearity is induced easily in the vicinity of the anode-side glass surface, the information on its surface structure is required in order to clarify origin of the seocnd-harmonic generation.

In the IR reflectance spectra, it was observed that the intensity around $635\,cm^{-1}$ decreased at the anode-side surface in comparison with the as-annealed and cathode-side surfaces. This means a decrease in the number of Te-O_{ax} bonds. In other words, the poling caused the breaking of the tellurite glass network at the anode-side surface. However, this change in reflectance disappeared after etching of anode-side surface with a $5\,\mu m$ thick which is thinner than the observed SHG-active layer. Hence, it is not clear whether the change in IR spectrum directly relates to the induction of second-order nonlinearity.

Another influence of poling is the modification of glass composition. The XPS data of the anode-side revealed a depletion of Zn^{2+} ions and an increase in the number of Na^+ ions implanted from the borosilicate glass, which was placed between the sample and the anode during poling. These results support that the second-order nonlinearity is induced via $\chi^{(2)} = 3\,\chi^{(3)} \cdot E_{dc}$ process where E_{dc} is the static electric field in space charge layer such as the Zn^{2+} ion-depleted and Na^+ ion-accumulated region. Considering a difference in decay time of the second-harmonic intensity between $30ZnO{\cdot}70TeO_2$ and $30NaO_{1/2}{\cdot}70TeO_2$ glasses, it can be speculated that the Zn^{2+} ion-depleted region plays an important role in the second-harmonic generation in the $30ZnO{\cdot}70TeO_2$ glass.

4.2 XPS, IR and ESR studies on the structure of poled WO_3-TeO_2 glasses

4.2.1 Introduction

Second-order nonlinearity of poled oxide glasses has been extensively studied in a decade because of great potential applications to high speed modulators and frequency upconversion devices [8 10]. From the fundamental viewpoint as well as the practical one, an attempt has been made to clarify how the poling induces the second-order nonlinearity in glass materials which originally do not show any second-order nonlinear phenomena such as second-harmonic generation [5.11 13]. As a result of SHG measurements, it is generally accepted for poled oxide glasses that a SHG-active region is restricted in the vicinity of an anode-side glass surface. This implies that a modification of structure by poling occurs preferentially at surface region. Therefore, information on surface structure of poled oxide glasses is very important to deduce an induction process of second-order nonlinearity.

In this section, X-ray photoelectron spectroscopy and IR reflectance measurements were carried out for the purpose of investigating glass composition and network structure at surface of poled $20WO_3{\cdot}80TeO_2$ glasses with second-order nonlinearity. As reported by Kim *et al.* [14], tellurite glass systems possess a third-order nonlinear susceptibility $\chi^{(3)}$ by about two orders of magnitude larger than silica and silicate glasses. The larger $\chi^{(3)}$ possibly leads to a larger $\chi^{(2)}$ by poling if a process of $\chi^{(2)} = 3\,\chi^{(3)}{\cdot}E_{dc}$ is available. Besides, according to the Miller's rule which predicts that $\chi^{(3)}$ is proportional to the fourth power of the linear susceptibility, it can be deduced that $20WO_3{\cdot}80TeO_2$ glass has a large third- and second-order nonlinearity due to its high refractive index. Actually, as demonstrated in Chapter 2.2, $\chi^{(2)}_{33} = 2.1\,\mathrm{pm/V}$ was achieved for the poled $20WO_3{\cdot}80TeO_2$ glass, which is larger than those of other tellurite glasses employed in the present thesis.

Further, the poling effect on oxidation state of W ion has been examined using an electron spin resonance (ESR). Also, the relaxation behavior of second-harmonic intensity for the poled $20WO_3{\cdot}80TeO_2$ glass is discussed in terms of a comparison with those for $30NaO_{\frac{1}{2}}{\cdot}70TeO_2$ and $30ZnO{\cdot}70TeO_2$ glasses.

4.2.2 Experimental procedure

4.2.2.1 Sample preparation

Glass with a nominal composition of $20WO_3{\cdot}80TeO_2$ (mol%) was prepared from WO_3 and TeO_2 as starting materials. The purity of raw materials was 99.9 %. The mixture of the raw materials was melted in a platinum crucible at 850 °C for 30 min in air. The melt was rapidly cooled by pouring onto a carbon plate. Glass thus obtained was annealed around its glass transition temperature determined by means of differential scanning calorimetry (Rigaku. DSC-8230B). The as-annealed glass was cut into a plate and both surfaces of the plate-like glass were polished with CeO_2 slurry. The resultant glass specimen had a thickness of 0.50 or 1.00 mm.

Poling of the glass sample was performed as follows. The glass sample was sandwiched in between two commercial borosilicate glass plates with a thickness of 0.15 mm and contacted physically with electrodes made of stainless steel, as stated before. The glass sample sandwiched with the electrodes was put into an electric furnace and heated at the aimed temperature for 30 min. Then, a dc voltage of 3 kV was applied for 30 min at the temperature. After poling, the glass sample was taken out from the furnace and kept at room temperature for 60 min with the voltage applied.

4.2.2.2 Characterization of sample structure

Surfaces of both the as-annealed and poled glasses with a thickness of 0.50 mm were examined by means of XPS and IR reflectance measurements.

The poling was performed at 240 °C. The XPS (ULVAC-phi. MT-5500) measurements were carried out using MgKα X-ray as an excitation source in a pressure range of 10^{-8} to 10^{-9} Pa. The IR reflectance spectra were measured with a FT-IR spectrometer (Japan Spectroscopic. FT/IR-550) in a wave number range of 4000 to 400 cm^{-1} in air. Samples were placed at the angle of incidence of 10°. The reference was an aluminum mirror. The obtained data were corrected by subtracting reflectance due to atmospheric CO_2.

The glass specimens pulverized after poling at 250 °C were placed in a silica tube, and subjected to the ESR measurements. For a comparison, the ESR spectrum was measured for the as-annealed glass as well as the poled ones. The measurements were carried out at room temperature using a Varian E-Line spectrometer operating at the X-band frequency (ν=9.4 GHz) with a magnetic field modulation of 100 kHz. The magnetic modulation width was 5×10^{-4} T and the time constant was 0.1 s.

4.2.2.3 SHG measurements

Second-harmonic generation of the poled glass samples was measured using the Maker fringe method. A pulsed Nd:YAG laser (Spectra Physics. GCR-11) operated in a Q-switched mode with a 10 Hz repetition rate was used as a light source. After the pulse at 1064 nm with 9 ns duration was p-polarized, it was incident on the sample which was rotated around an axis perpendicular to the incident plane so that angle of incidence varied from $-65°$ to 65°. The beam diameter was 1 mm. The output light from the poled glass sample was passed through IR cut filters and a monochromator (Spex, 270M) to eliminate the fundamental wave at 1064 nm completely. The second-harmonic wave at 532 nm was detected with a photomultiplier (Hamamatsu Photonics, R955). The signal from the photomultiplier was integrated by using a digital oscilloscope (Hewlett Packard, 54522A). The second-harmonic intensity from a Y-cut quartz with a thickness of

1.046mm and $d_{11} = 0.34$ pm/V was also measured for the purpose of determining input light power. The experimental second-harmonic intensity thus obtained was analyzed by the Maker fringe theory to determine the second-order nonlinear susceptibility, $\chi^{(2)}$, and thickness of the SHG-active layer, L.

4.2.3 Results

Figure 4.5 shows relation between second-harmonic intensity and angle of incidence, namely, Maker fringe pattern for the $20WO_3{\cdot}80TeO_2$ glass with a thickness of 0.50 mm poled at 240 °C. The closed circles and solid curve denote the experimental and theoretical Maker fringe patterns, respectively. Using the Maker fringe theory, the theoretical one was drawn with the refractive indices at 532 nm, $n_{532} = 2.168$, and 1064 nm, $n_{1064} = 2.105$. Thus obtained fitting parameters are a non-zero component of second-order nonlinear susceptibility tensor, $\chi^{(2)}_{33} = 1.2$ pm/V, and a thickness of SHG-active layer, $L = 6.3\,\mu$m.

Figure 4.6 shows the second-harmonic intensity as a function of the etched thickness from the anode-side surface. The intensity decreased to about a tenth part when the anode-side surface was removed mechanically with a thickness of 10 μm, and completely disappeared with a thickness of 19 μm removed. These facts indicate that the second-order nonlinearity was induced mainly beneath the anode-side surface.

Figure 4.7 shows the variation of O 1s photoelectron spectrum with a depth from the anode-side surface. For a comparison, the spectrum of as-annealed specimen is depicted at the bottom. The O 1s main peak was observed at 530 eV in all the spectra, indicating no significant change in an electronic state of oxygen after poling, whereas a shoulder appeared at around 532 eV, i.e., on the larger binding energy side of the main peak, for the anode-side surface. The intensity of this shoulder gradually decreased when the surface was etched mechanically up to 20 μm. Himei *et al.* re-

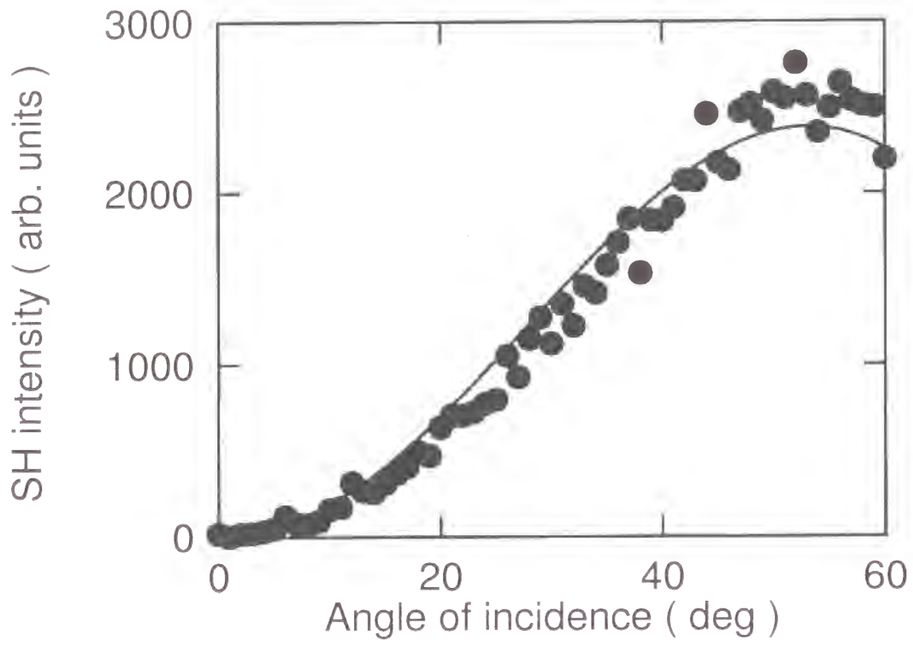

Fig. 4.5: Dependence of second-harmonic intensity on angle of incidence, namely, Maker fringe pattern for poled $20WO_3{\cdot}80TeO_2$ glass with a 0.50 mm thick. The poling temperature was 240 °C. The closed circles and solid curve denote the experimental and theoretical Maker fringe patterns, respectively. The theoretical one was drawn with $\chi^{(2)}_{33} = 1.2\,\mathrm{pm/V}$ and $L = 6.3\,\mu\mathrm{m}$.

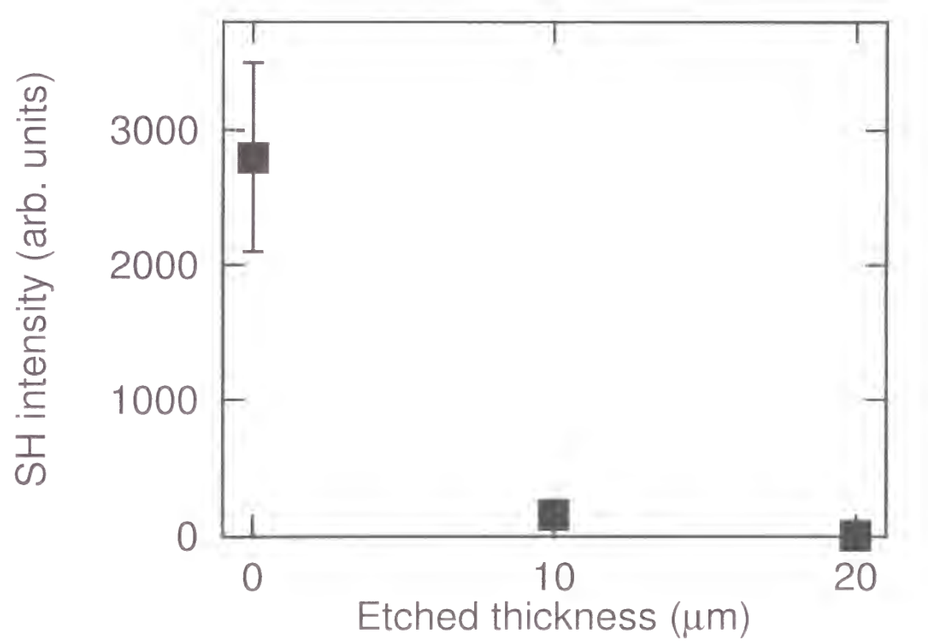

Fig. 4.6: Second-harmonic intensity as a function of etched thickness from the anode side surface of the poled $20WO_3{\cdot}80TeO_2$ glass.

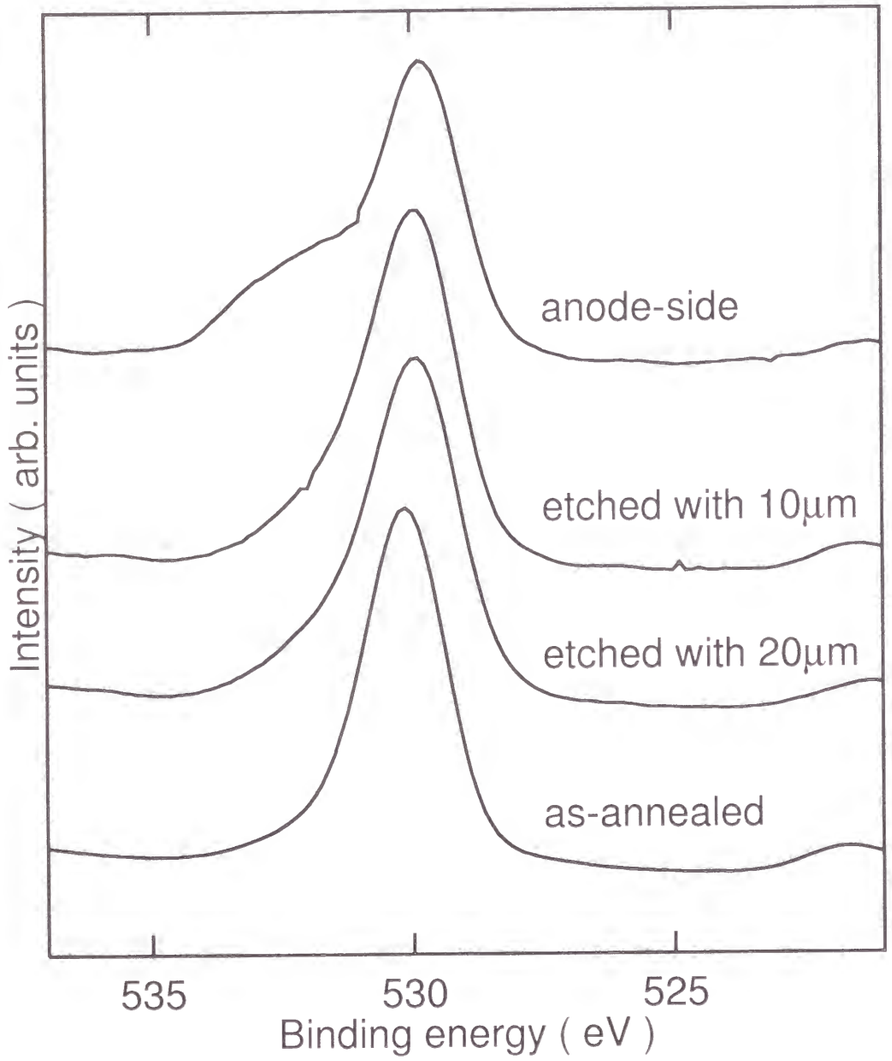

Fig. 4.7: Variation of O 1s photoelectron spectrum with a depth from the anode-side surface for the poled $20WO_3{\cdot}80TeO_2$ glass. For a comparison, the spectrum of the as-annealed glass is shown at the bottom.

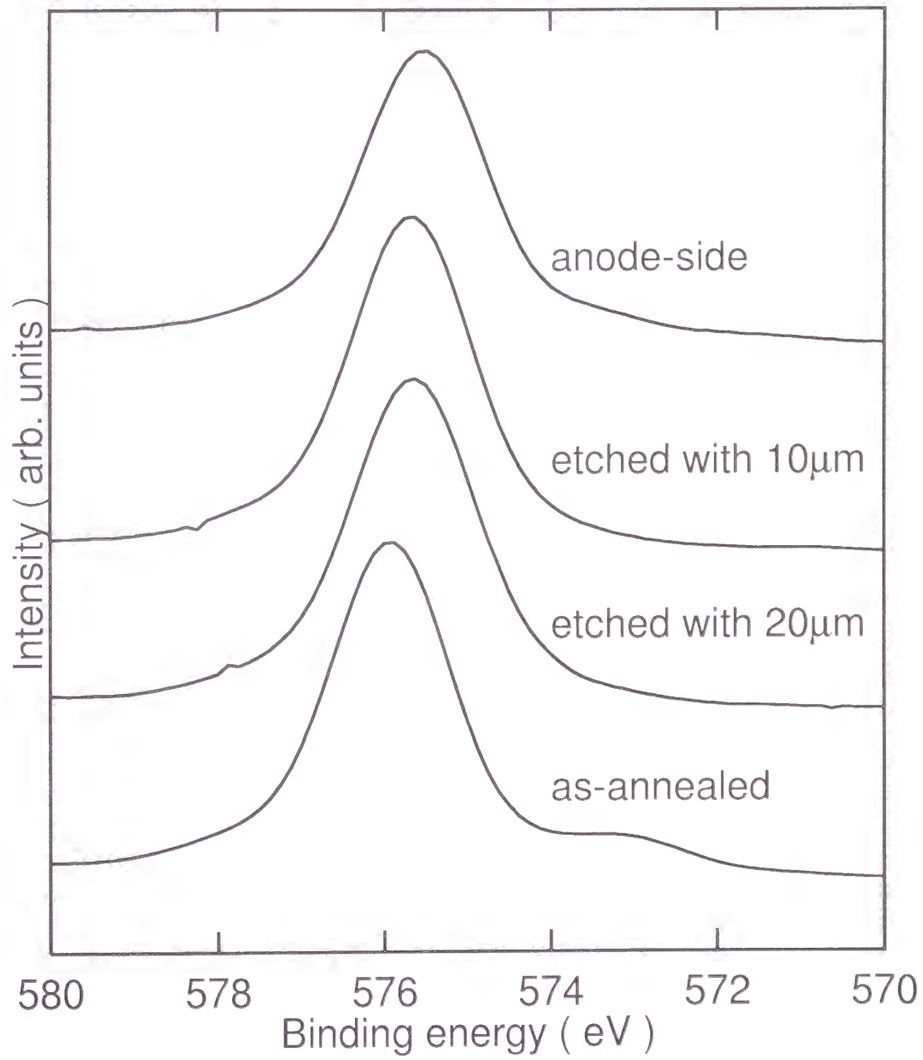

Fig. 4.8: Variation of Te $3d_{5/2}$ photoelectron spectrum with a depth from the anode-side surface for the poled $20WO_3{\cdot}80TeO_2$ glass.

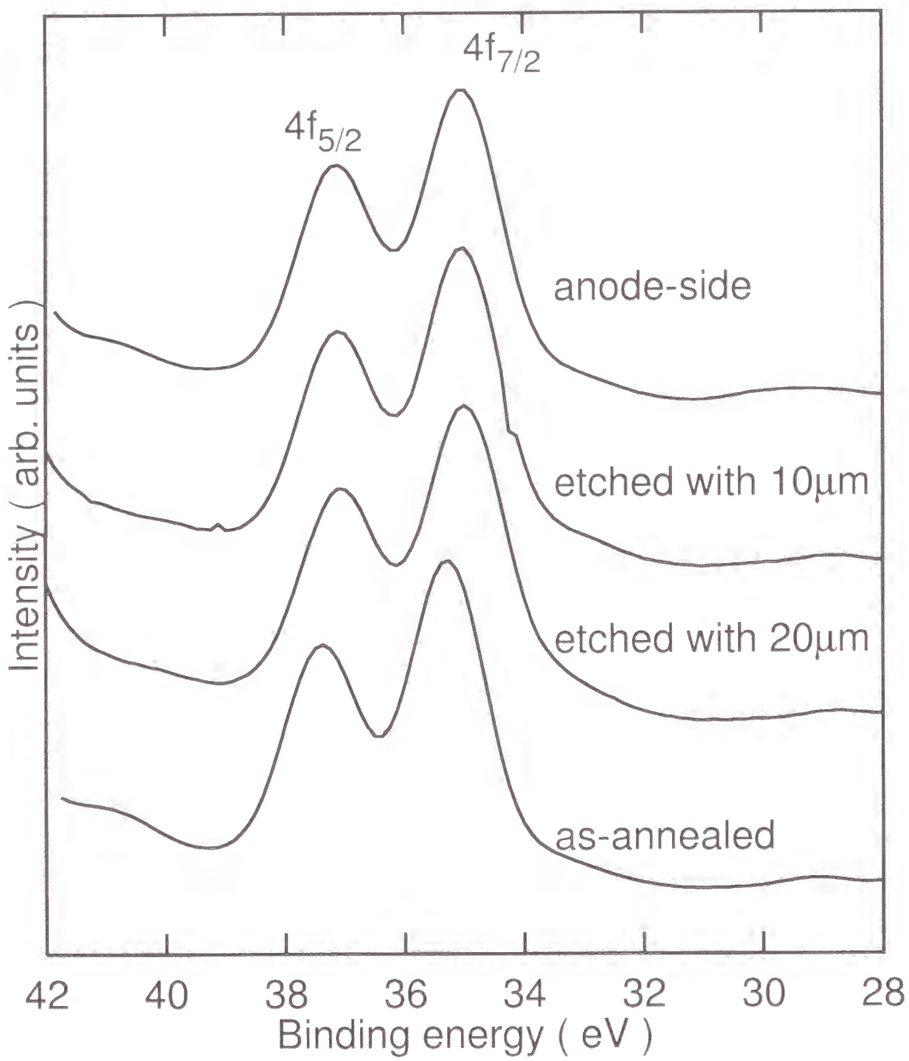

Fig. 4.9: Variation of W 4f photoelectron spectrum with a depth from the anode-side surface for the poled $20WO_3{\cdot}80TeO_2$ glass.

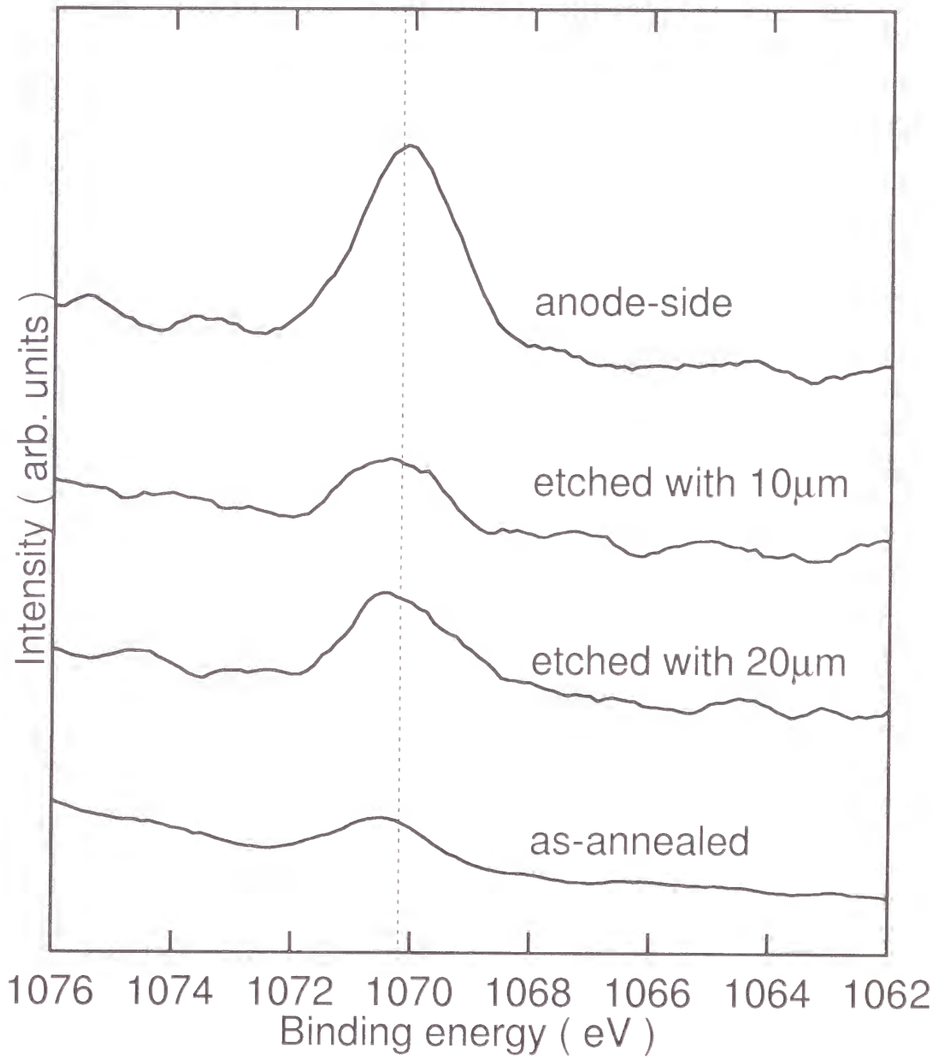

Fig. 4.10: Variation of Na 1s photoelectron spectrum with a depth from the anode side surface for the poled $20WO_3{\cdot}80TeO_2$ glass.

ported for alkali tellurite glasses that O 1s peak of the surface exposed in air can be decomposed into two components at 530 and 532 eV, and that the latter was assigned to the oxygen atoms in adsorbed compounds such as carbonates or hydroxides [15]. This is because only a single and symmetric Gaussian-Lorentzian O 1s peak at 530 eV was observable for the fresh surface fractured in a vacuum for the same glasses. Such behavior of O 1s photoelectron peak in tellurite glasses is different from that in silicate glass systems; the latter has intrinsic two components at 530 and 532 eV assignable to non-bridging and bridging oxygen, respectively, irrespective of surface condition [16]. Himei *et al.* also suggested that the single component of O 1s photoelectron in tellurite glasses is due to an equalization of the electronic density in the valence shell between bridging and non-bridging oxygens. However, in the present results, the component at around 532 cm^{-1} monotonically decreased with an increase of etched depth. Therefore, it is difficult to identify simply the O1s photoelectron at around 532 eV as compounds adsorbed during poling. Based on this result, the poling effect on the glass composition at the surface will be discussed in terms of the concentration ratio of glass-constituents except for the O element.

Figures 4.8 and 4.9 show the variation of Te $3d_{\frac{5}{2}}$ and W 4f photoelectron spectra with a depth from the anode-side surface. As for Te and W elements, no evident change in shape and position of the photoelectron peaks was observed after poling and etching.

In addition to the intentional glass-constituents, the photoelectron peak of Na element was observed for all the specimens, as shown in Fig. 4.10. The intensity of Na 1s peak at the anode-side surface is larger than as-annealed one. The increase in intensity at the anode-side is attributable to penetration of Na^+ ions into the tellurite glass sample from a borosilicate glass plate during poling. The concentration ratio of Na to Te was calculated using the photoelectron peak area divided by the atomic sensitivity. The ratios thus estimated are shown as a function of the distance from the original anode-side surface in Fig. 4.11. When the initial surface

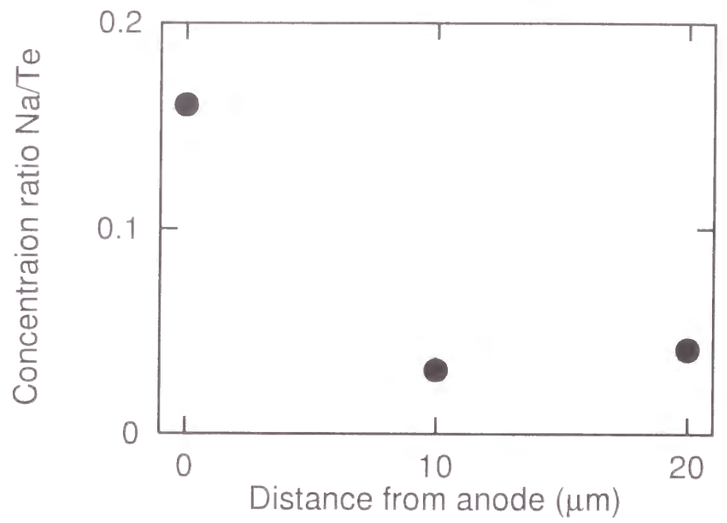

Fig. 4.11: Depth profile of the concentration ratio of Na/Te from the anode side surface for the $20WO_3{\cdot}80TeO_2$ glass.

was removed with a thickness of 10 μm, the ratio of Na/Te drastically decreased. It is clear that the penetration of a large number of Na^+ ions into the anode-side surface region, where the SHG-active structure existed as indicated in Fig. 4.6, was brought about by poling.

Table 4.3 lists the concentration ratio of Na to Te for the as-annealed and poled $20WO_3{\cdot}80TeO_2$ glass surfaces. Although the value of Na/Te ratio at the cathode-side increased by about four times compared with that of the as-annealed glass, the ratio at the anode-side is larger by nine times than the original one. Here, it should be mentioned that a small amount of Na^+ ions in as-annealed glass were identified as impurities. These suggest that the concentration of Na^+ ions becomes a maximum in the vicinity of the anode-side surface.

IR reflectance spectra at the surfaces of the as-annealed and poled glasses are shown in Fig. 4.12. In the tellurite glass systems, Mochida *et al.* reported the transmission spectra from 4000 to 350 cm^{-1} and assigned some peaks observed in a wave number range of 600-700 cm^{-1} to the vibrational modes of Te-O bonds in TeO_4 trigonal bipyramid or TeO_3 trigonal

Table 4.3: Concentration ratio of Na to Te for $20WO_3{\cdot}80TeO_2$ glass.

	Concentration ratio
	Na/Te
anode-side	0.16
cathode-sid	0.068
as-annealed	0.018

pyramid [1]. On the other hand, Bürger *et al.* assigned an absorption around 3000 cm^{-1} to free OH groups [17]. As shown in Fig. 4.12, there is no obvious change in the reflectance at the wave number from 4000 to 400 cm^{-1} after poling. This suggests that poling does not remarkably affect glass network and OH content in the WO_3-TeO_2 glass system.

The ESR spectra are shown for both poled and as-annealed $20WO_3{\cdot}80TeO_2$ glasses in Fig. 4.13.

The decay of the second-harmonic intensity is shown in Fig. 4.14 for the poled $20WO_3{\cdot}80TeO_2$, $30ZnO{\cdot}70TeO_2$ and $30NaO_{\frac{1}{2}}{\cdot}70TeO_2$ glasses with a thickness of 1.00 mm. The poling temperature was set at 280 °C for both the $20WO_3{\cdot}80TeO_2$ and $30ZnO{\cdot}70TeO_2$ glasses. whereas the $30NaO_{\frac{1}{2}}{\cdot}70TeO_2$ glass was poled at 220 °C. These data were fitted using the stretched exponential decay function. presented as Eq. (2.1). The fitting parameters τ and β are listed in Table. 4.4. τ for the $20WO_3{\cdot}80TeO_2$ glass is 4.0×10^2 h. which is larger than 1.0×10 h for the $30NaO_{\frac{1}{2}}{\cdot}70TeO_2$ glass and much smaller than 8.0×10^4 h for the $30ZnO{\cdot}70TeO_2$ glass.

Table 4.4: Relaxation time τ and stretched exponential parameter β for $20WO_3{\cdot}80TeO_2$ $30ZnO{\cdot}70TeO_2$ and $30NaO_{\frac{1}{2}}{\cdot}70TeO_2$ glasses.

Glass composition	Fitting parameters	
	τ (h)	β
$20WO_3{\cdot}80TeO_2$	4.0×10^2	0.6
$30ZnO{\cdot}70TeO_2$	8.0×10^4	1
$30NaO_{\frac{1}{2}}{\cdot}70TeO_2$	1.0×10	0.6

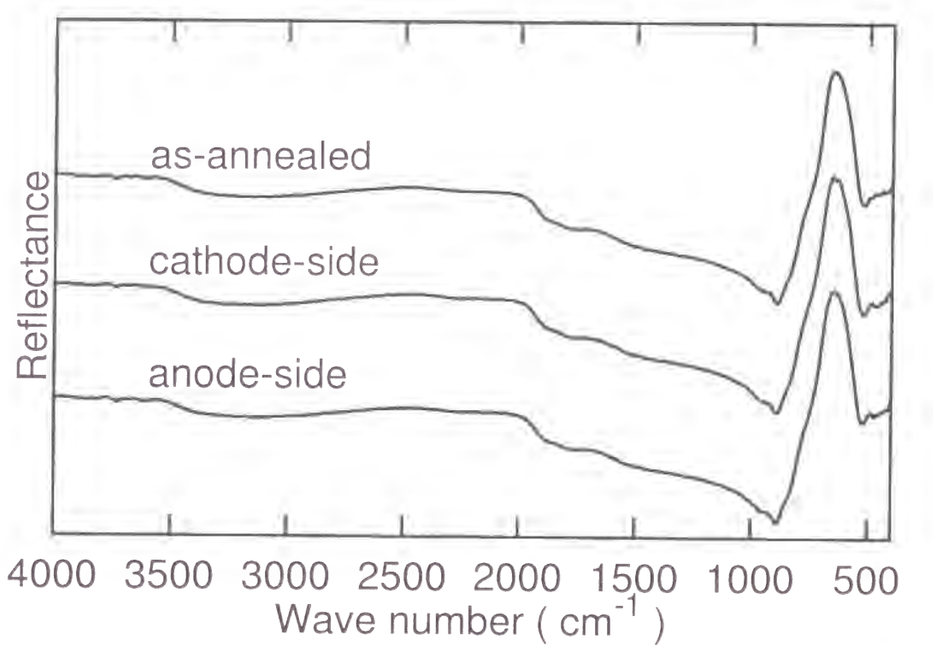

Fig. 4.12: Reflectance spectra from 4000 to 400 cm^{-1} for $20WO_3{\cdot}80TeO_2$ glass.

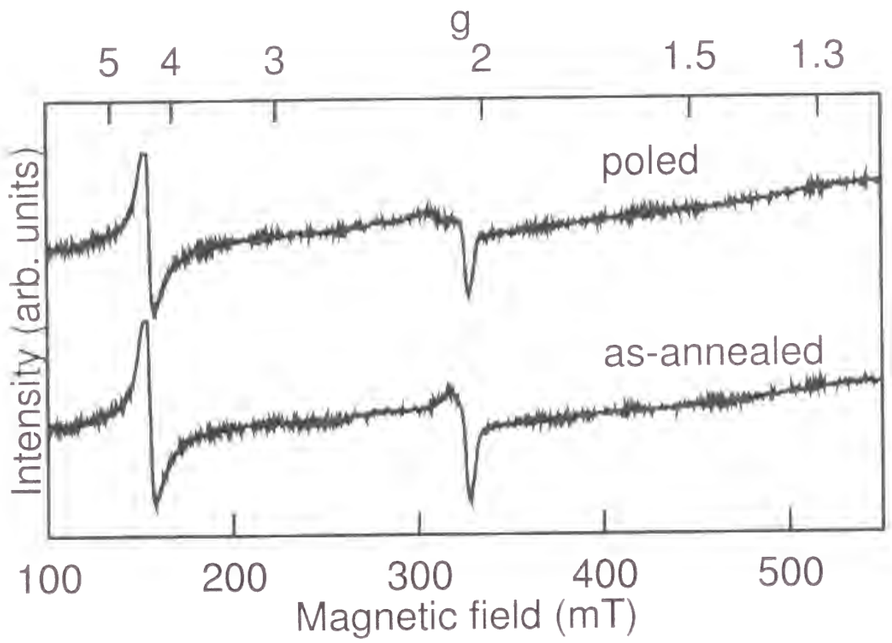

Fig. 4.13: ESR spectra of as-annealed and poled $20WO_3{\cdot}80TeO_2$ glasses at room temperature.

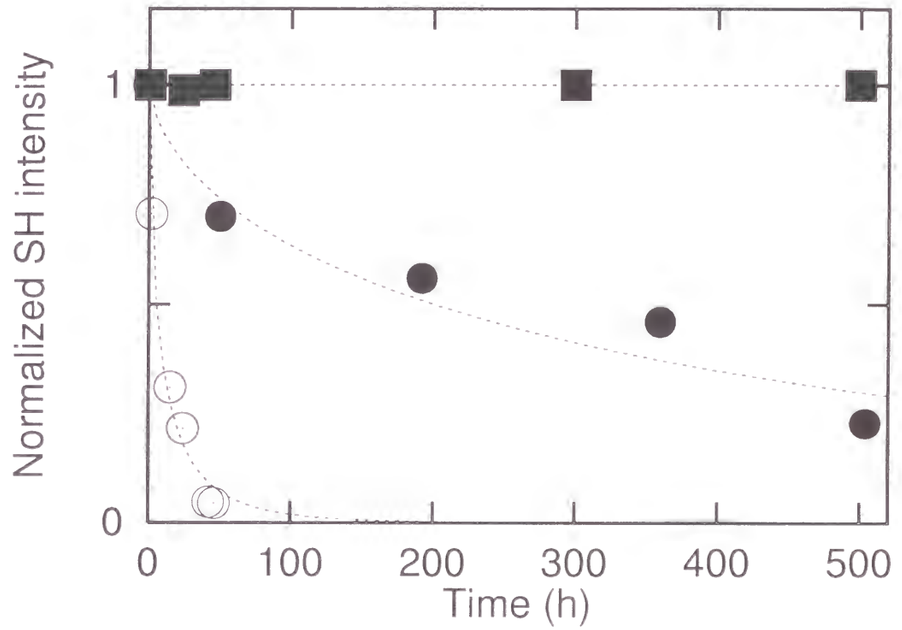

Fig. 4.14: Relaxation behavior of second-harmonic intensity for $20WO_3{\cdot}80TeO_2$ (closed circles), $30ZnO{\cdot}70TeO_2$ (closed squares) and $30NaO_{\frac{1}{2}}{\cdot}70TeO_2$ (open circles) glasses. The poling was performed at 280 °C for both $20WO_3{\cdot}80TeO_2$ and $30ZnO{\cdot}70TeO_2$ glasses. The $30NaO_{\frac{1}{2}}{\cdot}70TeO_2$ glass was poled at 220 °C. The experimental data were fitted using Eq. (2.1) with parameters τ and β listed in Table 4.4.

4.2.4 Discussion

It has been reported for various kinds of oxide glasses that the poling induced the second-order nonlinearity preferentially in a thin layer beneath an anode-side surface. Similarly, it was observed in the $20WO_3{\cdot}80TeO_2$ glasses that a SHG-active region was restricted in the vicinity of an anode-side, as shown in Fig. 4.6. One of the possible explanations for the localization of the second-order nonlinearity is as follows. When a dc voltage is applied during poling, relatively mobile cations in oxide glasses such as alkali ions drift toward a cathode in order to screen the applied voltage. Because of non-bridging oxygens with less mobility, the drift of mobile cations results in a formation of a cation-depleted layer with a net minus charge at the anode-side. Then, the depleted region induces the second-order nonlinear susceptibility via the $\chi^{(3)} \cdot E_{dc}$ process.

On the other hand, the WO_3-TeO_2 glass system does not contain mobile cations with mono- and divalent oxidation states as nominal glass-constituents. However, according to the XPS results, the concentration ratio of Na to Te increased in a thin layer at the anode-side after poling. In other words, the poling caused the penetration of Na^+ ions from the borosilicate glass plate followed by an accumulation in the vicinity of the anode-side. Therefore, it is a possible explanation for the localization of second-order nonlinearity at the anode-side surface of poled $20WO_3{\cdot}80TeO_2$ glasses that the penetrated Na^+ ions screen the applied external voltage and consequently create a static electric field in the vicinity of the anode-side.

Oxide glass materials including transition metal ions which are stable with more than two oxidation states, namely, mixed valence states, in the glass, tend to exhibit electronic conduction via the electron hopping process through the mixed-valence cations. For instance, when the TeO_2-WO_3 glass is fabricated by melting in a hydrogen atmosphere followed by a rapid cooling, the resultant glass contains both W^{6+} and W^{5+} ions, and exhibits high electronic conductivity at elevated temperatures.

As for the as-annealed and poled $20WO_3{\cdot}80TeO_2$ glasses employed in the present work, no ESR peak assignable to W^{5+} ion was observed. Judging from this fact, such electronic conduction via valence-exchange between W^{6+} and W^{5+} ions did not occur during poling, and never contributed to the induction of second-order nonlinearity.

As seen in Fig. 4.12, the IR reflectance at the wave number of 4000-400 cm^{-1} from the surfaces of poled $20WO_3{\cdot}80TeO_2$ glass is similar to that of the as-annealed one. The reflectance peaks in the lower wave number range are assignable to the vibration of Te-O bonds, as mentioned above. Hence, it is suggested that the poling did not change the glass network composed of TeO_n structural units. In contrast, for the $30ZnO{\cdot}70TeO_2$ glass poled at 280 °C, the IR reflectance from the anode-side surface showed a decrease in intensity at around 635 cm^{-1} compared with the as-annealed one, indicating that poling treatment brought about the breaking down of the glass network. A possible explanation for the drastic change in IR reflectance is the depletion of Zn^{2+} ions caused by poling which was observed by XPS measurements. Another explanation is that the $30ZnO{\cdot}70TeO_2$ glass was poled at higher temperature than 240 °C at which the poling of $20WO_3{\cdot}80TeO_2$ glass was performed in the present work.

Relaxation behavior of second-order nonlinearity significantly depends on the glass composition, as demonstrated in Fig. 4.14. This dependence provides a useful information about the SHG-active structure as well as its relaxation process. The relaxation time of poled $20WO_3{\cdot}80TeO_2$ glass is much shorter than that of $30ZnO{\cdot}70TeO_2$ glass. Supposing that an induction of second-order nonlinearity is made through the process of $\chi^{(2)} = 3\,\chi^{(3)} \cdot E_{dc}$, the decay of second-harmonic intensity with time corresponds to a decrease in E_{dc}. That is, the difference in the relaxation time between $20WO_3{\cdot}80TeO_2$ and $30ZnO{\cdot}70TeO_2$ glasses is describable in terms of the difference in kinds of cations which participate in the formation of E_{dc}. Consequently, it can be concluded that cations such as the implanted Na^+ ions with larger mobility than Zn^{2+} ions take part in the formation of E_{dc} in the WO_3-TeO_2 glass system. On the other hand,

the relaxation time of the $20WO_3{\cdot}80TeO_2$ glass is longer than that of the $30NaO_{\frac{1}{2}}{\cdot}70TeO_2$ glass. In order to discuss the difference in relaxation behavior between poled $20WO_3{\cdot}80TeO_2$ and $30NaO_{\frac{1}{2}}{\cdot}70TeO_2$ glasses, it is needed to take into account a difference in the poling temperature; the poling temperature of the former glass is higher by 60 °C than the temperature where the poling of the latter was performed. Thus, further studies on the effect of poling temperature on relaxation time are needed to clarify the difference in relaxation time between them.

4.2.5 Conclusions

Surface structure was examined for the poled $20WO_3{\cdot}80TeO_2$ glass with second-order nonlinearity. It was observed that the second-order nonlinearity was induced mainly beneath an anode-side glass surface. This fact indicates that the $\chi^{(2)} = 3\,\chi^{(3)}{\cdot}E_{dc}$ process is the dominant source of induction of second-order nonlinearity. The detail investigation of the anode-side surface was carried out using the X-ray photoelectron and IR reflectance spectroscopies. The XPS data exhibit the penetration of Na^+ ions followed by their accumulation in the vicinity of the anode-side; such Na^+ ions come from the borosilicate glass plate which was placed between the tellurite glass and an anode. On the other hand, there was no obvious change of IR reflectance after poling. This implies that poling does not affect glass network significantly for the poled $20WO_3{\cdot}80TeO_2$ glass, which is different from the $30ZnO{\cdot}70TeO_2$ glass poled at higher temperature. A possibility of electronic conduction via valence-exchange between W^{6+}-W^{5+} ions was also examined by the electron spin resonance technique. As a result, there were no W^{5+} ions in both an as-annealed and poled glasses. As revealed from the decay of second-harmonic intensity with time, the difference in relaxation time among WO_3-TeO_2 , ZnO-TeO_2 , and Na_2O-TeO_2 glass systems supports that the penetrated Na^+ ions play an important role in the formation of E_{dc} accompanied with the second-order nonlinearity.

References

[1] N. Mochida, K. Takahashi, K. Nakata, and S. Shibusawa, J. Ceram. Soc. Jpn. **86**, 316 (1978).

[2] H. Bürger, W. Vogel, and V. Kozhukharov, Infrared Phys. **25**, 395 (1985).

[3] A. Narazaki, K. Tanaka, K. Hirao, and N. Soga, J. Appl. Phys. **83**, 3986 (1998).

[4] A. Narazaki, K. Tanaka, K. Hirao, and N. Soga, J. Am. Ceram. Soc. **81**, 2735 (1998).

[5] A. Narazaki, K. Tanaka, K. Hirao, and N. Soga, J. Appl. Phys. **85**, 2046 (1999).

[6] D. E. Carlson, J. Am. Ceram. Soc. **57**, 291 (1974).

[7] D. E. Carlson, K. W. Hang, and G. F. Stockdale, J. Am. Ceram. Soc. **57**, 295 (1974).

[8] X. C. Long, R. A. Myers, and S. R. J. Brueck, Opt. Lett. **19**, 1819 (1994).

[9] O. Sugihara, T. Hirama, H. Fujimura, and N. Okamoto, Opt. Rev. **3**, 150 (1996).

[10] P. G. Kazansky, A. Kamal, and P. S. J. Russell, Opt. Lett. **18**, 1141 (1993).

[11] H. Nasu, H. Okamoto, A. Mito, J. Matsuoka, and K. Kamiya, Jpn. J. Appl. Phys. **32**, 180 (1993).

[12] T. G. Alley, R. A. Myers, and S. R. J. Brueck, in Bragg Gratings, Photosensitivity, and Poling in Glass Fibers and Waveguides: Applications and Fundamentals **17**, 293 (1997).

[13] H. Imai, S. Horinouchi, N. Asakuma, K. Fukao, D. Matsuki, H. Hirashima, and K. Sasaki, J. Appl. Phys. **15**, 5415 (1998).

[14] S. H. Kim, T. Yoko, and S. Sakka, J. Am. Ceram. Soc. **76**, 2486 (1993).

[15] Y. Himei, Y. Miura, T. Nanba, and A. Osaka, J. Non-Cryst. Solids **211**, 64 (1997).

[16] S. Matsumoto, Y. Miura, T. Nanba, and A. Osaka, Proc. 17th Int. Congress on Glass **3**, 72 (1995).

[17] B. V. Tatarintsev and A. K. Yahnkind, Sov. J. Opt. Technol. **42**, 210 (1975).

Chapter 5

Second-order nonlinearity in transparent tellurite glass-ceramics

5.1 Second-harmonic generation in glass-ceramics containing $BaTiO_3$ crystallites

5.1.1 Introduction

In the previous chapters, the poling effect on tellurite glass structure and the resultant second-order nonlinearity have been investigated when poling was performed at below the glass transition temperature. Another interesting application of poling to amorphous materials is demonstrated in Chapter 5.2; an attempt is made to control the crystallization behavior of tellurite glasses by means of the application of a high voltage around and above the glass transition temperature. In this section, a modification of the Maker fringe equation which was presented in Chapter 1 is carried out to analyze the second-harmonic generation from glass-ceramics, in particular, the surface-crystallized ones.

Transparent glass-ceramics containing ferroelectric crystalline phases have been attracting a lot attention because of their potential application to optical devices, for instance, an excellent frequency converter utilizing large second-order nonlinearity, as well as easiness to fabricate [1–8]. However, the efficiency of second-harmonic generation has been limited due to a relatively low transparency as well as a restriction of the ferroelectric

transition by a rigid glass matrix [9], the size effect [7], and so forth. Therefore, for the purpose of achieving large second-order nonlinearity and high transparency simultaneously, it is desirable that the difference in refractive index between glass matrix and crystallite is small enough to reduce the light scattering near boundaries. Recently, Komatsu *et al.* [10] succeeded in preparing transparent glass-ceramics containing $BaTiO_3$ crystallites from tellurite-based glasses; the refractive indices of tellurite glass and $BaTiO_3$ are almost the same. Tanaka *et al.* [4,11] subsequently found that surface crystallization of $BaTiO_3$ as well as other crystalline phases occurred in the same glass system and observed second-harmonic generation in the glass-ceramics, although the ratio of lattice parameters, c/a, of $BaTiO_3$ crystals precipitated was closer to the value of the paraelectric cubic phase than that of the ferroelectric tetragonal phase as estimated from the position of the X-ray diffraction line. Nonetheless, an origin of the second-harmonic generation has still remained unclear. According to the simple relation between polarization and electric field, the structure of a solid that shows the second-order nonlinearity is restricted to that without the inversion symmetry. Based on this restriction, the origin of the second harmonic generation in such a glass-ceramic material is attributable to a slight tetragonal strain of precipitated $BaTiO_3$, any other crystalline phases, or a stress with $C_{\infty v}$ symmetry caused by the surface crystallization.

In this section, it is tried to make clear what factors play an important role in the second-order nonlinear phenomenon of the glass-ceramics containing $BaTiO_3$ crystallites by comparing the results of second-harmonic generation with those of glass-ceramics without a ferroelectric crystalline phase. The SrO-TiO_2-TeO_2 glass system is chosen for comparison because $SrTiO_3$ is not ferroelectric at room temperature even if it is precipitated. Accordingly, a modified Maker fringe equation is applied to the $BaTiO_3$-based glass-ceramics, leading to the successful evaluation of the magnitude of second-order nonlinear susceptibility.

5.1.2 Experimental procedure

5.1.2.1 Sample preparation

Powders of reagent-grade $BaCO_3$, $SrCO_3$, TiO_2 and TeO_2 were mixed thoroughly to make nominal compositions of $15BaO{\cdot}15TiO_2{\cdot}70TeO_2$ and $15SrO{\cdot}15TiO_2{\cdot}70TeO_2$ (in mol%). The mixture was melted in a platinum crucible at 1000 °C for 30 min, and then the melt was poured into an alumina boat. The inside and the surface of the samples were amorphous, as ascertained by both powder and thin-film X-ray diffraction (XRD) measurements (Rigaku, RINT1400 and RINT2500) with Cu Kα radiation. The diffraction intensities were measured from 10° to 70° in 2θ for each measurement. After the glass samples were annealed for 30 min at 380 °C, which is around the glass transition temperature determined by differential thermal analysis (Rigaku, TG-DTA8112BH) for both compositions, they were cut into a plate of 5 mm×7 mm×1 mm and polished with CeO_2 powder for optical measurements.

Glass-ceramics were fabricated as follows. $15BaO{\cdot}15TiO_2{\cdot}70TeO_2$ and $15SrO{\cdot}15TiO_2{\cdot}70TeO_2$ glasses were put in electric furnaces and heated from room temperature to 415 and 455 °C, respectively. The heat treatment was performed for 0.5 to 12 h, followed by gradual cooling to room temperature in the furnaces (the cooling rate ≈ 5 K/min). In Table 5.1 are listed the heat treatment conditions along with the notation of samples, which is hereafter referred to.

Table 5.1: Heat treatment conditions performed in the preparation of glass-ceramics from $15BaO{\cdot}15TiO_2{\cdot}70TeO_2$ and $15SrO{\cdot}15TiO_2{\cdot}70TeO_2$ glasses.

Notation of glass-ceramics	Original glass composition (mol%)	Temperature (°C)	Time (h)
BTO-0.5	$15BaO{\cdot}15TiO_2{\cdot}70TeO_2$	415	0.5
BTO-12	$15BaO{\cdot}15TiO_2{\cdot}70TeO_2$	115	12
STO-0.5	$15SrO{\cdot}15TiO_2{\cdot}70TeO_2$	455	0.5
STO-12	$15SrO{\cdot}15TiO_2{\cdot}70TeO_2$	455	12

5.1.2.2 Characterization of heat-treated specimens

Thin-film XRD measurements were carried out to identify crystalline phases precipitated at the surfaces of the resultant heat-treated specimens. In order to identify phases crystallized below the surface, diffraction patterns were also obtained for the specimens after the surface was etched mechanically.

The size of the crystals was estimated using a scanning electron microscope (SEM, Hitachi, S-510). The surface and fractured cross section were also observed.

Second-harmonic generation was measured using the Maker fringe method. A Q-switched pulsed Nd:YAG laser (Spectra-Physics, GCR-11) was operated as a light source at 1064 nm with a duration of 9 ns. The *p*- or *s*-polarized fundamental light at 1064 nm was incident on a sample, which was rotated around an axis perpendicular to the incident plane. The fundamental wave was mostly eliminated by using infrared (IR) cut filters behind the sample, whereas the second-harmonic wave generated in the sample was passed thorough a polarizer, which was *p*- or *s*-polarized. Thus, only the polarized second-harmonic light at 532 nm was detected by means of a monochromator (Spex, 270M) equipped with a photomultiplier (Hamamatsu Photonics, R955). The signal from the photomultiplier was accumulated using a digital oscilloscope (Hewlett Packard, 54522A). Then, the data were obtained by computing the integration of stored wave form. For the purpose of acquiring the input light power, Y-cut quartz with the thickness of 1.046 mm and d_{11} of 0.34 pm/V was employed as a reference material.

5.1.3 Results

Figure 5.1 shows differential thermal analysis (DTA) curves for $15BaO{\cdot}15TiO_2{\cdot}70TeO_2$ and $15SrO{\cdot}15TiO_2{\cdot}70TeO_2$ glasses. For the measurements, the glass samples were pulverized. The former glass exhibits

the glass transition temperature, T_g = 398 °C and temperature of crystallization peak, T_{xp} = 452 °C, whereas the latter has T_g = 414 °C and T_{xp} = 490 °C. The $15BaO{\cdot}15TiO_2{\cdot}70TeO_2$ and $15SrO{\cdot}15TiO_2{\cdot}70TeO_2$ glasses were heat-treated around 420 and 460 °C, respectively, to prevent a loss of transparency due to overgrowth of crystalline phases.

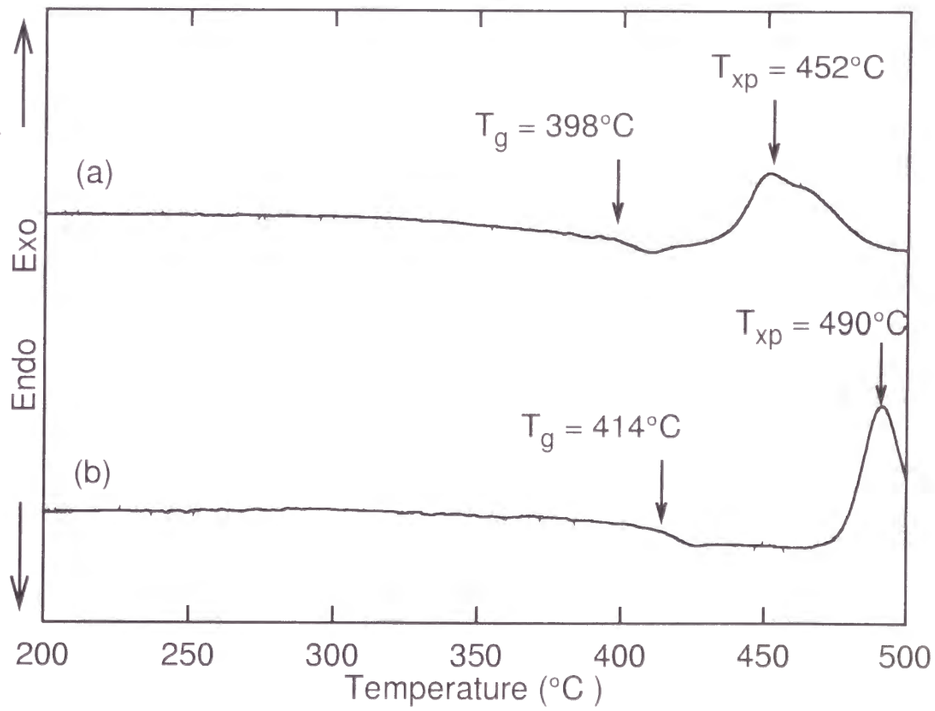

Fig. 5.1: Differential thermal analysis curves for pulverized (a) $15BaO{\cdot}15TiO_2{\cdot}70TeO_2$ and (b) $15SrO{\cdot}15TiO_2{\cdot}70TeO_2$ glasses. T_g and T_{xp} indicate temperatures of glass transition and crystallization, respectively.

Figures 5.2 (a) and (b) show thin-film XRD patterns of the glass-ceramics BTO-0.5 and BTO-12 designated in Table 5.1, respectively. The patterns from the top to the bottom (Fig. 5.2(b)) were measured after mechanical etching with a depth of 0, 50 and 140 μm from the original surface. Irrespective of the heat treatment time, the as-prepared glass-ceramic exhibits four main diffraction peaks at $2\theta = 23.4°$, $27.1°$, $31.4°$ and $53.1°$, which are assigned to TeO_2, $BaTeO_3$, $BaTiO_3$ and $TeO_2(H_2O)_n$, respectively. The line at $2\theta = 31.4°$ is attributable to the Bragg reflection from (101) or (110) plane of $BaTiO_3$; it is located between diffraction angles corresponding to cubic and tetragonal phases of $BaTiO_3$ reported in JCPDS cards. In addition to the above-listed main diffraction lines, a small line can be observed at $2\theta = 65.3°$. This line is probably assigned to the reflection from (202) or (220) plane of $BaTiO_3$, although the discrepancy from the value in the JCPDS cards is somewhat large. From the change in diffraction intensity with the depth etched mechanically from the initial surface, the behavior of surface crystallization can be summarized as follows. First, $BaTiO_3$ phase keeps its orientation as far as the depth of 140 μm. Second, $TeO_2(H_2O)_n$ crystal is present only at the near-surface region, the thickness of which is smaller than 50 μm. Finally, the crystalline phase that is observable at the deepest region from the surface is $BaTeO_3$.

A scanning electron micrograph (SEM) of the surface of BTO-12 is shown in Fig. 5.3. The SEM observation reveals that the precipitated particle has a diameter of about 0.5-1.5 μm, whereas the particle size is distributed in a range of 0.2-0.9 μm in the case of BTO-0.5. Figures 5.4 (a) and (b) show SEMs of fractured cross sections for BTO-0.5 and BTO-12, respectively. A clear boundary between glass and crystallized layer is recognized for both glass-ceramics. From this observation, the thickness of surface crystallized layer is estimated to be about 10 μm and over 100 μm for BTO-0.5 and BTO-12, respectively. This result is coincident with that derived from the thin film XRD.

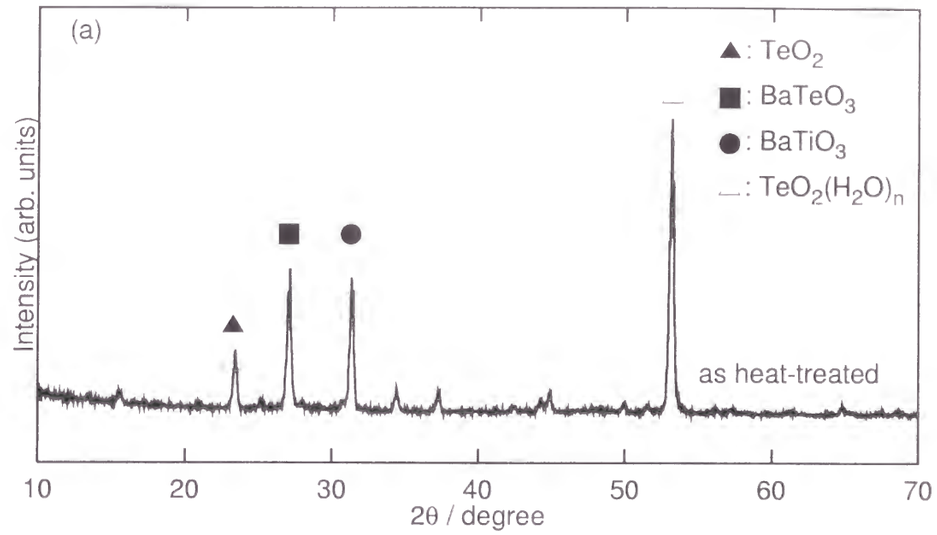

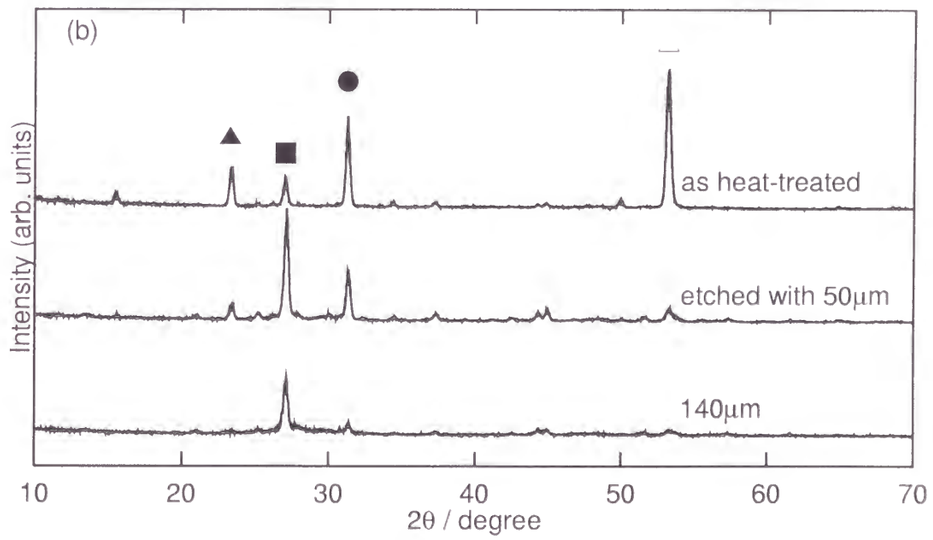

Fig. 5.2: Thin-film X-ray diffraction (XRD) patterns for (a) BTO-0.5 and (b) BTO-12. The XRD measurements of BTO-12 were carried out for specimens the surface of which was etched mechanically as well as the as-heated specimen. The closed circle and square represent $BaTiO_3$ and $BaTeO_3$, respectively. The open and closed triangles denote $TeO_2(H_2O)_n$ and TeO_2, respectively.

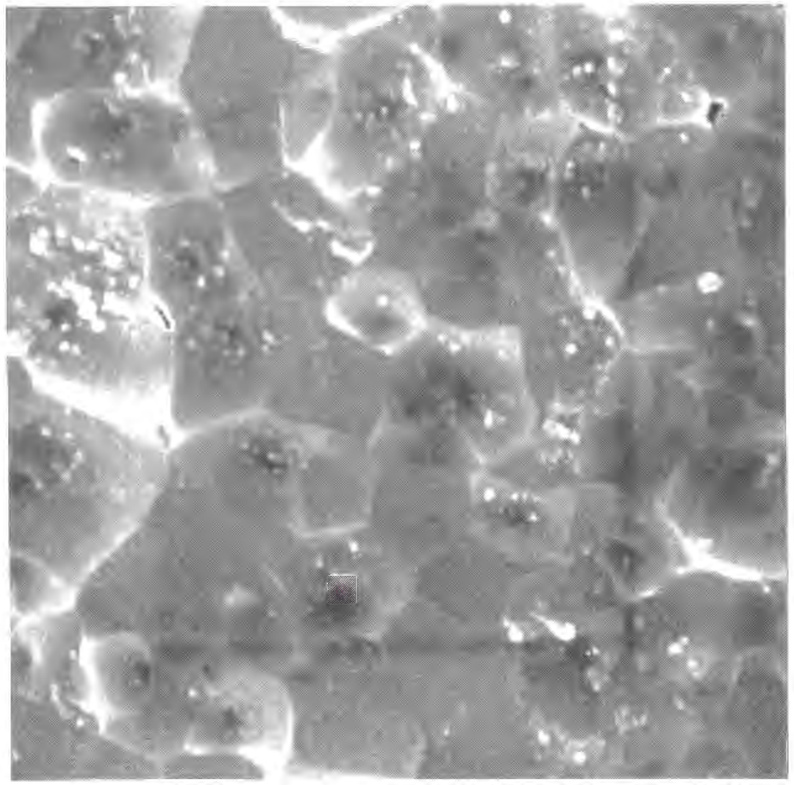

Fig. 5.3: Scanning electron micrograph of the surface of BTO-12.

(a)

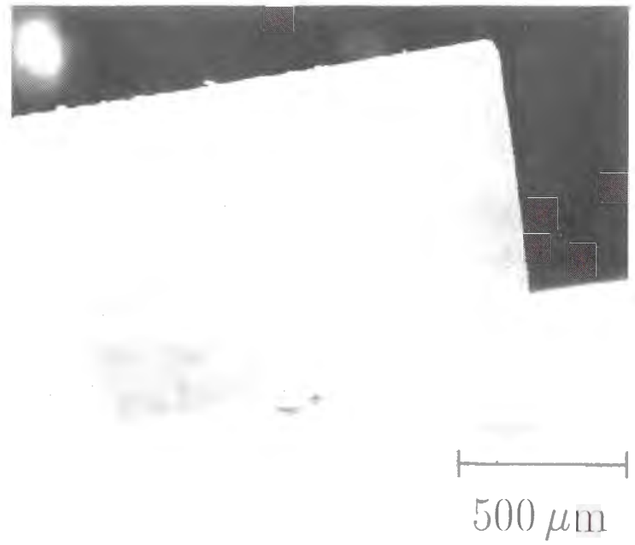

(b)

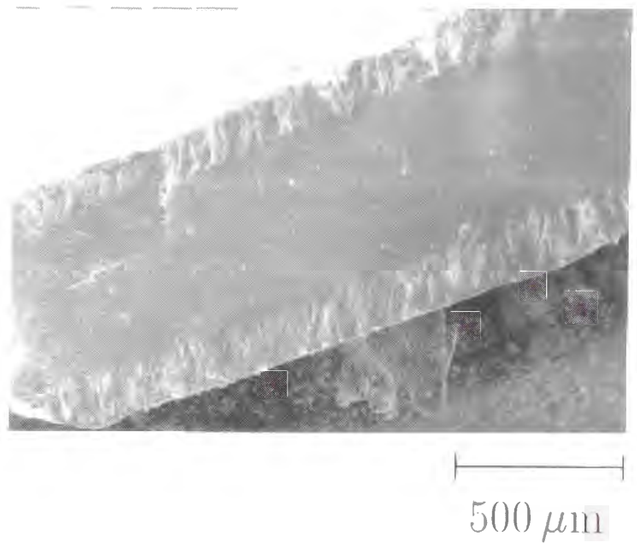

Fig. 5.4: Scanning electron micrographs of fractured cross sections for (a) BTO-0.5 and (b) BTO-12.

The dependence of second-harmonic intensity on angle of incidence, that is, Maker fringe pattern, is shown for BTO-0.5 and BTO-12 (Figs. 5.5 and 5.6). These patterns were measured under the condition of *pp*-polarization, which means that the plane of polarization is parallel to the incident plane for both fundamental and second-harmonic waves. The second-harmonic intensity of BTO-0.5 experiences a maximum at about 40°, and the maximum intensity is ten times larger than that of BTO-12 around 0°. In addition, the behavior of second-harmonic generation in BTO-0.5 is distinguished from that in BTO-12 in terms of the dependence of Maker fringe pattern on the plane of polarization; the second-harmonic intensity of the former glass-ceramic under *sp*-polarization is only one tenth of the intensity with *pp*-polarization, and the second-harmonic wave is not observed at all under the other conditions, whereas the Maker fringe pattern of the latter does not change even though the polarization condition is varied.

The thin-film XRD patterns of STO-12, which are shown in Fig. 5.7, are quite similar to those of the glass-ceramics containing $BaTiO_3$ shown in Fig. 5.2. Namely, the precipitation of several kinds of crystalline phases, which include TeO_2, $SrTeO_3$, $SrTe_2O_5$, Sr_2TiO_4 and $TeO_2(H_2O)_n$, is observed only at the near-surface region with a depth of smaller than 50 μm. A similar result was obtained for STO-0.5. The only difference between glass-ceramics in the SrO-TiO_2-TeO_2 system and the $BaTiO_3$- containing ones lies in the fact the glass-ceramics derived from $15SrO{\cdot}15TiO_2{\cdot}70TeO_2$ glasses do not show the second-harmonic generation under any polarization conditions.

5.1.4 Discussion

$BaTiO_3$ bulk crystal is well known to exhibit the displacive transition at around 130 °C between cubic and ferroelectric tetragonal phases; the latter shows a large second-order nonlinearity at room temperature [12].

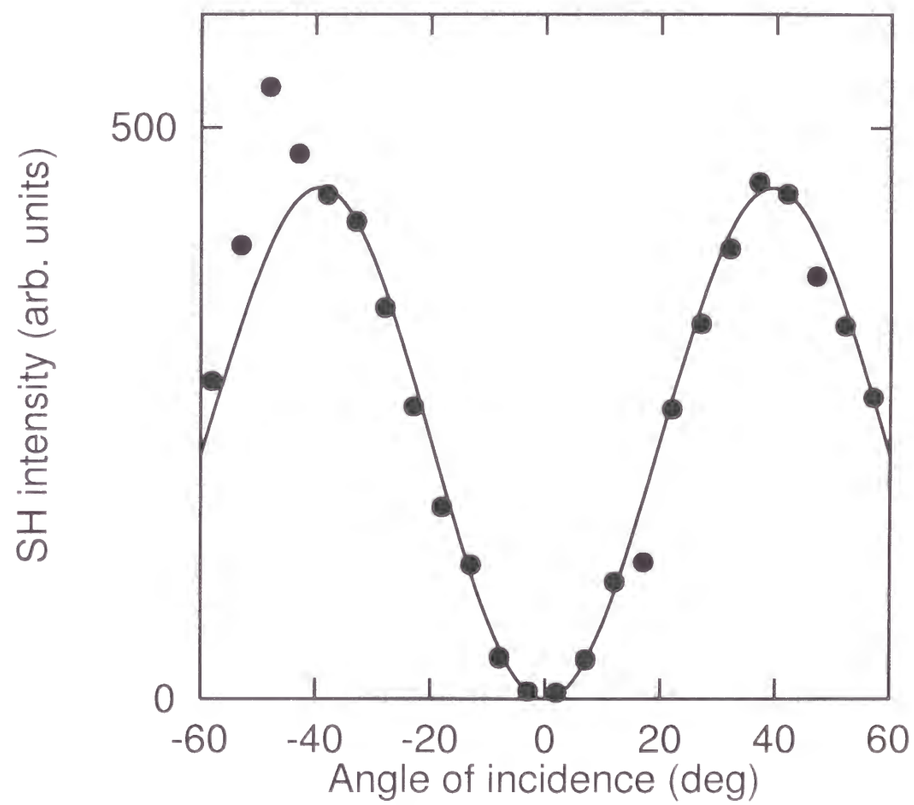

Fig. 5.5: Variation of second-harmonic intensity with angle of incidence, i.e., Maker fringe pattern, for BTO-0.5. Closed circles denote experimental pattern measured under conditions that both fundamental and second-harmonic waves were *p*-polarized. Theoretical pattern (solid curve) was drawn with $L = 3.43\,\mu$m and non-zero component of second-order nonlinear tensor, $d_{33} = 3.65$ pm/V.

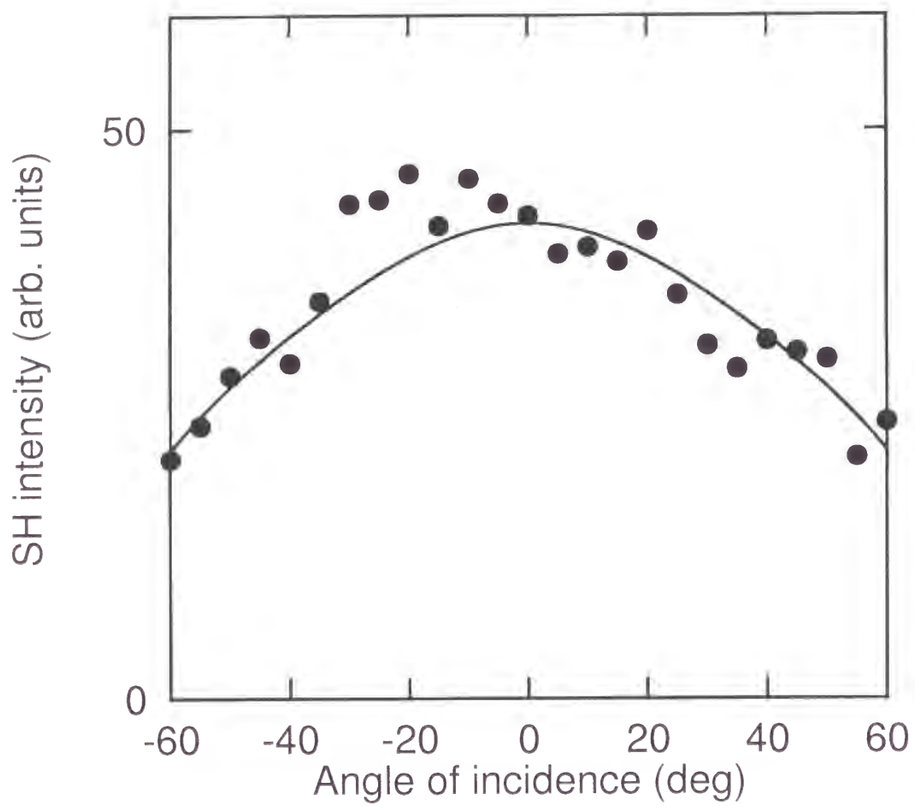

Fig. 5.6: Experimental (closed circles) and theoretical (solid curve) Maker fringe patterns of BTO-12. The p-polarized second-harmonic wave converted from p-polarized fundamental light was detected. By fitting the solid curve to the experimental data, L and $d^{(2)}$ were obtained: $L = 300\,\mu$m and $d_{15} = d_{24} = 0.31$ pm/V, $d_{31} = d_{32} = 0.29$ pm/V, $d_{33} = 0.12$ pm/V.

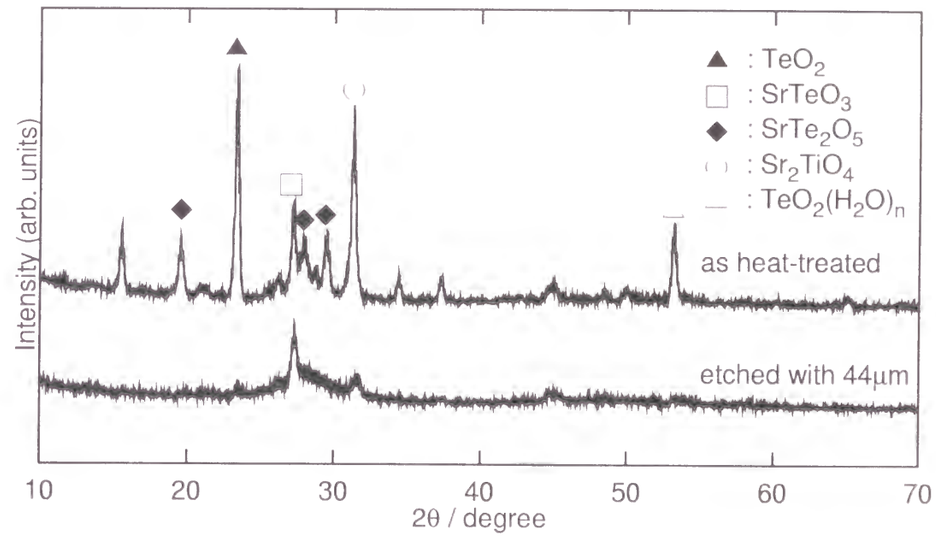

Fig. 5.7: Thin-film XRD patterns for STO-12 derived from $15SrO{\cdot}15TiO_2{\cdot}70TeO_2$ glass. Like the glass-ceramics prepared from $15BaO{\cdot}15TiO_2{\cdot}70TeO_2$ glasses, crystalline phases were observed only at both surfaces of the glass-ceramics.

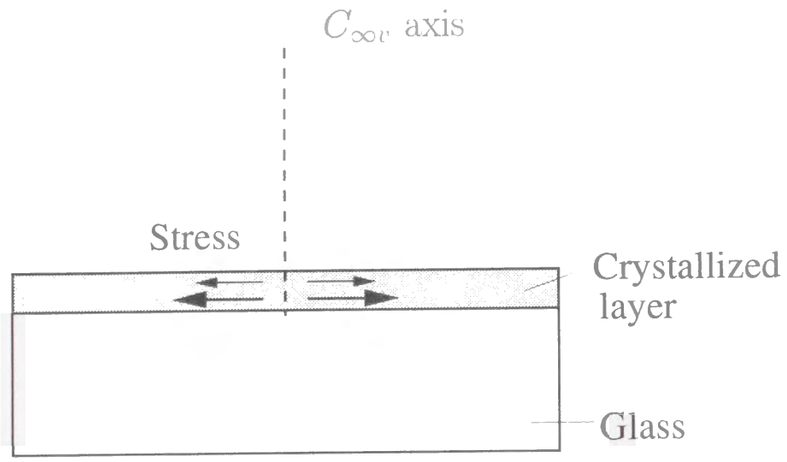

Fig. 5.8: Schematic illustration of an induced stress, which possibly brings about $C_{\infty v}$ symmetry after surface crystallization of glass. This stress is caused by a difference in thermal expansion coefficient between glass and precipitated crystals. It depends upon the magnitude of thermal expansion coefficient, although it is unclear whether the stress at the crystallized layer is tensile or compressive.

It has been reported, however, that in $BaTiO_3$ ceramics consisting of grains with submicron-size, the ferroelectric-paraelectric phase transition temperature decreases and the ferroelectricity ceases with decreasing the grain size, resulting in the stabilization of the pseudo-cubic phase below 130 °C [6, 13, 14]. Similarly, it is anticipated that for the present $BaTiO_3$ crystallites, which were precipitated as a cubic phase when the glass was heated above 400 °C, the transformation into the tetragonal phase during the cooling to room temperature is suppressed to some extent. As a result, the $BaTiO_3$ crystallite is closer to cubic than to the tetragonal phase at room temperature as indicated by the XRD results.

For the glass-ceramics containing $BaTiO_3$, we can take the following origins as a source of the second-harmonic generation. One is the $BaTiO_3$ crystallites the tetragonal phase of which is well known to possess large second-order nonlinear susceptibility. Another is crystalline phases other than $BaTiO_3$. In addition, a stress induced by the surface crystallization like that shown in the schematic illustration in Fig. 5.8 is a possible origin

as well. This stress may be caused by a difference in the thermal expansion coefficient between glass and precipitated crystals during the cooling from heat treatment temperature to room temperature. Based on the fact that no second-harmonic signal was detected from the glass-ceramics fabricated via surface crystallization of $15SrO{\cdot}15TiO_2{\cdot}70TeO_2$ glass, the contribution of TeO_2, $TeO_2(H_2O)_n$ and the above-described stress to the second-harmonic generation can be excluded. Moreover, the sample containing only $BaTeO_3$ obtained by removing the surface layer with 140 μm did not generate a second-harmonic wave, indicating that the $BaTeO_3$ crystal is not an origin of the second-harmonic generation. It can be said, that the $BaTiO_3$ crystallites play an important role in the second-order nonlinear phenomenon, although they are more likely to be cubic than tetragonal. It can be speculated that a small tetragonal strain from the cubic structure is responsible for the second-order nonlinearity.

It was found that the Maker fringe pattern of the glass-ceramics containing $BaTiO_3$ drastically changes with an increase in heat treatment time. Furthermore, an increase in heat treatment temperature gives rise to the similar variation [11]; the glass-ceramic heat-treated at 415°C exhibits zero intensity at the incident angle of 0° like the pattern in Fig. 5.5, whereas the fringe pattern of the glass-ceramic heat-treated at 422.5°C is similar to that of BTO-12 in Fig. 5.6, which shows a maximum intensity at 0°. These facts suggest that some change is imposed on the origin of second-harmonic generation, namely $BaTiO_3$ crystal, as the crystallization proceeds. According to the Maker fringe patterns in Figs. 5.5 and 5.6, this change corresponds to an induction of $d^{(2)}$ component parallel to the sample surface instead of a disappearance of $d^{(2)}$ component normal to the surface, where $d^{(2)}$ represents the second-order nonlinear optical coefficient.

For the aim of estimating the second-order nonlinear tensor components of the $BaTiO_3$-containing glass-ceramics, an attempt to analyze the experimental second-harmonic intensity in Figs. 5.5 and 5.6 utilizing the Maker fringe equations introduced in Chapter 1 was made. It should be mentioned that $R(\theta)$ which represents the multiple reflection coefficient is

approximately unity, and that its dependence on the angle of incidence is negligible because refractive indices of the present glass-ceramics are about 2. In this theory the material is assumed to have no loss of transmitted light due to scattering or absorption, which reduces the interference among the generated harmonic waves and results in a disappearance of the oscillation of second-harmonic intensity. The scattering, however, increases as the crystallization proceeds with heat treatment time. As a result, for BTO-12, the Maker fringe equations are inappropriate and should be improved. Actually, the behavior of oscillation in Maker fringe pattern of BTO-0.5 varied clearly, depending on the thickness of the surface crystallized layer, L, as demonstrated by etching, whereas the Maker fringe pattern of BTO-12 did not change even though the etching of surface was carried out.

The solid curve in Fig. 5.5 is the theoretical Maker fringe pattern drawn with Eqs. (1.2) to (1.10) since the variation of Maker fringe pattern with the polarization condition was similar to that of poled glasses which have d_{eff} written as Eq. (1.10). The parameters thus obtained are $L = 3.43\,\mu$m and $d_{33} = 3.65$ pm/V. Although the d_{33} value estimated is about one fifth of d_{15} for $BaTiO_3$ single crystal, it is comparable to or larger than the d-value of $BaTiO_3$ thin films deposited by other methods such as metalorganic chemical vapor deposition [15] and pulsed-laser deposition [16]. Here, it should be noted that the present value of d_{33} was calculated from the macroscopic symmetry of $BaTiO_3$- based polycrystalline film on the BTO-0.5 glass-ceramic.

As described in the previous part of this section, Eqs. (1.2) to (1.10) are not suitable for the analysis of the Maker fringe pattern for BTO-12. Therefore, the following equation is introduced in order to analyze the experimental second-harmonic intensity for BTO-12:

$$I_{2\omega} = C\, d_{eff}^2\, t_\omega^4\, T_{2\omega} \frac{1}{(n_\omega^2 - n_{2\omega}^2)^2} \times \int_0^L I_\omega^2 \exp\{-\frac{z}{\cos\theta_\omega} 2\alpha_\omega \ln 10 - \frac{(L-z)}{\cos\theta_{2\omega}} \alpha_{2\omega} \ln 10\} dz \ . \quad (5.1)$$

Here, α is the absorbance per unit length in the surface crystallized layer,

i.e., $\alpha_\omega = 1.4\ \mathrm{mm}^{-1}$ and $\alpha_{2\omega} = 2.8\ \mathrm{mm}^{-1}$, and z is the depth from the input surface to the position where the second-harmonic wave is generated. In this equation $\sin^2\Psi$ in Eq. (1.2) is changed for the last integral term because of lack of interference among the harmonic waves and presence of finite absorption or scattering loss. Contrary to the case of BTO-0.5, the second-harmonic intensity did not depend on the polarization of light, which suggests that the source of second-harmonic generation, namely the c-axis of $BaTiO_3$, is distributed randomly in the plane parallel to the surface. Thus, we calculated d_{eff} for BTO-12 by assuming that $BaTiO_3$ crystallites were precipitated with (101)- or (110)-orientation as ascertained by the XRD pattern. Under these assumptions, the solid curve in Fig. 5.6 was drawn with the parameters, $L = 300\,\mu$m which corresponds to both surface regions of BTO-12, $d_{15} = d_{24} = 0.31$ pm/V , $d_{31} = d_{32} = 0.29$ pm/V and $d_{33} = 0.12$ pm/V. It should be noted that the Maker fringe pattern and the polarization dependence of second-harmonic intensity of BTO-12 are coincident with the XRD and SEM data, but that a relation between the Maker fringe pattern and $BaTiO_3$ crystal structure derived from XRD results has not been made clear yet for BTO-0.5.

5.1.5 Conclusions

The second-harmonic generation was examined for the glass-ceramics fabricated via surface crystallization of both $15BaO{\cdot}15TiO_2{\cdot}70TeO_2$ and $15SrO{\cdot}15TiO_2{\cdot}70TeO_2$ glasses. The former, containing (101)- or (110)-oriented $BaTiO_3$ crystallites, exhibited second-harmonic generation, whereas no second-harmonic signal was detected from the latter, leading to the conclusion that $BaTiO_3$ crystallites play an important role in the second-order nonlinear phenomena although they are more likely to be cubic rather than tetragonal. Additionally, the Maker fringe pattern of the $BaTiO_3$-containing glass-ceramics was found to change drastically as the surface crystallization proceeded with an increase in the heat treatment time and

temperature. In order to evaluate the second-order nonlinearity for the glass-ceramics containing $BaTiO_3$, the analyses were carried out using the original and improved Maker fringe equations written as Eqs. (1.2) and (5.1), respectively. The second-order nonlinear tensor component d_{15} of BTO-12 thus obtained is 0.31 pm/V. For the sample BTO-0.5, d_{33}, which only reflects the macroscopic symmetry of $BaTiO_3$-based polycrystalline film on the surface of the glass-ceramic, is estimated to be 3.65 pm/V. This value is larger than that reported for $BaTiO_3$ polycrystalline thin films prepared by metalorganic chemical vapor deposition and pulsed-laser deposition.

5.2 Poling effect on crystallization of tetragonal $BaTiO_3$ and second-harmonic generation

5.2.1 Introduction

As revealed in Chapter 5.1, the glass-ceramics containing $BaTiO_3$ crystallites on their surfaces were successfully fabricated via heat treatment of $15BaO{\cdot}15TiO_2{\cdot}70TeO_2$ glass and exhibited the second-harmonic generation, although the XRD results indicate that the precipitated $BaTiO_3$ crystals are likely to be rather paraelectric cubic phase than ferroelectric tetragonal one. Namely, the suppression of paraelectric-ferroelectric transition of $BaTiO_3$ crystallites occurred. A similar result was reported for glass-ceramics in the system PbO-BaO-TiO_2-B_2O_3 by Lynch *et al.* [9]: the cubic $PbTiO_3$ precipitated at elevated temperature was quenched to room temperature after heat treatment of glass without the ferroelectric transition characteristic of bulk $PbTiO_3$ crystal. This was explained by assuming that the lattice strain between glass matrix and precipitated crystallite restricted the phase transition of $PbTiO_3$ crystal into ferroelectric phase, which is known as crystal clamping. They also found that the effect of crystal clamping could be efficiently excluded when the glass transition

temperature of the residual glass was decreased below the Curie temperature of $PbTiO_3$, i.e., 490 °C. However, as for $BaTiO_3$ crystal, this method is not available because of its lower Curie temperature of 120 °C.

In this study, the application of a dc voltage, i.e., poling during crystallization of $15BaO{\cdot}15TiO_2{\cdot}70TeO_2$ glass is carried out to fabricate transparent glass-ceramics with ferroelectric-like properties such as large optical nonlinearity. The effect of poling on ferroelectricity and related optical nonlinearity of the precipitated crystalline phase has been little investigated thus far [5]. Therefore, the effect of poling on both crystallization of $15BaO{\cdot}15TiO_2{\cdot}70TeO_2$ glass and second-order nonlinearity of the resultant glass-ceramics is examined by means of measurements of X-ray diffraction and second-harmonic generation. The behavior of crystallization of other crystalline phases as well as $BaTiO_3$ crystal caused by an external voltage is discussed in terms of the effect of both the electric field and the Joule heat.

5.2.2 Experimental procedure

$15BaO{\cdot}15TiO_2{\cdot}70TeO_2$ (in mol%) glass was prepared from reagent-grade $BaCO_3$, TiO_2 and TeO_2 as starting materials. The mixture of raw materials was melted in a platinum crucible at 1000 °C for 30 min, and then was poured into an alumina boat. The glass transition temperature of the sample was determined using differential thermal analysis (Rigaku, TG-DTA 8112BH). After annealing for 30 min at 380 °C which is around its glass transition temperatures, the sample was polished with CeO_2 powders into a plate of 5 mm × 7 mm × 1 mm. The inside and surface of as-annealed specimen were ascertained to be amorphous by powder and bulk X-ray diffraction (XRD) measurements (Rigaku, RINT1400). Cu K_α radiation was used and diffraction intensity was measured at $2\theta = 10°$ to 70°.

Poling treatment was performed as follows. The glass specimen was

sandwiched in between two commercial borosilicate glass plates with a size of 18mm × 18mm × 0.15 mm and contacted with electrodes made of stainless steel. The borosilicate glasses were used for the suppression of leakage current at the sample surface. The glass specimen with electrodes was put in an electric furnace and heated to an aimed temperature which ranged from 380 to 420 °C. Then, a dc voltage of 0-1 kV was applied at the temperature for 3 h followed by gradual cooling to room temperature with the voltage applied. It should be noted that the actual voltage applied to the specimen was smaller than the intentionally applied external voltage due to the use of borosilicate glass plates. The XRD pattern for the surface of the resultant specimen was measured in order to identify crystalline phases if precipitated.

Second-harmonic generation was examined for all the heat-treated specimens at room temperature using the Maker fringe method. The *p*-polarized fundamental light at 1064 nm from a Q-switched pulsed Nd:YAG laser (Spectra-Physics, GCR-11) was incident on the sample which was rotated around an axis perpendicular to the incident plane. The fundamental wave which passed through the sample was reduced in its intensity using two IR cut filters and eliminated perfectly by a monochromator (Spex. 270M), whereas the second-harmonic light at 532 nm generated in the sample was passed thorough a polarizer to be *p*-polarized. Thus, only the *p*-polarized second-harmonic light at 532 nm was detected by using a photomultiplier (Hamamatsu Photonics, R955). The signal from the photomultiplier was accumulated using a digital oscilloscope (Hewlett Packard. 54522A). The input fundamental light power was estimated by measuring the second-harmonic intensity of Y-cut quartz with $L = 1.046$ mm and $d_{11} = 0.34$ pm/V as a reference material, where L and d_{11} are the thickness and the component of second-order nonlinear coefficient tensor, respectively.

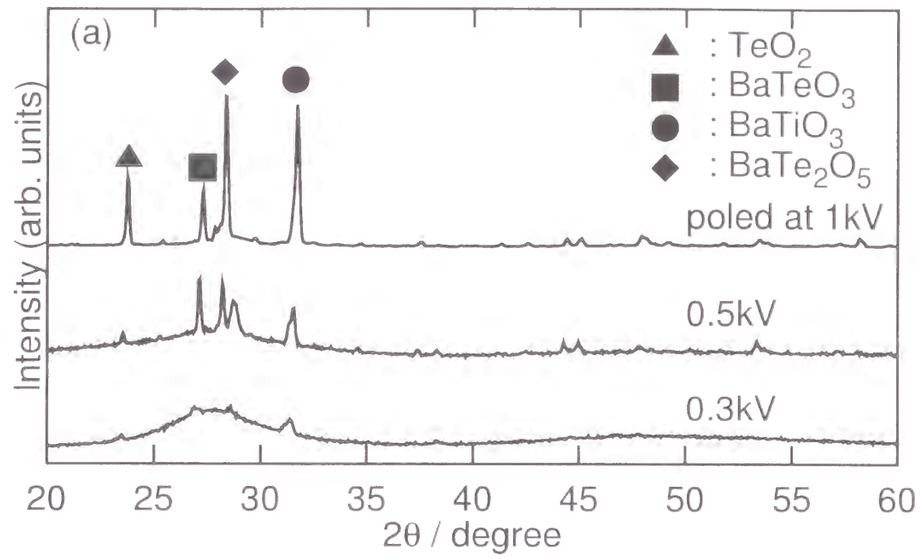

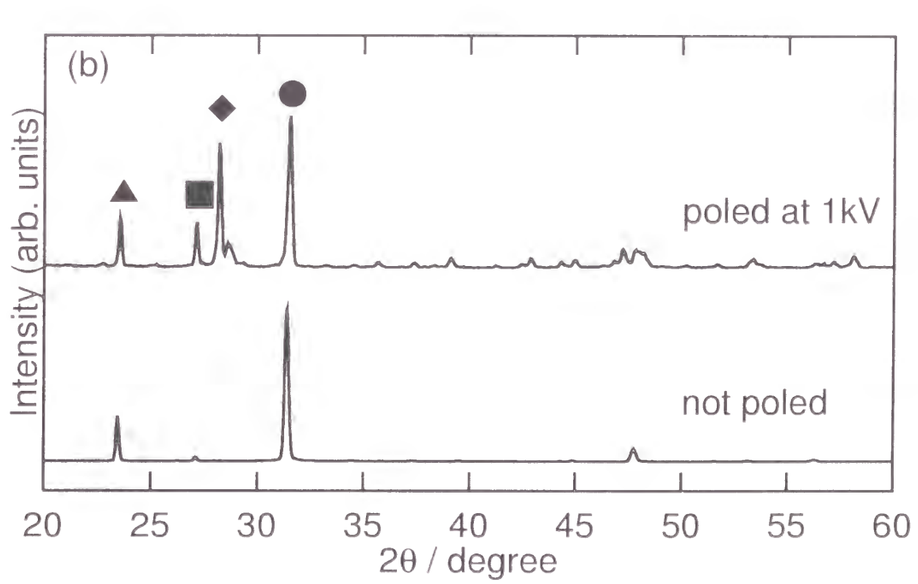

Fig. 5.9: XRD patterns for the specimens prepared by heat treatment at (a) 100 °C and (b) 420 °C, respectively. The patterns from bottom to top in (a) correspond to the samples heat-treated at an applied voltage of 0.3, 0.5 and 1 kV/mm. The upper and lower patterns in (b) represent the XRD lines for the glass-ceramics heat-treated with a voltage of 1 kV and without a voltage.

5.2.3 Results and discussion

Figures 5.9 (a) and (b) show XRD patterns for an anode-side surface of the bulk specimens heat-treated at 400 and 420 °C, respectively. The XRD patterns in Fig. 5.9 (a) correspond to the samples poled at several voltages indicated in the figure during the heat treatment. In the case of the poling voltage of 1 kV, the diffraction lines were observed at around 2θ = 23.6, 27.2, 28.2 and 31.7 °. These lines can be assigned to TeO_2, $BaTeO_3$, $BaTe_2O_5$ and $BaTiO_3$ crystalline phases, respectively. The intensity of these diffraction lines was decreased with a decrease in the applied voltage. The diffraction lines eventually disappeared for the sample without poling which was identified as an amorphous phase by XRD. Here, it should be noted that the powder XRD patterns of all the heat-treated samples, irrespective of poling conditions, exhibited only a broad hallow peak characteristic of an amorphous material. This fact indicates that the crystallization did not occur uniformly inside the bulk $15BaO{\cdot}15TiO_2{\cdot}70TeO_2$ glass, but took place only at the surface-region of the glass. Thus, it can be said that the surface crystallization was promoted by the application of a dc voltage during the heat treatment. The application of voltage possibly has an influence on the crystallization behavior through effect of an electric field or the Joule heat. Whereas the former is considered to bring about the transfer of ions, the latter causes an increase in actual sample temperature. Based on the measured specific heat of about 0.4 $J{\cdot}g^{-1}{\cdot}K^{-1}$ at 400 °C for $15BaO{\cdot}15TiO_2{\cdot}70TeO_2$ glass and the measured poling current of less than 0.1 μA, the increase of sample temperature due to the Joule heat was estimated to be about 10 K at most when the glass was poled at an external voltage of 1 kV. Therefore, it is plausible that the increase in sample temperature is possibly one of the important factors for the occurrence of crystallization at this temperature.

Being similar to the glass-ceramics poled at 400 °C, the XRD pattern of the poled glass-ceramic in Fig. 5.9 (b) show sharp peaks at around 23.6, 27.2, 28.2 and 31.6 °. On the other hand, the glass-ceramic prepared with

no voltage applied shows the Bragg reflection lines at 23.6, 27.2 and 31.4 °, but dose not exhibit any lines assignable to $BaTe_2O_5$ crystalline phase. The fact that $BaTe_2O_5$ was observed for only the poled glass-ceramics suggests that the electric field, i.e., movement of ions brought about the change in the crystallization behavior.

The XRD peaks due to the Bragg reflection from (101) and (110) plane of $BaTiO_3$ crystalline phase are shown for the glass-ceramics prepared at 400 and 420 °C in Figs. 5.10 (a) and (b), respectively. The higher the applied voltage was during heat treatment, the larger shift in 2θ these peaks experienced, whereas the diffraction lines attributable to the other crystalline phases exhibited no change in their peak position. According to JCPDS cards, the paraelectric cubic phase of $BaTiO_3$ crystal shows the XRD line from (110) plane at 2θ = 31.4°. On the other hand, the ferroelectric tetragonal $BaTiO_3$ has the diffraction peaks corresponding to (101) or (110) plane at 31.50 and 31.64°, respectively. Therefore, it can be pointed out that the poling made $BaTiO_3$ crystallites rather close to tetragonal phase than cubic phase.

Figure 5.11 shows the variation of second-harmonic intensity with angle of incidence, i.e., Maker fringe pattern for the glass-ceramic prepared at 400 °C with poling at 1 kV. Whereas the second-harmonic generation was observable for the glass-ceramics poled at 0.5 and 1 kV, no second-harmonic signals were detected from the specimens heat-treated with a voltage in the range of 0-0.3 kV applied. This observation indicates that in the present experiments the surface-crystallization is necessary for the second-harmonic generation. Two types of possibilities should be considered as a source of the second-order nonlinearity induced by the surface crystallization of $15BaO{\cdot}15TiO_2{\cdot}70TeO_2$ glass. One of them is the $BaTiO_3$ crystallites the tetragonal phase of which has large second-order nonlinearity. Another is a stress caused during the cooling process from heat treatment temperature to room temperature because of difference in thermal expansion coefficient between glass and precipitated crystals, as schematically described in Fig. 5.8. However, this kind of stress leads to $C_{\infty v}$ symmetry like poled

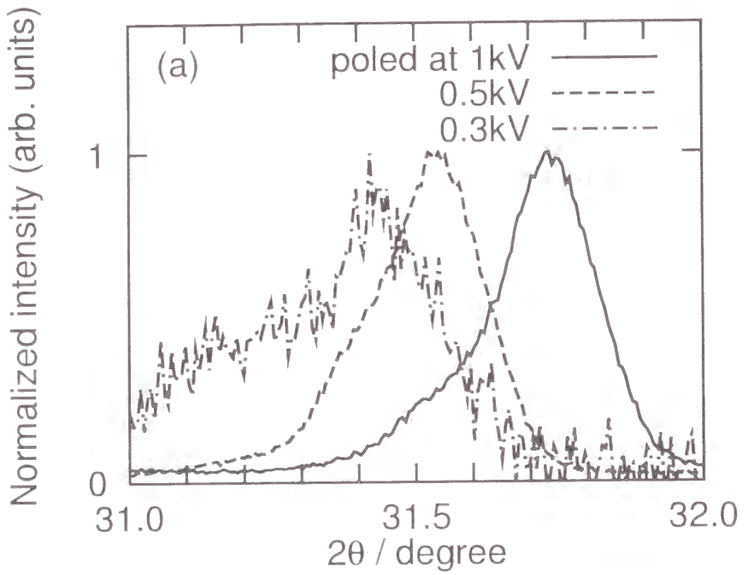

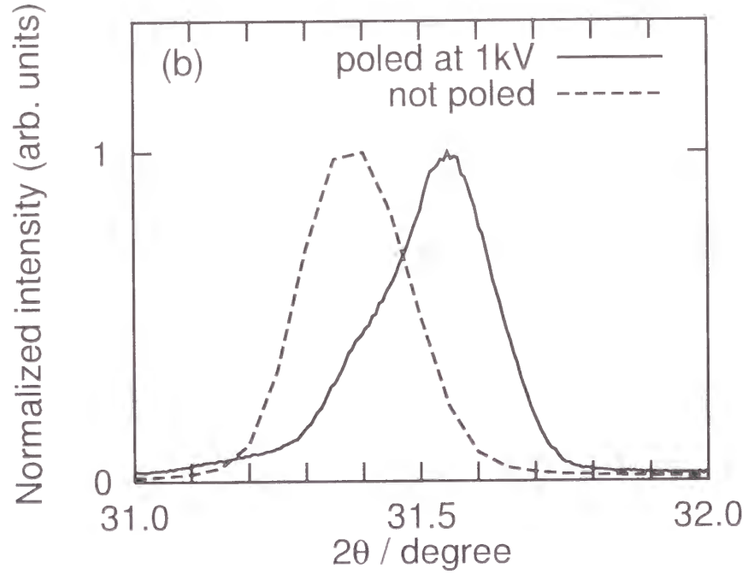

Fig. 5.10: XRD lines, which can be assigned to $BaTiO_3$ crystal, for the glass-ceramics fabricated via heat treatment at (a) 400 °C and (b) 420 °C, respectively. According to the JCPDS cards, diffraction line at around $2\theta = 31.4°$ is due to the Bragg reflection from (110) plane of cubic phase, whereas diffraction peaks at 31.50° and 31.64° are attributable to (101) and (110) planes of tetragonal one, respectively.

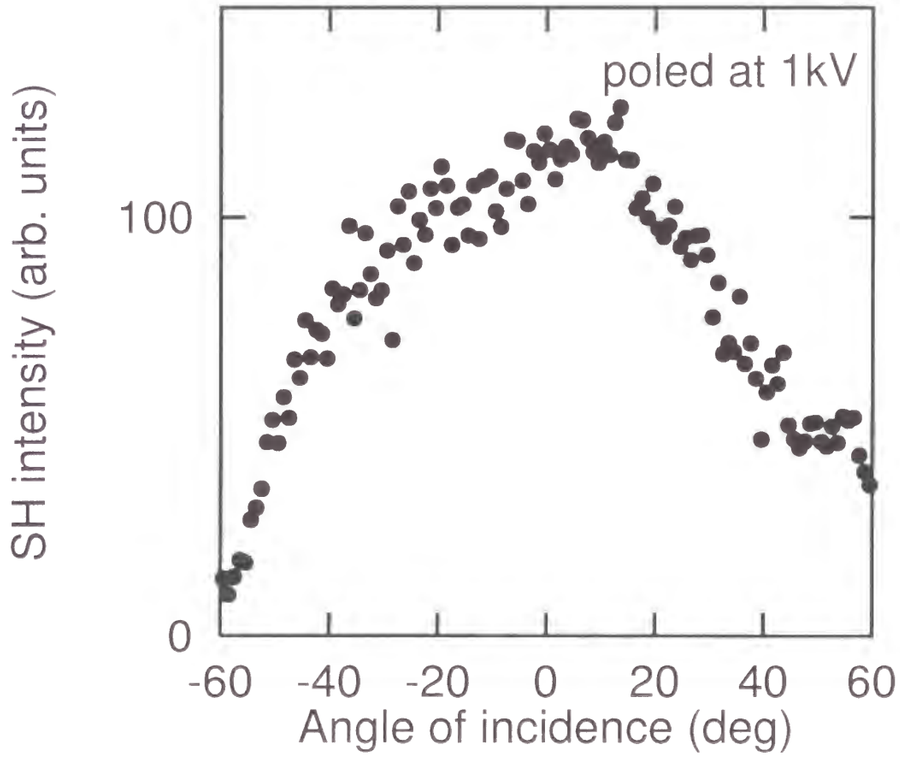

Fig. 5.11: Variation of the second-harmonic intensity with incident angle, i. e., Maker fringe pattern for the glass-ceramic prepared at 400 °C with an applied voltage of 1 kV.

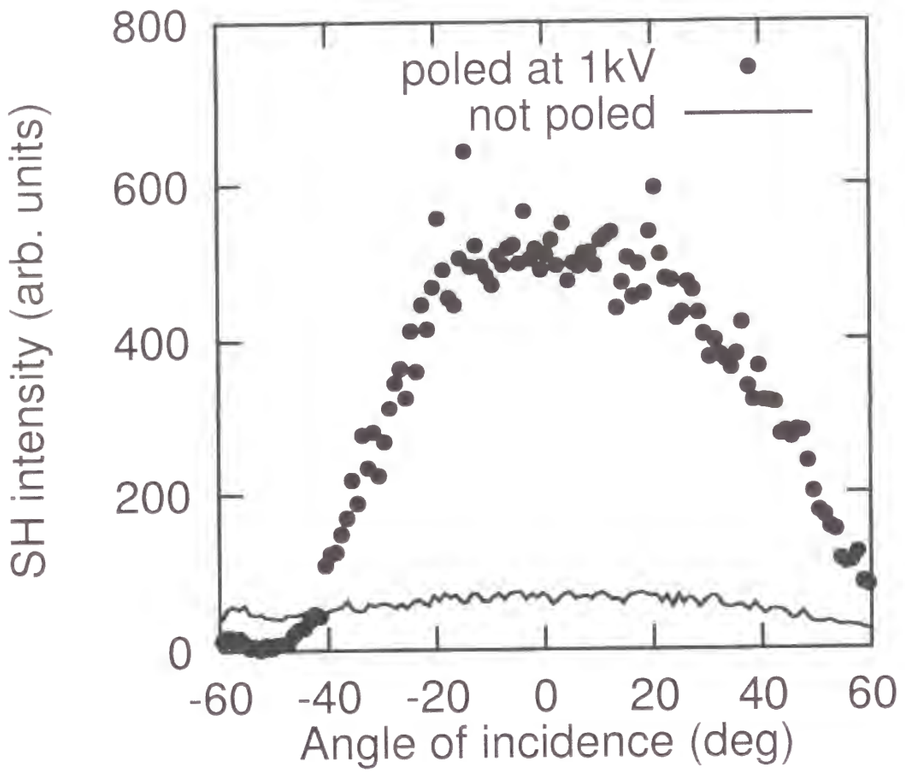

Fig. 5.12: Maker fringe patterns for the glass-ceramics heat-treated at 420 °C. The solid curve and closed circles denote the second-harmonic intensity for the specimens crystallized without and with an external voltage, respectively.

glass materials which show no second-harmonic generation at 0° but have a maximum intensity at a larger angle, as shown in the previous chapters. According to the Maker fringe pattern in Fig. 5.11, such a stress can be excluded from the origins for second-harmonic generation in the present glass-ceramics.

The Maker fringe patterns of the glass-ceramics heat-treated at 420 °C are demonstrated in Fig. 5.12. The solid curve and closed circles represent the second-harmonic intensity from the glass-ceramics without and with poling, respectively. The latter intensity is ten times larger than the former one, indicating that the poling treatment enhanced the second-harmonic generation. The possible explanation for this enhancement is an increase in amount or tetragonality of precipitated $BaTiO_3$. On the other hand, it was revealed by SEM observations that the longer-period heat treatment made the crystallized layer thicker: the thickness varied from a few to more than 100 μm, resulting in an increase in the amount of precipitated $BaTiO_3$. However, the glass-ceramic with a thicker surface-crystallized layer showed smaller intensity of second-harmonic light because of a decrease in transparency. Therefore, it takes a more important role in the enhancement of second-harmonic generation by poling that $BaTiO_3$ crystal precipitates as the tetragonal phase.

5.2.4 Conclusions

The effect of poling on both the surface crystallization behavior of $BaTiO_3$ in $15BaO{\cdot}15TiO_2{\cdot}70TeO_2$ glass and the second-harmonic generation in the resultant glass-ceramics was investigated. The poling proceeded not only the surface-crystallization of $BaTiO_3$ at lower temperature but also the stabilization of tetragonal $BaTiO_3$ phase. The poled glass-ceramics exhibited larger second-harmonic intensity, which can be ascribed to the increase in tetragonality of $BaTiO_3$ crystalline phase.

References

[1] Y. H. Kao. Y. Hu. H. Zheng. J. D. Mackenzie. K. Perry. G. Bourhill. and J. W. Perry. J. Non-Cryst. Solids **167**. 247 (1994).

[2] Y. Ding. Y. Miura. and A. Osaka. J. Mater. Res. **11**. 495 (1996).

[3] Y. Ding. A. Osaka. Y. Miura. H. Toratani. and Y. Matsuoka. J. Appl. Phys. **77**. 2208 (1995).

[4] K. Tanaka. H. Kuroda. K. Hirao. and N. Soga. Mater. Res. Soc. Symp. Proc. **453**. 271 (1997).

[5] N. F. Borrelli and M. M. Layton, J. Non-Cryst. Solids **6**, 197 (1971).

[6] M. M. Layton and J. W. Smith, J. Am. Ceram. Soc. **58**, 435 (1975).

[7] M. J. Reece, C. A. Worrell, G. J. Hill, and R. Morrell. J. Am. Ceram. Soc. **79**, 17 (1996).

[8] M. Todorovic, L. Radonjic, and J. Dumic, Key Engineering Materials **132-136**, 193 (1997).

[9] S. M. Lynch and J. E. Shelby, J. Am. Ceram. Soc. **67**. 424 (1984).

[10] T. Komatsu, H. Tawarayama, and K. Matusita. J. Ceram. Soc. Jpn. **101**, 48 (1993).

[11] K. Tanaka, H. Kuroda, A. Narazaki, K. Hirao, and N. Soga, J. Mater. Sci. Lett. **17**, 1063 (1998).

[12] A. Dubey and P. Sen, Solid State Commun. **105**, 739 (1998).

[13] K. Uchino, E. Sadanaga, and T. Hirose, J. Am. Ceram. Soc. **72**, 1555 (1989).

[14] Y. Park, K. M. Knowles, and K. Cho. J. Appl. Phys. **83**, 5702 (1998).

[15] B. Bihari, J. Kumar, G. T. Stauf, P. C. V. Buskirk, and C. S. Hwang, J. Appl. Phys. **76**, 1169 (1994).

[16] T. Okada. Y. Nakata. H. Kaibara. and M. Maeda. Jpn. J. Appl. Phys. **34**. L1536 (1995).

Summary

In the present thesis, optical second-order nonlinear properties in poled tellurite glasses were investigated by second-harmonic generation measurements utilizing the Maker fringe method. Poling effect on surface structure of tellurite glasses was also examined in detail by means of X-ray photoelectron spectroscopic (XPS) and infrared reflectance techniques, which was discussed in connection with the second-order nonlinearity. Besides, the influence of poling on crystallinity and ferroelectricity as well as nonlinearity of $BaTiO_3$ crystallites in tellurite glass-ceramics was explored. The results obtained are summarized as follows.

In General introduction, the general background and purpose of the present study were outlined. Poling was introduced as an attractive technique for the improvement of the optical properties and structure of oxide glasses. Additionally, some interesting phenomena in the nonlinear optical properties of poled glasses were described and the unresolved problems concerning the induced structure by means of poling and second-order nonlinear properties were suggested.

In Chapter 1, tellurite glasses containing mono- and/or divalent cations such as alkali, alkaline earth and some transition metal ions were prepared by the conventional melting-quenching method, and then poled at various temperatures below the glass transition temperature. Second-harmonic generation measurements were carried out for poled tellurite glasses in order to evaluate nonlinear optical properties with second-order. For the poling temperature dependence of second-harmonic generation, it is a characteristic of all the tellurite glass systems that the generated second-harmonic intensity increases, manifests a maximum, and then begins to decrease just

below its glass transition temperature, with an increase in poling temperature. This decrease in second-harmonic intensity was explained in terms of some electrochemical reactions at the anode-side surface which diminish the induced SHG-active structure. Furthermore, a linear relationship between an optimum poling temperature, which results in a maximum second-harmonic intensity, and glass transition temperature was found out through all the tellurite glasses employed in this chapter. On the other hand, the compositional dependence of second-order nonlinearity was discussed in the light of the mixed alkali effect. It was shown that the thermal stability of mixed alkali glass is higher than that of single alkali glass. As a result, the temperature range within the poling is effective is wider for the former glass.

In Chapter 2, the incident angular dependence of second-harmonic intensity, so-called Maker fringe pattern, was examined in detail for Na_2O-ZnO-TeO_2 glass system. According to the analysis of the second-harmonic intensity for the glasses poled at the optimum poling temperature using the Maker fringe theory, it was revealed that the SHG-active layer has a thickness of only several micrometers which is much thiner than a whole sample thickness. This agrees the observation that the second-harmonic generation perfectly disappeared when an anode-side surface region was mechanically removed. Based on these results, it was concluded that the second-order nonlinear susceptibility, $\chi^{(2)}$, is induced preferentially in the vicinity of the anode-side glass surface. The value of $\chi^{(2)}$ was explained by considering the $\chi^{(3)}$ process associated with a frozen electric field E_{dc} created in the tellurite glass, which is described as $\chi^{(2)} = 3\,\chi^{(3)} \cdot E_{dc}$. The magnitude of $\chi^{(2)}$ estimated on the assumption of the above process is comparable to the value obtained experimentally, supporting the idea that a formation of the static electric field E_{dc} is responsible for the induction of second-order nonlinearity by poling. On the other hand, the relaxation behavior of second-harmonic intensity was strikingly influenced by glass composition; the intensity decayed rapidly for alkali tellurite glasses, whereas the glass containing divalent cations exhibited longer relaxation time. Consequently, in the glass containing Zn^{2+} ions, the second-order nonlinearity was attained to be stable enough to the practical applications. Simultaneously, an attempt was made to realize a large second-order nonlinearity in WO_3-TeO_2 glass system. This is because the WO_3-TeO_2 glass possesses a large refractive index which possibly leads to a large third-order nonlinearity due to the Miller's law, resulting in a large magnitude of second-order nonlinearity via the induction process of $\chi^{(2)} = 3\,\chi^{(3)} \cdot E_{dc}$. Actually, the obtained $\chi^{(2)}_{33}$ reached 2.1 pm/V. This value is approximately 40% of $\chi^{(2)}_{22}$ of $LiNbO_3$ crystal.

In Chapter 3, second-harmonic generation was examined as a function of time at elevated temperatures as well as at room temperature for the WO_3-TeO_2 glasses. In order to explore the effect of poling temperature on both the second-harmonic intensity and its decay, poling was performed at various temperatures. The stretched exponential decay function was applied to analysis of the observed relaxation behavior, which leads to the estimation of both relaxation time and stretched exponential parameter; the latter describes a deviation from an exponential decay curve. Not only the dependence of the decay of second-order nonlinearity on poling temperature but also the temperature dependence of the decay time was investigated. First, the relaxation time increased with an increase in poling temperature, suggesting that the activation energy and/or frequency factor for a relaxation process increased with raising poling temperature. In other words, the SHG-active structure induced at higher temperature is more stable. Secondly, it was shown that the relaxation behavior deviates from an exponential curve when the poling temperature is high. As for the T-dependence of the relaxation time, the decay rate rapidly increased with the measurement temperature. The plots of the relaxation time versus a reciprocal of temperature, namely, the Arrhenius plots, show a linear correlation. From this, the activation energy for the decay of second-order nonlinearity was estimated to be 47 kJ·mol^{-1}. This value was compared with those reported for the electronic conductivity of alkali ions and the viscous flow in alkali tellurite glasses. As a result, it was concluded that

the relaxation of second-order nonlinearity is not caused by the viscous flow and the motion of non-bridging oxygen, which is stuck to the tellurite glass network, but is attributable to the ionic motion such as conduction and diffusion of Na^+ ion.

In Chapter 4, surface structure of poled tellurite glasses was characterized by means of X-ray photoelectron and IR reflectance spectroscopies in order to obtain the poling effect on glass composition and glass network at the anode-side surface where the second-order nonlinearity was mainly induced as indicated in the previous chapters. The XPS data for the binary tellurite glass containing Zn^{2+} ions indicate that the concentrational ratio of Zn to Te decreased at the anode-side, whereas it increased at the cathode-side, after poling. This suggests the formation of Zn^{2+} ion-depleted region in the vicinity of the anode-side surface. Moreover, the photoelectron spectra showed that Na^+ ions exist at both surfaces of the $30ZnO{\cdot}70TeO_2$ glass after poling, mainly accumulating at the anode-side surface. This fact was explained by assuming penetration of Na^+ ions from the borosilicate glass plate which was placed between the tellurite glass specimen and an anode to avoid precipitation of metallic tellurium and a discharge between electrodes. In addition to these results, the persistent second-order nonlinearity in the ZnO-TeO_2 glass, which manifested significant difference from the rapid decay of second-harmonic intensity in binary tellurite glasses containing Na^+ ions, led to conclusion that the Zn^{2+} ions with lower mobility than Na^+ ions play a dominant role in the formation of E_{dc}, that is, the induction of second-order nonlinearity. For the WO_3-TeO_2 glass system, the penetration of Na^+ ions was also observed, while there was no obvious change in the ratio of W/Te after poling. It was thought from this fact that the Na^+ ions are responsible for the induction of second-order nonlinearity in WO_3-TeO_2 glass system.

In Chapter 5, the second-order nonlinear properties of transparent glass-ceramics containing $BaTiO_3$ crystallites fabricated via heat treatment of BaO-TiO_2-TeO_2 glasses were discussed. Besides, in order to clarify the poling effect on the crystallization behavior and the second-harmonic generation, the poling technique was performed for these glasses above the glass transition temperature. From the scanning electron microscopic and thin-film X-ray diffraction observations, it was shown that the $BaTiO_3$ crystallite was precipitated with (100) and/or (110) orientations in the glass surface region. In other words, the surface crystallization was dominant. The surface-crystallized layer exhibited the second-harmonic generation, and the obtained Maker fringe pattern drastically varied when the thickness of the crystallized layer was changed, resulting in two types of patterns. As for the glass-ceramics with thin crystallized layer, the second-order nonlinear coefficient was calculated using the Maker fringe theory to be 3.65 pm/V which is larger than those reported for the polycrystalline films prepared by metalorganic chemical vapor deposition and pulsed-laser deposition. For the glass-ceramics containing a large amount of $BaTiO_3$, the modified Maker fringe theory was introduced due to their relatively low transmittance. In these glass-ceramics, however, the $BaTiO_3$ crystals were precipitated likely to be rather paraelectric cubic phase than ferroelectric tetragonal phase, as indicated by the position of X-ray diffraction lines. This suppression of paraelecrtic-ferroelectric transition has been reported in many glass-ceramics, and a lot of efforts has been made to obtain ferroelectric-like glass-ceramics. In the present glass-ceramics, the X-ray diffraction data indicated that the stability of tetragonal or ferroelectric phase was enhanced by the application of a dc voltage, that is, poling. Consequently, the enhancement of second-harmonic generation was accomplished by the poling-induced crystallization of $BaTiO_3$ in the tellurite glass.

List of publications

Chapter 1.

"Effect of poling temperature on optical second harmonic intensity of sodium zinc tellurite glasses",
Aiko Narazaki, Katsuhisa Tanaka, Kazuyuki Hirao and Naohiro Soga,
J. Appl. Phys. **83**, 3986-3990 (1998).

"Effect of poling temperature on optical second-harmonic intensity of lithium sodium tellurite glass",
Aiko Narazaki, Katsuhisa Tanaka, Kazuyuki Hirao and Naohiro Soga,
J. Am. Ceram. Soc. **81**, 2735-2737 (1998).

"Poling temperature dependence of optical second-harmonic intensity of MgO-ZnO-TeO_2 glasses",
Katsuhisa Tanaka, Aiko Narazaki, Kazuyuki Hirao and Naohiro Soga,
J. Appl. Phys. **79**, 3798-3800 (1996).

"Optical second harmonic generation in poled MgO-ZnO-TeO_2 and B_2O_3-TeO_2 glasses",
Katsuhisa Tanaka, Aiko Narazaki, Kazuyuki Hirao and Naohiro Soga,
J. Non-Cryst. Solids **203**, 49-54 (1996).

Chapter 2.

"Induction and relaxation of optical second-order nonlinearity in tellurite glasses",
Aiko Narazaki, Katsuhisa Tanaka, Kazuyuki Hirao and Naohiro Soga,
J. Appl. Phys. **85**, 2046-2051 (1999).

"Large optical second-order nonlinearity of poled WO_3-TeO_2 glass",
Katsuhisa Tanaka, Aiko Narazaki and Kazuyuki Hirao.
Opt. Lett., 2000, in press.

Chapter 3.

"Relaxation behavior of second-order nonlinearity in poled WO_3-TeO_2 glasses",
Aiko Narazaki, Katsuhisa Tanaka and Kazuyuki Hirao.
submitted to Opt. Lett.

Chapter 4.

"IR and XPS studies on surface structure of poled ZnO-TeO_2 glasses with second-order nonlinearity",
Aiko Narazaki, Katsuhisa Tanaka and Kazuyuki Hirao,
submitted to J. Am. Ceram. Soc.

"Poling effect on second-order nonlinearity and surface structure in WO_3-TeO_2 glass system",
Aiko Narazaki, Katsuhisa Tanaka and Kazuyuki Hirao,
to be submitted.

Chapter 5.

"Optical second-order nonlinearity of transparent glass-ceramics containing $BaTiO_3$ precipitated via surface crystallization",
Aiko Narazaki, Katsuhisa Tanaka and Kazuyuki Hirao,
J. Mater. Res. **14**, 3640-3646 (1999).

"Poling-induced crystallization of tetragonal $BaTiO_3$ and enhancement of optical second-harmonic intensity in BaO-TiO_2-TeO_2 glass system",
Aiko Narazaki, Katsuhisa Tanaka and Kazuyuki Hirao,
Appl. Phys. Lett. **75**, 3399-3401 (1999).

"Second harmonic generation in $BaTiO_3$ film crystallized on tellurite glass surface",
Katsuhisa Tanaka, Hisako Kuroda, Aiko Narazaki, Kazuyuki Hirao and Naohiro Soga.
J. Mater. Sci. Lett. **17**, 1063-1065 (1998).

Related publication

"Effect of poling on TeO_2-based glasses",
Katsuhisa Tanaka, Aiko Narazaki and Kazuyuki Hirao,
New Glass **14**, 7-11 (1999) (In Japanese).

Acknowledgments

The present thesis has been carried out under the direction of Professor Kazuyuki Hirao at Graduate School of Engineering in Kyoto University.

The author wishes to express her sincere gratitude to Professor Kazuyuki Hirao and Emeritus Professor Naohiro Soga for their continuous encouragement and valuable advice all through the duration of the present work. The author is also grateful to Professor Tadashi Kokubo and Professor Toshinobu Yoko for useful suggestions on the present thesis. The author would like to express her grateful appreciations to Professor Katsuhisa Tanaka at Faculty of Engineering and Design in Kyoto Institute of Technology for his informative discussion and helpful advice on numerous occasions through this work. The profitable suggestions given by Professor Teiichi Hanada, Professor Kazuki Nakanishi, Dr. Setsuhisa Tanabe, Dr. Koji Fujita and Mr. Koichi Kajihara are also appreciated. Hearty thanks are made to all the students and staffs of Hirao's laboratory for their collaboration.

The author wishes to thank Professor Hiroyuki Nasu in Mie University and Dr. Jun Matsuoka in University of Shiga Prefecture for their informative discussion. The author also thanks to the financial support of Research Fellowship of the Japan Society for the Promotion of Science for Young Scientists.

Finally, the author thanks Mr. Kyoji Narazaki and Mrs. Reiko Narazaki, her parents, and Mr. Hideki Sato, her husband, for their support and encouragement.

Kyoto, winter 2000 Aiko NARAZAKI